Folia Histochemica et Cytobiologica

Scientific quarterly devoted to problems of histochemistry, cytochemistry and cell & tissue biology

www.fhc.viamedica.pl

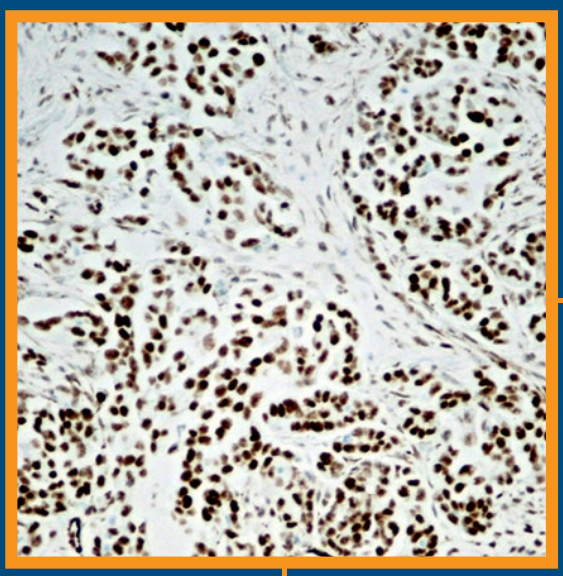

Vol. 58
No. 3
2020

ISSN 0239-8508

VIA MEDICA

Folia Histochemica et Cytobiologica

Scientific quarterly devoted to problems of histochemistry, cytochemistry and cell & tissue biology

www.journals.viamedica.pl/folia_histochemica_cytobiologica

Vol. 58
No. 3
2020

Official Journal of the Polish Society for Histochemistry and Cytochemistry

EDITORIAL OFFICE:
Department of Histology
Medical University of Gdansk
Debinki St. 1, 80–210 Gdansk, Poland
tel.: + 48 58 349 14 37
fax: + 48 58 349 14 19
e-mail: zkmiec@gumed.edu.pl
http://www.journals.viamedica.pl/folia_histochemica_cytobiologica

Folia Histochemica et Cytobiologica (pISSN 0239–8508, eISSN 1897–5631) is published quarterly, one volume a year, by the Polish Society for Histochemistry and Cytochemistry at VM Media sp. z.o.o VM Group sp.k., Gdansk.
Indexed in: Index Medicus/MEDLINE, Excerpta Medica/EMBASE, Chemical Abstracts/CAS, SCI Expanded, SciSearch, Biochemistry & Biophysics Citation Index, ISI Alerting Services, Biosis Previews Index Copernicus, Biological Abstracts, SCOPUS, Research Alert, ProQuest, EBSCO, DOAJ, Ulrich's Periodicals Directory.

POLISH SOCIETY FOR HISTOCHEMISTRY AND CYTOCHEMISTRY STATEMENT OF FOLIA HISTOCHEMICA ET CYTOBIOLOGICA EDITORIAL POLICY

Folia Histochemica et Cytobiologica is an international, English-language journal devoted to the rapidly developing fields of histochemistry, cytochemistry, cell and tissue biology.

The Folia Histochemica et Cytobiologica publishes papers that meet the needs and intellectual interests of medical professionals, basic scientists, college and university teachers and students. Prospective authors should read most recent issues of FHC to determine the appropriateness of a possible contribution. However, such an examination does not provide an infallible guide because editorial policy is always under review. Technical correctness is necessary, but it is not the only condition for acceptance. Clarity of exposition and potential interest of the readers are important considerations; it is the reader, not the author, who must receive the benefit of the doubt.

Folia Histochemica et Cytobiologica publishes review articles, original articles, short communications and proceedings of scientific congresses/symposia. Fields of particular interests include development and application of modern techniques in histochemistry and cell biology, cell biology and pathology, cell-microenvironment interactions, tissue organization and pathology.

Manuscripts announcing new theoretical or experimental results, or manuscripts questioning well-established and successful theories, are highly desirable and are a subject for evaluation by specialists. Manuscripts describing original research that clarifies past misunderstandings or allows a broader view of a subject are acceptable. Manuscripts that demonstrate new relations between apparently unrelated areas of fields of interests are appropriate. Manuscripts that show new ways of understanding, demonstrating, or deriving familiar results are also acceptable. Such manuscripts must provide some original cytobiological insight and not just a clever derivation.

Regularly, review or tutorial articles are published, often of a length greater than that of the average article. Most of these articles are a subject of a review; authors planning such articles are asked to consult with the editors at an early stage.

Most readers of a particular article will be specialists in the subject matter presented; the context within which the paper is presented should be established in the order given in Instructions for Authors. Manuscripts must be technically correct and must take proper cognizance of previous work on the same subject regardless of where it may have appeared. Such referencing is especially important for reminders of once well known ideas, proofs, or techniques that may have again become useful to readers. It is the responsibility of the author to provide adequate references; editors and referees will not do the literature search that should have been done by the authors. The references are a matter of review though.

Contributions considered include: Regular Articles (Papers), Short Communications, Review Articles, Conference Proceeding, Book Reviews and Technical Notes, which describe new laboratory methods or substantial improvements of the existing techniques. Regular articles should be about five journal pages or less in length. Short communications are usually confined to the discussion of a single concept and should be about two journal pages in length. Review articles are confined to a broad discussion and should contain the most recent knowledge about the subject.

Instructions concerning the preparation of manuscripts are given in the Information for Authors. Care in following those instructions will permit editors and referees to devote more time to thoughtful evaluation of contributions and will ultimately lead to a better, more interesting Journal.

SUBSCRIPTION

Folia Histochemica et Cytobiologica is available for paper subscription (print on demand).
To read and download articles for free as pdf document, visit http://czasopisma.viamedica.pl/fhc

Publisher: VM Media sp. z o.o. VM Group sp.k., Swietokrzyska St. 73, 80–180 Gdansk, http://www.viamedica.pl, wap.viamedica.pl

Illustration on the cover: *Wilms' tumor 1 antigen immunoreactivity in epithelial ovarian cancer — diagnostic and prognostic value* (see: Zarychta E *et al.*, pp. 198–207)

Folia Histochemica et Cytobiologica

Scientific quarterly devoted to problems of histochemistry, cytochemistry and cell & tissue biology

www.journals.viamedica.pl/folia_histochemica_cytobiologica

Vol. 58
No. 3
2020

Official Journal of the Polish Society for Histochemistry and Cytochemistry

FOLIA HISTOCHEMICA ET CYTOBIOLOGICA
Vol. 58, No. 3, 2020
pp. 163–173

REVIEW

VIA MEDICA

An overview of applications of CRISPR-Cas technologies in biomedical engineering

Saleh Jamehdor[1, 2, 3]*, Kasra Arbabi Zaboli[4]*, Sina Naserian[5, 6], Jose Thekkiniath[7], Honey Alef Omidy[8], Ali Teimoori[1], Behrooz Johari[4], Amir Hossein Taromchi[4], Yu Sasano[9], Saeed Kaboli[4]

[1]Department of Virology, Faculty of Medicine, Hamadan University of Medical Sciences, Hamadan, Iran
[2]Department of Molecular Medicine, Institute of Medical Biotechnology, National Institute of Genetic Engineering and Biotechnology, Tehran, Iran
[3]Department of Biology, Faculty of Sciences, University of Sistan and Baluchestan, Zahedan, Iran
[4]Department of Medical Biotechnology, School of Medicine, Zanjan University of Medical Sciences, Zanjan, Iran
[5]INSERM UMR-S-MD 1197/Ministry of the Armed Forces, Biomedical Research Institute of the Armed Forces (IRBA), Paul-Brousse Hospital Villejuif, and CTSA Clamart, France
[6]SivanCell, Sivan Aryo Pharmed, Tehran, Iran
[7]Fuller Laboratories, Fullerton, CA, USA
[8]Department of Biochemistry and Molecular Biology, University of Southern California, Los Angeles, CA, USA
[9]Department of Applied Microbial Technology, Faculty of Biotechnology and Life Science, Sojo University, Kumamoto, Japan

*Saleh Jamehdor and Kasra Arbabi Zaboli equally contributed to work

Abstract
Clustered Regulatory Interspaced Short Palindromic Repeats (CRISPR) is one of the major genome editing systems and allows changing DNA levels of an organism. Among several CRISPR categories, the CRISPR-Cas9 system has shown a remarkable progression rate over its lifetime. Recently, other tools including CRISPR-Cas12 and CRISPR-Cas13 have been introduced. CRISPR-Cas9 system has played a key role in the industrial cell factory's production and improved our understanding of genome function. Additionally, this system has been used as one of the major genome editing systems for the diagnosis and treatment of several infectious and non-infectious diseases. In this review, we discuss CRISPR biology, its versatility, and its application in biomedical engineering. *(Folia Histochemica et Cytobiologica 2020, Vol. 58, No. 3, 163–173)*

Key words: Genome editing; sgRNA; CRISPR-Cas9; CRISPR-Cas12; CRISPR-Cas13

Abbreviations: AAV — adeno-associated virus; ADAR — adenosine deaminases acting on RNA; Cas9 — CRISPR-associated endonuclease 9; saCas9 — Cas9 from *Staphylococcus aureus*; spCas9 — Cas9 from *Streptococcus pyogenes*; HDR — homology-directed repair; HNH — an endonuclease domain named for characteristic histidine and asparagine residues; HPRT — hypoxanthine phosphoribosyltransferase; Indel — insertion and/or deletion; MHC — Major Histocompatibility Complex; NAG — Nucleotide-Adenine-Guanine; NGG — Nucleotide-Guanine-Guanine; NHEJ — non-homologous end-joining; PAM — Protospacer Adjacent Motifs; RuvC — an endonuclease domain named for an *E. coli* protein involved in DNA repair

Correspondence address: Saeed Kaboli
Department of Medical Biotechnology,
School of Medicine, Zanjan University
of Medical Sciences, Zanjan, Iran
e-mail: kaboli2017@zums.ac.ir
Yu Sasano,
Department of Applied Microbial Technology,
Faculty of Biotechnology and Life Science,
Sojo University, Kumamoto, Japan
e-mail: sasano@bio.sojo-u.ac.jp

Introduction

CRISPR-Cas (Clustered Regularly Interspaced Short Palindromic Repeats-CRISPR associated Cas enzyme) is an advanced adaptive immune system in bacteria and most archaea which protects them through the degradation of invasive DNA [1]. The history of the exploration of the CRISPR-Cas system turns back to 1987 when Ishino and co-workers at Osaka University reported repeated DNA fragments in cluster form in the *Escherichia coli* genome [2]. While they were attempting to investigate the alkaline phosphatase isozyme encoding gene, a special repetitive sequence was observed downstream of the gene. This repetitive sequence was composed of five completely similar repetitive 29 nucleotides sequences that are dispersed by 32 nucleotide unique sequences [2]. In the following years, similar repetitive sequences were found in other *E. coli* strains and in enterobacteria that are closely related to *E.coli* as well as in *Shigella dysenteria* [3]. Several 36-base pair (bp) direct repeats interspaced by 35-46 bp unparalleled spacers were reported in *Mycobacterium tuberculosis* [4]. The repetitive sequence of the CRISPR in archaea was discovered in 1993, while Mojica and co-workers were investigating the salinity effects on the growth of *Haloferax mediterranei.* These researchers observed a long DNA sequence in the genome of these archaea which composed of regulatory repeats, although there was no similarity between these sequences and *E.coli* repeats [5]. The function of these repeats remained unclear for almost 20 years after its discovery. Several names including multiple direct repeats (DRs) [6], short regulatory spaced repeats (SRSR) [7], and large clusters of tandem repeats (LCTR) [8] have been suggested.

The term CRISPR was coined by Jansen and coworkers [9] and became accepted by researchers as this acronym reflects the structural features of repeats. In this review, we summarize CRISPR-Cas mechanisms and its applications in biotechnology and biomedical engineering. We propose insights into our understanding of CRISPR-Cas and discuss the open questions in the field.

Molecular mechanisms of CRISPR-Cas system

In the CRISPR-Cas system, RNA harboring the spacer sequence supports the CRISPR-associated (Cas) proteins to recognize and cleave foreign pathogenic DNA which is followed by cell repairing. There have been two repairing mechanisms discovered; non-homologous end-joining (NHEJ) (with more probability) and homology-directed repair (HDR) mechanisms. To knock-out a specific gene by the CRISPR system, NHEJ has been used (cells naturally use this mechanism with a high percentage to escape death after a double-strand break). On the other hand, HDR has been used for knock-in and occurs at a low percentage (Fig. 1). For HDR knock-in of any DNA fragments, either a single-stranded oligodeoxynucleotide (ssODN) or a double-stranded donor plasmid (dsODN) is used as a template in combination with nucleases to achieve accurately targeted and efficient insertion into the target DNA site. Previous studies have shown that ssODN-mediated knock-in is more efficient as compared to double-stranded plasmid-mediated knock-in [10–12].

CRISPR-Cas system consists of a crRNA (CRISPR RNA) complemented with targeted DNA which causes the attachment of crRNA to this DNA and is involved in recognition. RNA that is attached to the 3' end of crRNA is called tracrRNA (trans-activating CRISPR RNA) which transcribes from the same cluster of the CRISPR locus. For recognition and double-stranded DNA cleaving, annealing of these two RNAs to create a single guide RNA (sgRNA) and subsequent attachment of sgRNA to Cas9 protein is required [1, 13]. One of the major sequences called Protospacer Adjacent Motif (PAM) is also involved in recognition, while the length and number of this sequence may vary in different bacterial systems. This sequence is located close to the ~20 nucleotides sequence which is recognized by crRNA. The stem-loops formed at 3' end of tracrRNA are critical for the function of CRISPR [14, 15].

Types of CRISPR systems

Based on CRISPR/Cas loci, CRISPR systems have been classified into six types (I–VI) and all of them contain a distinctive Cas nuclease along the interference stage [1]. Of these, type I and III systems use a large multi-Cas protein complex to promote the target sequence cleavage, whereas the type II system utilizes a single nuclease called Cas9 [15, 16]. Cas12 and Cas13 are nuclease proteins belonging to type V and VI, respectively [17]. In this review, we focus on three important types of CRISPR/Cas systems.

CRISPR-Cas9

Among the several types of CRISPR-Cas systems, CRISPR-Cas9 has been most commonly used and is derived from *Streptococcus pyogenes*. CRISPR-Cas9 system has been harnessed to mediate genome editing in several cell types and can be exploited to generate gene knock-outs (*via* insertion/deletion) or knock-ins (*via* the HDR). PAM sequence of this bacterium

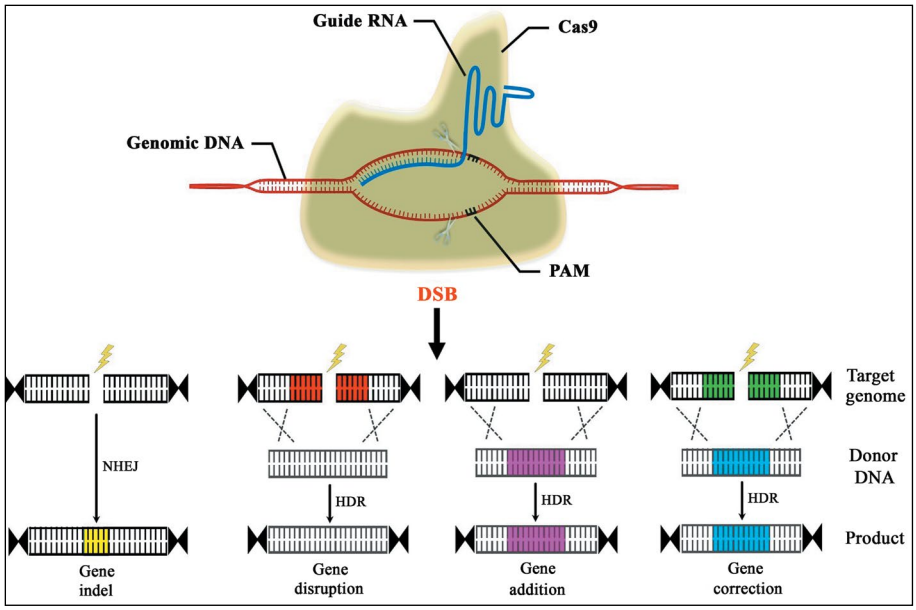

Figure 1. Illustration of the CRISPR-Cas9 mediated gene editing. The CRISPR/Cas9 system which has been functioned in different organisms has a sgRNA consisting of a backbone with three stem-loops and a complementary sequence with a 20-nucleotide target (shown in blue color). It also has a PAM (shown in black color) that in 80% of cases is NGG and in 20% of cases is NAG. After binding of 20-nucleotide to the target DNA, endonuclease distinguishes it and cuts three nucleotides after the PAM as blunt end using its endonuclease property (Some studies showed that Cas9 is first attached to sgRNA, and then the target DNA is detected). Afterward, the cell uses an NHEJ repair method to add or reduce some nucleotides (gene indel, shown in yellow color). This method is used to knock out genes. If the cell uses HDR repair, it uses a DNA similar to the cut-off region as a template and performs repair. This type of repair is used to create knock-in in the cell and destroy, add, and correct the gene (shown in no color, pink, and blue respectively).

is 80 percent NGG and could be 20 percent NAG, while other CRISPR systems may contain different PAM sequences [14]. Bioinformatics tools have been used to link tracrRNA to crRNA resulting in a single unique RNA that can be used in genome editing. Several vectors have been generated to exploit the potentials of CRISPR-Cas9 technology [18, 19]. Molecular studies showed that Cas9 endonuclease has two domains (RuvC and HNH) on Cas9 protein and each domain cut one strand in a double-stranded DNA. While D10 (aspartic acid 10) that exists on the RuvC domain is involved in cutting the non-complementary strand with sgRNA, H840 (histidine 840) located on the HNH domain is required for cutting the complementary strand with sgRNA. To create a Cas9 that only connects to the guided location without applying a double-stranded break (Dead Cas9 or dCas9), both nuclease domains need to be mutated [20, 21] (Fig. 2). On the other hand, effector domains could be connected to carboxyl-terminal of the dCas9 protein that may result in activation of gene expression by transcriptional activators such as VP64 (a transcription activator protein from *Herpes Simplex Virus*), inhibition of gene expression by KRAB effector (Krüppel associated box domain), epigenetic changes (KDM [histone lysine demethylase] or HAT/HDAC [histone acetyltransferase/ /histone deacetylase]), tracking of DNA (often with GFP [green fluorescent protein]) and specific DNA isolation by affinity tag (and base-changer deaminase domain) [22–25]. One such effector is adenosine deaminase enzyme (TadA), which can change adenine to inosine; thus, it can convert A-T to G-C [26]. This system enables researchers to make targeted point mutations with around 50 percent efficiency. Additionally, the cytidine deaminase enzyme has been applied in manipulating several bacterial species [27–30]. This system has been designed to induce an end-codon into a gene and make it possible to out the target gene purposefully and is known as CRISPR--stop. This approach has been efficiently used to inactivate several genes in mice zygote cells [31] as well as to identify critical amino acids in proteins [32]. Also, the cytidine deaminase enzyme has been used for induction of exon skipping, activation of alternative 3' or 5' splice site, switching between mutually exclusive exons, or targeted intron retention [33]. To ease recognition sites that could be identified by the CRISPR-Cas9 system and to reduce the off-target rate, web-based software has been used.

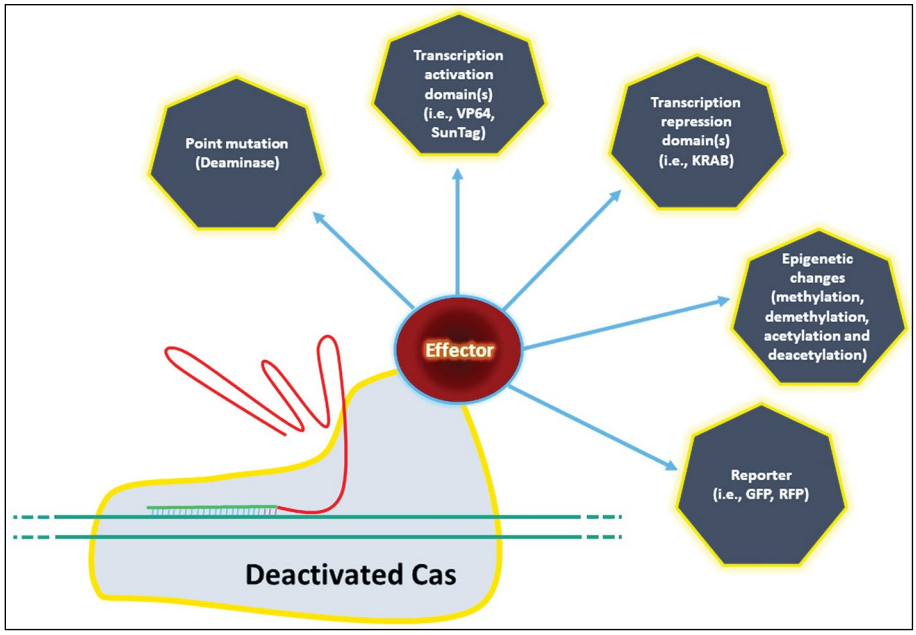

Figure 2. Researchers have mutated and inactivated Cas so that it can bind to DNA based on the sgRNA targeting sequence, but has lost its ability to cleave. By binding Cas to transcriptional activators (*e.g.*, VP64 [Virion Protein 64], SunTag [repetitive peptide epitopes that can be used to recruit multiple copies of an antibody-fusion protein to the target of interest]) and inhibition domains (*e.g.*, KRAB [Krüppel Associated Box]), epigenetic modulation domains, reporters (*e.g.*, GFP [Green Fluorescent Protein], RFP [Red Fluorescent Protein]), and deaminase (*i.e.*, adenosine deaminase), additional capabilities can be added to the Cas.

One of the major disadvantages of the CRISPR-Cas9 system is the "off-target effect". Although this system is highly efficient in prokaryotes, in the case of eukaryotes, there has been an increase in the off-target effect due to multiple increases in genome size. To overcome this effect, one specific mutation on Cas9 protein has been added to create a new protein called Cas9 nickase. This protein has a mutation in nuclease domains to cut complementary or non- complementary strand DNA with sgRNA (Fig. 2). It has been shown that using sgRNAs on opposite strands to create a double nickase resulted in 200–1500 fold reduction of off-target effect [19, 34, 35].

CRISPR-Cpf1 (Cas12)

One of the most important CRISPR-associated tools is CRISPR from *Prevotella* and *Francisella* 1 (CRISPR-Cpf1) which is analogous to the CRISPR-Cas9. Zhang and co-workers for the first time introduced the CRISPR-Cpf1 system in which the sgRNA-endonuclease protein differs from that of the CRISPR-Cas9 system [17] (Fig. 3). Crystallography of *Lachnospiraceae bacterium* ND2006-crRNA-DNA revealed that the Cpf1 consists of a binding domain with a looped-out helical domain (LHD), an oligonucleotide binding domain (OBD), a RuvC nuclease domain, and domains with unknown functions [36].

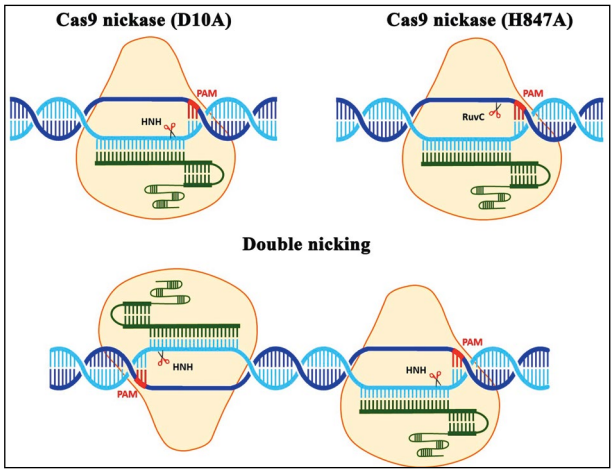

Figure 3. Single nickase and paired nickases systems. Researchers identified two amino acids in the Cas9 endonuclease protein (H840 and D10), that are involved in cutting one of the DNA strands. The amino acid H840 is located in the RuvC domain and the amino acid D10 is located in the HNH domain. Cas9 D10A cleaves the gRNA-targeting strand, while Cas9 H840A cleaves the non-targeted strand. In single nickase, the Cas9 can cut merely the strand complementary to the sgRNA; a couple of sgRNA-Cas9n complexes can nick both strands at the same time (paired nickases). When using paired nickases, additional considerations need to be given to gRNA design which includes producing a 5' overhang, the spacing between the two gRNAs, and the relative position of the two gRNA target sites. By using paired nickases, the off-target is greatly reduced, but cutting efficiency is also greatly reduced.

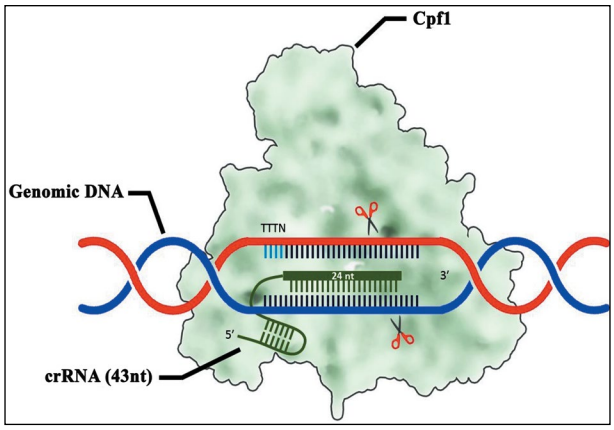

Figure 4. CRISPR-Cas12a (Cpf1) system. The Cas12a targets AT-rich regions of the genome (indicated with light blue color), in contrast to Cas9 which targets GC-rich sequences. The backbone of the sgRNA has one stem-loop and the sgRNA is composed of 43 nucleotides, of which 24 nucleotides are complementary to the target DNA (shown in dark green color). The mature crRNA required for the Cpf1 action is shorter than the guide RNA of the Cas9. The Cpf1 endonuclease protein has fewer nucleotides than the Cas9 and carries the cut as a sticky end, and the cut area is far from the PAM. Three well-studied orthologs of the Cpf1, including AsCpf1, FnCpf1, and LbCpf1 have been applied for genome editing in eukaryotic cells. The PAM sequences of the Cpf1 family proteins differ only in the number of thymidine.

A crystallography analysis on DNA-crRNA-*Acidaminococcus sp.* has shown that conformational transitions of the PAM interacting cleft and disordered seed sequence minimize the off-target in CRISPR-Cpf1 system suggesting PAM sequence plays a critical role in the stimulation of structural rearrangements [37] (Fig. 4). Using the Cpf1 endonuclease derived from *Acidaminococcus sp*. BV3L6 and *Lachnospiraceae* ND2006 bacteria, it was found that the effect of this system on eukaryotic cells is compatible with the CRISPR-Cas9 [38]. However, functional Cpf1 does not require the tracrRNA, but crRNA is needed. This promotes genome editing because the Cpf1 is not only smaller than the Cas9 but also has a smaller sgRNA molecule. Cas12a orthologs and BhCas12b have been used as powerful gene-editing tools [39, 40]. Catalytically inactive AsCpf1 protein in fusion with a transcription activator (dAsCpf1-VPR) was used for upregulation of targeted gene expression in mammalian cells [41]. The Cpf1 has also been effectively used for multiplex gene editing purposes [42–44]. Recently, Broughton *et al.* used a CRISPR–Cas12-based assay to detect SARS-CoV-2 from patient RNA, namely SARS-CoV-2 DNA Endonuclease Targeted CRISPR Trans Reporter (DETECTR) [45]. Some of the new subtypes of type-V CRISPR system including Cas12e, Cas12f, Cas12g, Cas12h, Cas12i, and Cas12k show programmable endonuclease activity [46–49].

CRISPR-Cas13

The type VI CRISPR-Cas systems also known as CRISPR-Cas13 only requires one Cas13 protein and a crRNA molecule. To date, four subtypes of this system have been recognized including VI-A (Cas13a/C2c2), VI-B (Cas13b/C2c6), VI-C (Cas13c/ /C2c7), and VI-D (Cas13d) [50, 51]. The presence of two HEPEN domains that are responsible for RNA-targeted nucleolytic activity is a common feature of all subtypes, even though they differ in size and sequence [50, 52]. While Cas13a is used to cut a particular RNA [51], catalytically-inactive Cas13 (dCas13) can only attach to RNA strands [53–55]. Similar to CRISPR-Cas9 which present base editing activity to revert an SNP without inducing a dsDNA break [56], RNA base editing for A-to-I edit [57] and C-to-U edit [58] were proven to be achieved by fusion of dCas13 with ADAR. These systems are used to make changes at RNA level as well as to treat diseases [59]. In contrast to other types of Cas13, Cas13d [60] and some examples of Cas13a do not require a Protospacer Flanking Sequence (PFS). Very recently, it has been shown that Cas13d can inhibit SARS-CoV-2 and influenza [61]. Among the Cas13 family, the Cas13d has fewer amino acids than others (930 amino acids). Due to the low number of Cas13 nucleotides, the insertion of this protein in vectors with a size limitation is much easier. Importantly, the Cas13d has more than 90% efficiency in cutting the RNA. These features of the Cas13d endonuclease has made it as one of the best tools for molecular biology studies.

Applications of CRISPR-Cas9 in biomedical engineering

The CRISPR-Cas system has demonstrated an incredible potential for utilization in several biomedical and biotechnological applications. In this review, we focus on some of the CRISPR applications in biomedical engineering. One of the major applications of the CRISPR-Cas system is the induction of disease models in animals become faster and cheaper than conventional methods. The creation of these models is intended to simulate human diseases in mouse; due to its genomic similarity to the human genome, the low distance between generations, and its cost-effectiveness [62–65]. However, problem with CRISPR-mediated creation of animal models is the generation of mosaic animals [66]. The frequency of mosaic animals generated *via* the CRISPR-Cas9 system may vary in different species [66]. Nevertheless,

this system has provided a good opportunity to study cancer in cell and animal models [67–69].

Regarding the importance of animal studies, the CRISPR has been used for knocking out the MHC system in pigs at the genome level [70] which represents a suitable source of organs for xenotransplantation. Due to its importance in the food and biomedical industry, genetically engineered pigs have been produced by introducing CRISPR components into developing zygotes using somatic cell nuclear transfer (SCNT) [71]. Also, it has been demonstrated that resistance to *Mycobacterium bovis* in cows can be generated through the integration of Nramp1 (natural resistance-associated macrophage protein-1) gene by the Cas9 nickase into the bovine genome [72]. CRISPR-based genome manipulation has been successfully used in other livestock animals including goat [73–76] and sheep [77–80].

CRISPR has been used in multiplexing and simultaneously targeting several genes on multiple chromosomes and modeling complex human diseases. This system has been successfully applied in patient-derived hematopoietic stem and progenitor cells [81], liver diseases including viral hepatitis caused by hepatitis B virus (HBV) and hepatitis C virus (HCV) [82], and neurological disorders including amyotrophic lateral sclerosis (ALS) and Parkinson's disease [83]. Effective delivery of CRISPR-Cas9 to target cells is critical for therapeutic editing outcomes. Using *in vivo* or *ex vivo* methods, Cas9 can be delivered directly in the form of ribonucleoprotein (RNP) complexes or indirectly as DNA or mRNA. While *in vivo* methods exploit direct delivery of CRISPR-Cas components into unhealthy cells of the body, *ex vivo* methods can be used to introduce the CRISPR-Cas components to cells harvested from patients, before reintroducing them into the patient [84]. *Ex vivo* gene editing is favorable to achieve good efficiency and safety in CRISPR-mediated genetic manipulation of the human-induced pluripotent stem cells (hiPSCs). This strategy has been implemented for treating HIV-1 infection and acute lymphoblastic leukemia [85]. *In vivo* gene editing therapy is more challenging as it requires more efficient and tissue-specific *in vivo* delivery methods. A recent preclinical study by Maeder *et al*. [86] documented efficient removal of a disease-causing mutation within the intron 26 of the CEP290 gene using AAV-saCas9, in both murine and primate models of Leber congenital amaurosis type 10.

In the context of biomedical applications, CRISPR system has been used in eliminating infectious agents such as viruses [87] and genome engineering of non-infectious microorganisms to achieve bio-based benefits [88, 89].

CRISPR-Cas9 libraries have been used in drug target discovery and such approaches offer promising results over RNA interference because of its ability to target the whole genome, complete knockdown, and remarkable reproducibility [90]. Genome-wide CRISPR library screens include CRISPR-based loss-of-function (CRISPR knock-out) for studying drug resistance [91]; CRISPR-based gene activation (CRISPRa) for studying gain-of-function [92]; and CRISPR-based gene inhibition (CRISPRi) for studying the loss of functions (Figure 4) [93]. Of these, CRISPR knock-out libraries employ original Cas9, while CRISPRa and CRISPRi libraries use dCas9 along with other elements including VP64 (activation) [94] or the Krüppel associated box (KRAB) repression (inhibition) [23]. The CRISPR-Cas screens have also been applied for assessing gene deletions linked to drug resistance. One such application of CRISPR-Cas9 involves knocking out HPRT1 leading to cells' resistance to 6-thioguanine which has been commonly used in cancer treatment [95]. Another study identified 51-long noncoding RNAs involved in modulating cancer cell growth [96].

In cancer research, the CRISPR system could improve cancer diagnostic platforms that impact hospital medicine [53, 57]. It has also been used for high-throughput screening to identify anti-cancer drugs [97]. CRISPR imaging systems using dCas9 [98–101] and dCas13 [54, 57, 101] have shown to be critical for tracking genomic content and transcriptional regulation in various tissues of healthy and ill people. In cancer immunotherapy, the CRISPR has been used to generate CAR-T cells as the CRISPR engineered T cells showed high potential in treating leukemia and lymphoma [102]. PD-1 has been identified as an important target for the engineering of T-cells [103, 104]. CRISPR technologies have been widely applied in stem cells and regenerative medicine [105–107]. In recent years, several methods of nanoparticle-mediated CRISPR/Cas9 delivery systems have been well established [108].

Perspectives and future directions

Genome editing is a modern science tool and has been considered as a promising strategy for treating several diseases at genomic level. Among genome editing tools, CRISPR-Cas is now being considered as a great interest to both scientists and clinicians. CRISPR/Cas9 system is simple, relatively cheaper and its *in vitro*, *in vivo* and *ex vivo* applications have been used to diagnose, cure or reduce the severity of a wide range of human diseases as well as HIV-1/ /AIDS and Kostmann disease [45, 109–113]. CRISPR technology is applicable at many biological levels and could be used for the treatment of many human

diseases including cancers, infectious diseases, and genetic disorders. It has also been shown that Cas9 protein can activate host immunity against itself [114]. Researchers have been attempting to overcome challenges including the targeted delivery of this editing system to the target area and reduction of off-target effects [115, 116]. The CRISPR system has an off-target limit in organisms with a large genome which can be minimized by using bioinformatics and engineering tools (*e.g.*, double nickase approach [34]. Besides, the possible immunogenicity of SpCas9 and SaCas9 proteins [114] need to be discussed for *in vivo* therapy. Another challenge is the large size of some Cas9 proteins (*e.g.*, spCas9 approximately is 160 kDa), which is a restriction in delivery approaches, as some viral vectors have a size limitation for integration. Ethical aspects should not be ignored when working with this system. A deep understanding of the challenges and differences between several CRISPR systems allows us to improve its performance functionality. Overall, the CRISPR-Cas system toolkits (including Cas9, Cas12, and Cas13 and their engineered derivatives) are endowed with the potential to revolutionize the field of biomedicine.

The recent developments in the CRISPR-Cas system and its vast number of biotechnological applications allowed us to study gene function and carry out translational research. In recent years, CRISPR technologies, including CRISPR-mediated genome editing, CRISPRa, and CRISPRi have been widely used in gene expression studies and genome sequence manipulation. Furthermore, these systems have been applied in stem cell engineering and regenerative medicine [105]. Although the effectiveness of the CRISPR-Cas system has been documented, safe and efficient delivery of the CRISPR components to desired cells in patients' needs to be addressed. For example, in cancer immunotherapy, the most efficient method of delivery would be utilizing nanoparticles to introduce the system's components [117]. In conclusion, the CRISPR system has created a revolution in molecular biology, biotechnology, and biomedicine which rapidly moves toward creating tremendous changes in clinical trials.

Funding information

This review article did not receive any specific grant from funding agencies in the public, commercial, or not-for-profit sectors.

Conflict of interest

The authors declare no conflict of interest, financial or otherwise.

References

1. Jiang F, Doudna JA. CRISPR-Cas9 structures and mechanisms. Annu Rev Biophys. 2017; 46: 505–529, doi: 10.1146/annurev-biophys-062215-010822, indexed in Pubmed: 28375731.
2. Ishino Y, Shinagawa H, Makino K, et al. Nucleotide sequence of the iap gene, responsible for alkaline phosphatase isozyme conversion in Escherichia coli, and identification of the gene product. J Bacteriol. 1987; 169(12): 5429–5433, doi: 10.1128/jb.169.12.5429-5433.1987, indexed in Pubmed: 3316184.
3. Nakata A, Amemura M, Makino K. Unusual nucleotide arrangement with repeated sequences in the Escherichia coli K-12 chromosome. J Bacteriol. 1989; 171(6): 3553–3556, doi: 10.1128/jb.171.6.3553-3556.1989, indexed in Pubmed: 2656660.
4. Hermans P, Van So, Bik E, et al. Insertion element IS987 from Mycobacterium bovis BCG is located in a hot-spot integration region for insertion elements in Mycobacterium tuberculosis complex strains. Infect Immun. 1991; 59(8): 2695–705, indexed in Pubmed: 1649798.
5. Mojica FJ, Juez G, Rodríguez-Valera F. Transcription at different salinities of Haloferax mediterranei sequences adjacent to partially modified PstI sites. Mol Microbiol. 1993; 9(3): 613–621, doi: 10.1111/j.1365-2958.1993.tb01721.x, indexed in Pubmed: 8412707.
6. Groenen PM, Bunschoten AE, van Soolingen D, et al. Nature of DNA polymorphism in the direct repeat cluster of Mycobacterium tuberculosis; application for strain differentiation by a novel typing method. Mol Microbiol. 1993; 10(5): 1057–1065, doi: 10.1111/j.1365-2958.1993.tb00976.x, indexed in Pubmed: 7934856.
7. Mojica FJ, Díez-Villaseñor C, Soria E, et al. Biological significance of a family of regularly spaced repeats in the genomes of Archaea, Bacteria and mitochondria. Mol Microbiol. 2000; 36(1): 244–246, doi: 10.1046/j.1365-2958.2000.01838.x, indexed in Pubmed: 10760181.
8. She Q, Singh RK, Confalonieri F, et al. The complete genome of the crenarchaeon Sulfolobus solfataricus P2. Proc Natl Acad Sci U S A. 2001; 98(14): 7835–7840, doi: 10.1073/pnas.141222098, indexed in Pubmed: 11427726.
9. Jansen R, Embden JD, Gaastra W, et al. Identification of genes that are associated with DNA repeats in prokaryotes. Mol Microbiol. 2002; 43(6): 1565–1575, doi: 10.1046/j.1365-2958.2002.02839.x, indexed in Pubmed: 11952905.
10. Storici F, Snipe JR, Chan GK, et al. Conservative repair of a chromosomal double-strand break by single-strand DNA through two steps of annealing. Mol Cell Biol. 2006; 26(20): 7645–7657, doi: 10.1128/MCB.00672-06, indexed in Pubmed: 16908537.
11. Yoshimi K, Kunihiro Y, Kaneko T, et al. ssODN-mediated knock-in with CRISPR-Cas for large genomic regions in zygotes. Nat Commun. 2016; 7: 10431, doi: 10.1038/ncomms10431, indexed in Pubmed: 26786405.
12. Bressan RB, Dewari PS, Kalantzaki M, et al. Efficient CRISPR/Cas9-assisted gene targeting enables rapid and precise genetic manipulation of mammalian neural stem cells. Development. 2017; 144(4): 635–648, doi: 10.1242/dev.140855, indexed in Pubmed: 28096221.
13. Zhang F, Wen Y, Guo X. CRISPR/Cas9 for genome editing: progress, implications and challenges. Hum Mol Genet. 2014; 23(R1): R40–R46, doi: 10.1093/hmg/ddu125, indexed in Pubmed: 24651067.
14. Jiang W, Bikard D, Cox D, et al. CRISPR-assisted editing of bacterial genomes. Nat Biotechnol. 2013; 31(3): 233, doi: 10.1038/nbt.2508, indexed in Pubmed: 23360965.

15. Kimura P, Nakane T, Ishitani R, et al. Molecular mechanism of CRISPR. J Appl Crystallogr. 2014; 156: 935–49.
16. Wu X, Kriz AJ, Sharp PA. Target specificity of the CRISPR-Cas9 system. Quant Biol. 2014; 2(2): 59–70, doi: 10.1007/s40484-014-0030-x, indexed in Pubmed: 25722925.
17. Yan F, Wang W, Zhang J. CRISPR-Cas12 and Cas13: the lesser known siblings of CRISPR-Cas9. Cell Biol Toxicol. 2019; 35(6): 489–492, doi: 10.1007/s10565-019-09489-1, indexed in Pubmed: 31468291.
18. Cong Le, Ran FA, Cox D, et al. Multiplex genome engineering using CRISPR/Cas systems. Science. 2013; 339(6121): 819–823, doi: 10.1126/science.1231143, indexed in Pubmed: 23287718.
19. Ran FA, Hsu PD, Wright J, et al. Genome engineering using the CRISPR-Cas9 system. Nat Protoc. 2013; 8(11): 2281–2308, doi: 10.1038/nprot.2013.143, indexed in Pubmed: 24157548.
20. Qi LS, Larson MH, Gilbert LA, et al. Repurposing CRISPR as an RNA-guided platform for sequence-specific control of gene expression. Cell. 2013; 152(5): 1173–1183, doi: 10.1016/j.cell.2013.02.022, indexed in Pubmed: 23452860.
21. Brezgin S, Kostyusheva A, Kostyushev D, et al. Dead cas systems: types, principles, and applications. Int J Mol Sci. 2019; 20(23), doi: 10.3390/ijms20236041, indexed in Pubmed: 31801211.
22. Perez-Pinera P, Kocak DD, Vockley CM, et al. RNA-guided gene activation by CRISPR-Cas9-based transcription factors. Nat Methods. 2013; 10 (10): 973–976, doi: 10.1038//nmeth.2600, indexed in Pubmed: 23892895.
23. Gilbert LA, Horlbeck MA, Adamson B, et al. Genome-scale CRISPR-mediated control of gene repression and activation. Cell. 2014; 159(3): 647–661, doi: 10.1016/j.cell.2014.09.029, indexed in Pubmed: 25307932.
24. Kwon DY, Zhao YT, Lamonica JM, et al. Locus-specific histone deacetylation using a synthetic CRISPR-Cas9-based HDAC. Nat Commun. 2017; 8: 15315, doi: 10.1038/ncomms15315, indexed in Pubmed: 28497787.
25. Pulecio J, Verma N, Mejía-Ramírez E, et al. CRISPR/Cas9-based engineering of the epigenome. Cell Stem Cell. 2017; 21(4): 431–447, doi: 10.1016/j.stem.2017.09.006, indexed in Pubmed: 28985525.
26. Gaudelli NM, Komor AC, Rees HA, et al. Programmable base editing of A•T to G•C in genomic DNA without DNA cleavage. Nature. 2017; 551(7681): 464–471, doi: 10.1038/nature24644, indexed in Pubmed: 29160308.
27. Zhou GS, Su ZY, Cai YuR, et al. Different effects of nanophase and conventional hydroxyapatite thin films on attachment, proliferation and osteogenic differentiation of bone marrow derived mesenchymal stem cells. Biomed Mater Eng. 2007; 17(6): 387–395, indexed in Pubmed: 18032820.
28. Wang Yu, Wang S, Chen W, et al. CRISPR-Cas9 and CRISPR-assisted cytidine deaminase enable precise and efficient genome editing in Klebsiella pneumoniae. Appl Environ Microbiol. 2018; 84(23), doi: 10.1128/AEM.01834-18, indexed in Pubmed: 30217854.
29. Zhao Y, Tian J, Zheng G, et al. Multiplex genome editing using a dCas9-cytidine deaminase fusion in Streptomyces. Sci China Life Sci. 2019; 63(7): 1053–1062, doi: 10.1007/s11427-019-1559-y.
30. Gu T, Zhao S, Pi Y, et al. Highly efficient base editing in Staphylococcus aureus using an engineered CRISPR RNA-guided cytidine deaminase. Chemical Science. 2018; 9(12): 3248–3253, doi: 10.1039/c8sc00637g.
31. Zhang He, Pan H, Zhou C, et al. Simultaneous zygotic inactivation of multiple genes in mouse through CRISPR/Cas9-mediated base editing. Development. 2018; 145(20), doi: 10.1242/dev.168906, indexed in Pubmed: 30275281.
32. Li Q, Li Y, Yang S, et al. CRISPR-Cas9-mediated base-editing screening in mice identifies DND1 amino acids that are critical for primordial germ cell development. Nat Cell Biol. 2018; 20(11): 1315–1325, doi: 10.1038/s41556-018-0202-4, indexed in Pubmed: 30275529.
33. Yuan J, Ma Y, Huang T, et al. Genetic modulation of RNA splicing with a CRISPR-guided cytidine deaminase. Mol Cell. 2018; 72(2): 380–394.e7, doi: 10.1016/j.molcel.2018.09.002, indexed in Pubmed: 30293782.
34. Chiang TWW, le Sage C, Larrieu D, et al. CRISPR-Cas9(-D10A) nickase-based genotypic and phenotypic screening to enhance genome editing. Sci Rep. 2016; 6: 24356, doi: 10.1038/srep24356, indexed in Pubmed: 27079678.
35. Rysenkova KD, Semina EV, Karagyaur MN, et al. CRISPR/Cas9 nickase mediated targeting of urokinase receptor gene inhibits neuroblastoma cell proliferation. Oncotarget. 2018; 9(50): 29414–29430, doi: 10.18632/oncotarget.25647, indexed in Pubmed: 30034627.
36. Dong De, Ren K, Qiu X, et al. The crystal structure of Cpf1 in complex with CRISPR RNA. Nature. 2016; 532(7600): 522––526, doi: 10.1038/nature17944, indexed in Pubmed: 27096363.
37. Nishimasu H, Ran FA, Hsu PD, et al. Crystal structure of Cas9 in complex with guide RNA and target DNA. Cell. 2014; 156(5): 935–949, doi: 10.1016/j.cell.2014.02.001, indexed in Pubmed: 24529477.
38. Safari F, Zare K, Negahdaripour M, et al. CRISPR Cpf1 proteins: structure, function and implications for genome editing. Cell Biosci. 2019; 9: 36, doi: 10.1186/s13578-019-0298-7, indexed in Pubmed: 31086658.
39. Teng F, Li J, Cui T, et al. Enhanced mammalian genome editing by new Cas12a orthologs with optimized crRNA scaffolds. Genome Biol. 2019; 20(1): 15, doi: 10.1186/s13059-019-1620-8, indexed in Pubmed: 30717767.
40. Strecker J, Jones S, Koopal B, et al. Engineering of CRISPR-Cas12b for human genome editing. Nat Commun. 2019; 10(1): 212, doi: 10.1038/s41467-018-08224-4, indexed in Pubmed: 30670702.
41. Choi J, Bae T, Byambasuren N, et al. CRISPR-Cf1 activation of endogenous BMP4 gene for osteogenic differentiation of umbilical cord-derived mesenchymal stem cells. Mol Ther Methods Clin Dev. 2020(17): 309–316, doi: 10.1016/j.omtm.2019.12.010, indexed in Pubmed: 32021879.
42. Świat MA, Dashko S, den Ri, et al. Fn Cpf1: a novel and efficient genome editing tool for Saccharomyces cerevisiae. Nucleic Acids Res. 2017; 45(21): 12585–98, doi: 10.1093/nar/gkx1007, indexed in Pubmed: 29106617.
43. Zetsche B, Heidenreich M, Mohanraju P, et al. Multiplex gene editing by CRISPR-Cpf1 using a single crRNA array. Nat Biotechnol. 2017; 35(1): 31–34, doi: 10.1038/nbt.3737, indexed in Pubmed: 27918548.
44. Yang Z, Edwards H, Xu P. CRISPR-Cas12a/Cpf1-assisted precise, efficient and multiplexed genome-editing in . Metab Eng Commun. 2020; 10: e00112, doi: 10.1016/j.mec.2019.e00112, indexed in Pubmed: 31867213.
45. Broughton JP, Deng X, Yu G, et al. CRISPR-Cas12-based detection of SARS-CoV-2. Nat Biotechnol. 2020; 38(7): 870–874, doi: 10.1038/s41587-020-0513-4, indexed in Pubmed: 32300245.
46. Liu J-J, Orlova N, Oakes BL, et al. CRISPR-CasX is an RNA-dominated enzyme active for human genome editing. Nature. 2019; 566(7743): 218, doi: 10.1038/s41586-019-0908-x, indexed in Pubmed: 30718774.

47. Yan WX, Hunnewell P, Alfonse LE, et al. Functionally diverse type V CRISPR-Cas systems. Science. 2019; 363(6422): 88–91, doi: 10.1126/science.aav7271, indexed in Pubmed: 30523077.
48. Karvelis T, Bigelyte G, Young JK, et al. et al.. PAM recognition by miniature CRISPR-Cas14 triggers programmable double-stranded DNA cleavage. Nucleic Acids Res. 2020; 48(9): 516–5023, doi: 10.1093/nar/gkaa208, indexed in Pubmed: 32246713.
49. Strecker J, Ladha A, Makarova KS, et al. RNA-guided DNA insertion with CRISPR-associated transposases. Science. 2019; 365(6448): 48–53, doi: 10.1126/science.aax9181, indexed in Pubmed: 31171706.
50. Shmakov S, Abudayyeh OO, Makarova KS, et al. Discovery and functional characterization of diverse class 2 CRISPR-Cas Systems. Mol Cell. 2015; 60(3): 385–397, doi: 10.1016/j.molcel.2015.10.008, indexed in Pubmed: 26593719.
51. Abudayyeh OO, Gootenberg JS, Konermann S, et al. C2c2 is a single-component programmable RNA-guided RNA-targeting CRISPR effector. Science. 2016; 353(6299): aaf5573, doi: 10.1126/science.aaf5573, indexed in Pubmed: 27256883.
52. Smargon AA, Cox DBT, Pyzocha NK, et al. Cas13b Is a Type VI-B CRISPR-associated RNA-guided rnase differentially regulated by accessory proteins Csx27 and Csx28. Mol Cell. 2017; 65(4): 618–630.e7, doi: 10.1016/j.molcel.2016.12.023, indexed in Pubmed: 28065598.
53. Gootenberg JS, Abudayyeh OO, Lee JW, et al. Nucleic acid detection with CRISPR-Cas13a/C2c2. Science. 2017; 356(6336): 438–442, doi: 10.1126/science.aam9321, indexed in Pubmed: 28408723.
54. Yang LZ, Wang Y, Li SQ, et al. Dynamic imaging of RNA in living cells by CRISPR-Cas13 systems. Mol Cell. 2019; 76(6): 981–997.e7, doi: 10.1016/j.molcel.2019.10.024, indexed in Pubmed: 31757757.
55. Kaminski MM, Alcantar MA, Lape IT, et al. A CRISPR-based assay for the detection of opportunistic infections post-transplantation and for the monitoring of transplant rejection. Nat Biomed Eng. 2020; 4(6): 601–609, doi: 10.1038/s41551-020-0546-5, indexed in Pubmed: 32284553.
56. Rees HA, Liu DR, Rees HA, et al. Base editing: precision chemistry on the genome and transcriptome of living cells. Nat Rev Genet. 2018; 19(12): 770–788, doi: 10.1038/s41576-018-0059-1, indexed in Pubmed: 30323312.
57. Abudayyeh OO, Gootenberg JS, Essletzbichler P, et al. RNA targeting with CRISPR-Cas13. Nature. 2017; 550(7675): 280––284, doi: 10.1038/nature24049, indexed in Pubmed: 28976959.
58. Abudayyeh OO, Gootenberg JS, Franklin B, et al. A cytosine deaminase for programmable single-base RNA editing. Science. 2019; 365(6451): 382–386, doi: 10.1126/science.aax7063, indexed in Pubmed: 31296651.
59. Fry LE, Peddle CF, Barnard AR, et al. RNA editing as a therapeutic approach for retinal gene therapy requiring long coding sequences. Int J Mol Sci. 2020; 21(3), doi: 10.3390/ijms21030777, indexed in Pubmed: 31991730.
60. Yan WX, Chong S, Zhang H, et al. Cas13d Is a compact RNA-targeting type VI CRISPR effector positively modulated by a WYL-domain-containing accessory protein. Mol Cell. 2018; 70(2): 327–339.e5, doi: 10.1016/j.molcel.2018.02.028, indexed in Pubmed: 29551514.
61. Abbott TR, Dhamdhere G, Liu Y, et al. Development of CRISPR as an antiviral strategy to combat SARS-CoV-2 and influenza. Cell. 2020; 181(4): 865–876.e12, doi: 10.1016/j.cell.2020.04.020, indexed in Pubmed: 32353252.
62. Inui M, Miyado M, Igarashi M, et al. Rapid generation of mouse models with defined point mutations by the CRISPR/Cas9 system. Sci Rep. 2014; 4: 5396, doi: 10.1038/srep05396, indexed in Pubmed: 24953798.
63. Chen S, Sanjana NE, Zheng K, et al. Genome-wide CRISPR screen in a mouse model of tumor growth and metastasis. Cell. 2015; 160(6): 1246–60, doi: 10.1016/j.cell.2015.02.038, indexed in Pubmed: 25748654.
64. Egorova TV, Zotova ED, Reshetov DA, et al. CRISPR/Cas9-generated mouse model of Duchenne muscular dystrophy recapitulating a newly identified large 430 kb deletion in the human gene. Dis Model Mech. 2019; 12(4), doi: 10.1242/dmm.037655, indexed in Pubmed: 31028078.
65. Lee H, Yoon DaE, Kim K. Genome editing methods in animal models. Anim Cells Syst (Seoul). 2020; 24(1): 8–16, doi: 10.1080/19768354.2020.1726462, indexed in Pubmed: 32158611.
66. Mehravar M, Shirazi A, Nazari M, et al. Mosaicism in CRISPR/Cas9-mediated genome editing. Dev Biol. 2019; 445(2): 156–162, doi: 10.1016/j.ydbio.2018.10.008, indexed in Pubmed: 30359560.
67. Maddalo D, Manchado E, Concepcion CP, et al. In vivo engineering of oncogenic chromosomal rearrangements with the CRISPR/Cas9 system. Nature. 2014; 516(7531): 423–427, doi: 10.1038/nature13902, indexed in Pubmed: 25337876.
68. Wen L, Zhao C, Song J, et al. CRISPR/Cas9-mediated TERT disruption in cancer cells. Int J Mol Sci. 2020; 21(2), doi: 10.3390/ijms21020653, indexed in Pubmed: 31963842.
69. Xu M, Weng Q, Ji J. Applications and advances of CRISPR/Cas9 in animal cancer model. Brief Funct Genomics. 2020; 19(3): 235–241, doi: 10.1093/bfgp/elaa002, indexed in Pubmed: 32124927.
70. Reyes LM, Estrada JL, Wang ZYu, et al. Creating class I MHC-null pigs using guide RNA and the Cas9 endonuclease. J Immunol. 2014; 193(11): 5751–5757, doi: 10.4049/jimmunol.1402059, indexed in Pubmed: 25339675.
71. Sheets TP, Park CH, Park KE, et al. Somatic cell nuclear transfer followed by CRIPSR/Cas9 microinjection results in highly efficient genome editing in cloned pigs. Int J Mol Sci. 2016; 17(12), doi: 10.3390/ijms17122031, indexed in Pubmed: 27918485.
72. Gao Y, Wu H, Wang Y, et al. Single Cas9 nickase induced generation of NRAMP1 knockin cattle with reduced off-target effects. Genome Biol. 2017; 18(1): 13, doi: 10.1186/s13059-016-1144-4, indexed in Pubmed: 28143571.
73. Ni W, Qiao J, Hu S, et al. Efficient gene knockout in goats using CRISPR/Cas9 system. PLoS One. 2014; 9(9): e106718, doi: 10.1371/journal.pone.0106718, indexed in Pubmed: 25188313.
74. Bharati J, Punetha M, Kumar BS, et al. Genome editing in animals: an overview. Genomics and biotechnological advances in veterinary, poultry, and fisheries. 2020: 75–104, doi: 10.1016/b978-0-12-816352-8.00003-5.
75. Niu Y, Zhao X, Zhou J, et al. Efficient generation of goats with defined point mutation (I397V) in GDF9 through CRISPR/Cas9. Reprod Fertil Dev. 2018; 30(2): 307–312, doi: 10.1071/RD17068, indexed in Pubmed: 28692815.
76. Li X, Hao F, Hu X, et al. Generation of Tβ4 knock-in Cashmere goat using CRISPR/Cas9. Int J Biol Sci. 2019; 15(8): 1743–1754, doi: 10.7150/ijbs.34820, indexed in Pubmed: 31360116.
77. Crispo M, Mulet AP, Tesson L, et al. Efficient generation of myostatin knock-out sheep using CRISPR/Cas9 technology and microinjection into zygotes. PLoS One. 2015; 10(8): e0136690, doi: 10.1371/journal.pone.0136690, indexed in Pubmed: 26305800.
78. Niu Y, Jin M, Li Y, et al. Biallelic β-carotene oxygenase 2 knockout results in yellow fat in sheep via CRISPR/Cas9.

Anim Genet. 2017; 48(2): 242–244, doi: 10.1111/age.12515, indexed in Pubmed: 27862083.
79. Kalds P, Zhou S, Cai B, et al. Sheep and goat genome engineering: from random transgenesis to the CRISPR era. Front Genet. 2019; 10: 750, doi: 10.3389/fgene.2019.00750, indexed in Pubmed: 31552084.
80. Eaton SL, Proudfoot C, Lillico SG, et al. CRISPR/Cas9 mediated generation of an ovine model for infantile neuronal ceroid lipofuscinosis (CLN1 disease). Sci Rep. 2019; 9(1): 9891, doi: 10.1038/s41598-019-45859-9, indexed in Pubmed: 31289301.
81. Hoban MD, Cost GJ, Mendel MC, et al. Correction of the sickle cell disease mutation in human hematopoietic stem/progenitor cells. Blood. 2015; 125(17): 2597–2604, doi: 10.1182/blood-2014-12-615948, indexed in Pubmed: 25733580.
82. Wang C, Jin H, Gao D, et al. A CRISPR screen identifies CDK7 as a therapeutic target in hepatocellular carcinoma. Cell Res. 2018; 28(6): 690–692, doi: 10.1038/s41422-018-0020-z, indexed in Pubmed: 29507396.
83. Chai N, Haney MS, Couthouis J, et al. Genome-wide synthetic lethal CRISPR screen identifies FIS1 as a genetic interactor of ALS-linked C9ORF72. Brain Res. 2020; 1728: 146601, doi: 10.1016/j.brainres.2019.146601, indexed in Pubmed: 31843624.
84. Acharya S, Maiti S, Chakraborty D. CRISPR-Cas9 for therapy: the challenges and ways to overcome them. Genome Engineering via CRISPR-Cas9 System. 2020: 101–110, doi: 10.1016/b978-0-12-818140-9.00009-x.
85. Xu L, Wang J, Liu Y, et al. CRISPR-Edited Stem Cells in a Patient with HIV and acute lymphocytic leukemia. N Engl J Med. 2019; 381(13): 1240–1247, doi: 10.1056/NEJMoa1817426, indexed in Pubmed: 31509667.
86. Maeder ML, Stefanidakis M, Wilson CJ, et al. Development of a gene-editing approach to restore vision loss in Leber congenital amaurosis type 10. Nat Med. 2019; 25(2): 229–233, doi: 10.1038/s41591-018-0327-9, indexed in Pubmed: 30664785.
87. Soppe JA, Lebbink RJ. Antiviral Goes Viral: Harnessing CRISPR/Cas9 to combat viruses in humans. Trends Microbiol. 2017; 25(10): 833–850, doi: 10.1016/j.tim.2017.04.005, indexed in Pubmed: 28522157.
88. Sasano Yu, Nagasawa K, Kaboli S, et al. CRISPR-PCS: a powerful new approach to inducing multiple chromosome splitting in Saccharomyces cerevisiae. Sci Rep. 2016; 6: 30278, doi: 10.1038/srep30278, indexed in Pubmed: 27530680.
89. Easmin F, Sasano Yu, Kimura S, et al. CRISPR-PCD and CRISPR-PCRep: Two novel technologies for simultaneous multiple segmental chromosomal deletion/replacement in Saccharomyces cerevisiae. J Biosci Bioeng. 2020; 129(2): 129–139, doi: 10.1016/j.jbiosc.2019.08.004, indexed in Pubmed: 31585858.
90. Wang T, Wei JJ, Sabatini DM, et al. Genetic screens in human cells using the CRISPR-Cas9 system. Science. 2014; 343(6166): 80–84, doi: 10.1126/science.1246981, indexed in Pubmed: 24336569.
91. Shalem O, Sanjana NE, Hartenian E, et al. Genome-scale CRISPR-Cas9 knockout screening in human cells. Science. 2014; 343(6166): 84–87, doi: 10.1126/science.1247005, indexed in Pubmed: 24336571.
92. Joung J, Konermann S, Gootenberg JS, et al. Genome-scale CRISPR-Cas9 knockout and transcriptional activation screening. Nat Protoc. 2017; 12(4): 828–863, doi: 10.1038/nprot.2017.016, indexed in Pubmed: 28333914.
93. Luo Ji. CRISPR/Cas9: From genome engineering to cancer drug discovery. Trends Cancer. 2016; 2(6): 313–324, doi: 10.1016/j.trecan.2016.05.001, indexed in Pubmed: 28603775.
94. Maeder ML, Linder SJ, Cascio VM, et al. CRISPR RNA-guided activation of endogenous human genes. Nat Methods. 2013; 10(10): 977–979, doi: 10.1038/nmeth.2598, indexed in Pubmed: 23892898.
95. Smurnyy Y, Cai Mi, Wu H, et al. DNA sequencing and CRISPR-Cas9 gene editing for target validation in mammalian cells. Nat Chem Biol. 2014; 10(8): 623–625, doi: 10.1038/nchembio.1550, indexed in Pubmed: 24929529.
96. Zhu S, Li W, Liu J, et al. Genome-scale deletion screening of human long non-coding RNAs using a paired-guide RNA CRISPR-Cas9 library. Nat Biotechnol. 2016; 34(12): 1279–1286, doi: 10.1038/nbt.3715, indexed in Pubmed: 27798563.
97. Shi J, Wang E, Milazzo JP, et al. Discovery of cancer drug targets by CRISPR-Cas9 screening of protein domains. Nat Biotechnol. 2015; 33(6): 661–667, doi: 10.1038/nbt.3235, indexed in Pubmed: 25961408.
98. Nelles DA, Fang MY, O'Connell MR, et al. Programmable RNA tracking in live cells with CRISPR/Cas9. Cell. 2016; 165(2): 488–496, doi: 10.1016/j.cell.2016.02.054, indexed in Pubmed: 26997482.
99. Gu Bo, Swigut T, Spencley A, et al. Transcription-coupled changes in nuclear mobility of mammalian cis-regulatory elements. Science. 2018; 359(6379): 1050–1055, doi: 10.1126/science.aao3136, indexed in Pubmed: 29371426.
100. Duan J, Lu G, Hong Yu, et al. Live imaging and tracking of genome regions in CRISPR/dCas9 knock-in mice. Genome Biol. 2018; 19(1): 192, doi: 10.1186/s13059-018-1530-1, indexed in Pubmed: 30409154.
101. Wang H, Nakamura M, Abbott TR, et al. CRISPR-mediated live imaging of genome editing and transcription. Science. 2019; 365(6459): 1301–1305, doi: 10.1126/science.aax7852, indexed in Pubmed: 31488703.
102. Maus MV, Grupp SA, Porter DL, et al. Antibody-modified T cells: CARs take the front seat for hematologic malignancies. Blood. 2014; 123(17): 2625–2635, doi: 10.1182/blood-2013-11-492231, indexed in Pubmed: 24578504.
103. Cyranoski D. CRISPR gene-editing tested in a person for the first time. Nature. 2016; 539(7630): 479, doi: 10.1038/nature.2016.20988, indexed in Pubmed: 27882996.
104. Choi BD, Yu X, Castano AP, et al. CRISPR-Cas9 disruption of PD-1 enhances activity of universal EGFRvIII CAR T cells in a preclinical model of human glioblastoma. J Immunother Cancer. 2019; 7(1): 304, doi: 10.1186/s40425-019-0806-7, indexed in Pubmed: 31727131.
105. Hsu MN, Chang YH, Truong VuA, et al. CRISPR technologies for stem cell engineering and regenerative medicine. Biotechnol Adv. 2019; 37(8): 107447, doi: 10.1016/j.biotechadv.2019.107447, indexed in Pubmed: 31513841.
106. Chen G, Cheng Du, Chen B. [Development of CRISPR technology and its application in bone and cartilage tissue engineering]. Nan Fang Yi Ke Da Xue Xue Bao. 2019; 39(12): 1515–1520, doi: 10.12122/j.issn.1673-4254.2019.12.19, indexed in Pubmed: 31907146.
107. Ali Q, Malik S, Malik A, et al. Role of modern technologies in tissue engineering. Arch Neurosci. 2020; 7(1), doi: 10.5812/ans.90394.
108. Aghamiri S, Ghavidel AA, Zandsalimi F, et al. Nanoparticles-mediated CRISPR/Cas9 delivery: Applications in cancer treatment and detection. J Drug Deliv Sci Technol.; 2020: 101533.
109. Baylis F, McLeod M. First-in-human Phase 1 CRISPR gene editing cancer trials: are we ready? Curr Gene Ther. 2017; 17(4): 309–319, doi: 10.2174/1566523217666171121165935, indexed in Pubmed: 29173170.
110. González-Romero E, Martínez-Valiente C, García-Ruiz C, et al. CRISPR to fix bad blood: a new tool in basic and

clinical hematology. Haematologica. 2019; 104(5): 881–893, doi: 10.3324/haematol.2018.211359, indexed in Pubmed: 30923099.
111. Xiao Q, Guo D, Chen S. Application of CRISPR/Cas9-based gene editing in HIV-1/AIDS therapy. Front Cell Infect Microbiol. 2019; 9: 69, doi: 10.3389/fcimb.2019.00069, indexed in Pubmed: 30968001.
112. Kostyusheva A, Brezgin S, Babin Y, et al. CRISPR-Cas Systems for Diagnosing Infectious Diseases, doi: 10.20944/preprints202002.0007.v1.
113. Pittermann E, Lachmann N, MacLean G, et al. Gene correction of reversed Kostmann disease phenotype in patient-specific induced pluripotent stem cells. Blood Adv. 2017; 1(14): 903–914, doi: 10.1182/bloodadvances.2016003798, indexed in Pubmed: 29296734.
114. Charlesworth CT, Deshpande PS, Dever DP, et al. Identification of preexisting adaptive immunity to Cas9 proteins in humans. Nat Med. 2019; 25(2): 249–254, doi: 10.1038/s41591-018-0326-x, indexed in Pubmed: 30692695.
115. Zhang XH, Tee LY, Wang XG, et al. Off-target Effects in CRISPR/Cas9-mediated genome engineering. Mol Ther Nucleic Acids. 2015; 4: e264, doi: 10.1038/mtna.2015.37, indexed in Pubmed: 26575098.
116. Lino CA, Harper JC, Carney JP, et al. Delivering CRISPR: a review of the challenges and approaches. Drug Deliv. 2018; 25(1): 1234–1257, doi: 10.1080/10717544.2018.1474964, indexed in Pubmed: 29801422.
117. Rahimi H, Salehiabar M, Charmi J, et al. Harnessing nanoparticles for the efficient delivery of the CRISPR/Cas9 system. Nano Today. 2020; 34: 100895, doi: 10.1016/j.nantod.2020.100895.

Submitted: 22 July, 2020
Accepted after reviews: 17 September, 2020
Available as AoP: 24 September, 2020

FOLIA HISTOCHEMICA ET CYTOBIOLOGICA
Vol. 58, No. 3, 2020
pp. 174–181

ORIGINAL PAPER

VIA MEDICA

A knockdown of the herpes simplex virus type-1 gene in all-in-one CRISPR vectors

Nastaran Khodadad[1, 2*], Mona Fani[1, 3*], Saleh Jamehdor[4], Rahil Nahidsamiei[1, 2], Manoochehr Makvandi[1, 2], Saeed Kaboli[5], Ali Teimoori[1, 2, 6], Jose Thekkiniath[7, 8]

[1]Cancer Research Center, Ahvaz Jundishapur University of Medical Sciences, Ahvaz, Iran
[2]Department of Virology, Ahvaz Jundishapur University of Medical Sciences, Ahvaz, Iran
[3]Department of Pathobiology and Laboratory Sciences, School of Medicine, North Khorasan University of Medical Sciences, Bojnurd, Iran
[4]Department of Biology, Faculty of Sciences, University of Sistan and Baluchestan, Zahedan, Iran
[5]Department of Medical Biotechnology and Cancer Gene Therapy Research Center, School of Medicine, Zanjan University of Medical Sciences, Zanjan, Iran
[6]Department of Virology, Faculty of Medicine, Hamadan University of Medical Sciences, Hamadan, Iran
[7]Fuller Laboratories, Fullerton, CA, USA
[8]Department of Internal Medicine, Section of Infectious Diseases, Yale School of Medicine, New Haven, CT, USA

*Nastaran Khodadad and Mona Fani contributed equally to this work.

Abstract

Introduction. Herpes simplex virus type 1 (HSV-1) is a virus that causes serious human disease and establishes a long-term latent infection. The latent form of this virus has shown to be resistant to antiviral drugs. Clustered Regularly Interspace Short Palindromic Repeats (CRISPR), is an important tool in genome engineering and composed of guide RNA (gRNA) and Cas9 nuclease that makes an RNA-protein complex to digest exclusive target sequences implementation of gRNA. Moreover, CRISPR-Cas9 system effectively suppresses HSV-1 infection by knockout of some viral genes.

Materials and methods. To survey the efficacy of Cas9 system on HSV-1 genome destruction, we designed several guide RNAs (gRNAs) that all packaged in one vector. Additionally, we performed a one-step restriction using *BamHI* and *Esp3I* enzymes.

Results. CRISPR/Cas9 system targeted against the gD gene of HSV-1 was transfected into HEK-AD cells that showed a significant reduction of HSV-1 infection by plaque assay and real-time PCR.

Conclusion. The *pCas-Guide-EF1a-GFP CRISPR* vector can create a fast and efficient method for gRNA cloning by restriction enzymes (*Esp3I* (*BsmBI*) and *BamHI*). Therefore, the CRISPR/Cas9 system may be utilized for the screening of genes critical for the HSV-1 infection and developing new strategies for targeted therapy of viral infections caused by HSV-1. *(Folia Histochemica et Cytobiologica 2020, Vol. 58, No. 3, 174–181)*

Key words: CRISPR; Cas9; gRNA; genome editing; HSV-1; HEK-AD cells

Correspondence address: Ali Teimoori,
Department of Virology, Faculty of Medicine,
Hamadan University of Medical Sciences, Hamadan, Iran;
phone: +98-9125116011
e-mail: teimooriali1982@gmail.com

Introduction

Herpes simplex virus type 1 (HSV-1) is a very contagious and lifetime infectious pathogen and remains an important problem worldwide [1, 2]. Herpes viruses are known to be involved in lytic infection in which viruses lyse their host cells or latent infection in which viruses remain silent within the host cells [1, 3].

In recent years, several studies have focused on DNA editing [4, 5] such as zinc-finger nucleases (ZFNs), transcription activator-like effector nucleases (TALENs) system. However, Clustered Regularly Interspace Short Palindromic Repeats (CRISPR) has been considered as an important acceptable system for genome editing [6]. CRISPR/Cas9 system which originated from a wide range of bacteria and archaea can be an adaptive bacterial immune system that mainly targets genome of bacterial invasive phages [7].

CRISPR-associated (Cas) genes are located adjacent to a CRISPR locus [8]. The CRISPR-Cas system is clustered into three major types (I, II, III) that CRISPR associated protein 9 (Cas9) is the signature gene of type II and also, the most efficient genome editing tool [9].

The Cas9 system consists of two major components including an endonuclease protein which can produce a double-strand break in DNA and two RNA components including trans-activating crRNA (tracrRNA) and mature CRISPR RNA (crRNA) which are responsible for identifying a short DNA sequence; 5'-NGG-3'; called the protospacer adjacent motif (PAM). The crRNA/tracrRNA complex associated with Cas9 creates an active ribonucleoprotein (RNP) complex [10]. In this system, crRNA can conduct the Cas9 protein as an RNA-guided endonuclease. Briefly, the crRNA 5'-end (twenty nucleotides) can interact with Guanine nucleotide of the PAM on the non-complementary DNA strand to form RNA-DNA complementarity due to the interaction between DNA backbone 5' and a phosphate-lock loop in Cas9. As mentioned above, Cas9 protein as an endonuclease protein cleaves the recognized target site to create a double-strand break (DSB) [10]. To fix this break, there have been two cellular repair mechanisms identified, including Non-Homologous End Joining (NHEJ) which joins the damaged ends of chromosomes and needs little to no DNA sequence homology.

Another mechanism is Homology Directed Repair (HDR) that has high precision to repair the DSB with the pattern of a DNA strand. For example, in humans, the NHEJ system has a higher recovery rate than the HDR [6, 11, 12].

In the CRISPR system, gRNA and Cas9 are needed to knock out or in any gene. Although there are many vectors for the gRNAs, p-Cas-Guide-EF1a-GFP CRISPR vector Origene Technologies (Rockville, MD, USA) as an all-in-one vector has both Cas9 and gRNA. Additionally, the vector contains an enhanced green fluorescent protein (EGFP) gene that can detect transfected cells. The gRNA and Cas9 protein are also under the control of the U6 promoter. For the high efficiency of gRNA transcription, U6 is an excellent housekeeping promoter, which is transcribed by RNA polymerase III [13].

One of the advantages of this system is the high and continuous transcription gRNA and Cas9 by stable functional promoters in p-Cas-Guide-EF1a-GFP CRISPR Vector. To design DNA with high-efficiency expression by U6 promoter, guanine should be considered as the first transcribed nucleotide. In the previous studies, multi-vector systems were used to knock out or in any gene, which was costly and time-consuming. For solving this problem, we designed a single vector CRISPR system in the present study.

The objective of this study is to establish a novel method to clone gRNA in p-Cas-Guide-EF1a-GFP CRISPR Vector by using *Bsm*BI and *Bam*HI restriction enzymes. These enzymes have specific detection sites (*Bam*HI: 5-GGATCC-3 and *Bsm*BI: 5-CGTCTC (N1) -3, 3-GCAGAG (N5) -5) and also, gRNAs can be easily and quickly clone between two restrictions sites. Here, we used a one-step restriction digestion method using *Esp3I* and *BamHI* and the ligation reaction (defined as a construction procedure of one g-RNA expression vector). Additionally the main goal of designing this new system is to perform knockouts in the HSV-1 genome and study the function of essential and non-essential genes in the virus.

Materials and methods

Software selection. Designing an efficient and functional sgRNA which can accurately join to the target DNA is the first step in the CRISPR system. However, this proposed gRNA is restricted to avoid off-target sites. In this regard, there have been several software programs currently used, and are listed in Table 1.

CHOPCHOP is one of the most powerful tools used to design CRISPR/Cas9, CRISPR/Cpf1, and TALEN systems. This software supports many features in order to design genome editing systems and allows us to add the undefined genomes of organisms. A target can be mentioned in both the name of the gene and the sequence (FASTA format).

Table 1. Several online software for gRNA design. These software are usually designed and supported by universities and research centers

Software	CHOPCHOP	E-CRISP	Cas-OFFinder	Genetic perturbation platform web portal
PAM	Ability to choose PAM	NGG	Different PAM	NGG, NNGRR, TTTV and enAsCas12a
Cas	Cas9, Cas12 and Cas13	Cas9	Cas9, Cas12 and MAD7 nuclease	Cas9 and Cas12
Target genome	It includes a large number of creatures and the ability to add genomes that non-defined in the software	55 Organisms	It includes a large number of creatures and the ability to add genomes that non-defined in the software	Human Mouse Rat
On target scoring	Doench *et al.* 2014 [22] Doench *et al.* 2016 [23] Xu *et al.* 2015 [24] Moreno-Mateos *et al.* 2015 [25] Shen *et al.*, 2014 [26]	Xu *et al.*, 2015 [24] Doench *et al.*, 2014 [22]		Doench, Fusi *et al.* 2016 [23] Snson, *et al.* 2018 [27] Kim, *et al.* 2018 [28]
Off target scoring	Hsu *et al.*, 2013 [29]	S-score	Standalone command--line program [30]	Use on target scoring for off target and on target prediction
Scientific institute or university	Harvard	German Cancer Research Center	Seoul National University	Broad Institute
Web site	http://chopchop.cbu.uib.no	http://www.e-crisp.org/E-CRISP/ /designcrispr.html	http://www.rgenome.net/cas-designer/	https://portals.broadinstitute.org/gpp/public/analysis-tools/sgrna-design

For example, the gene name refers to the area which can be designed for the gRNA (coding region, promoter, selected exons, 3' or 5' UTR, and splice sites). Other advantages of this software include selecting the PAM sequence (for different CRISPR systems), calculating the efficiency score method, detecting off-targets in the genome, calculating the number of bases (which can be self-complementary), and choosing different gRNA backbones. Furthermore, to increase transcriptional efficiency, the promoter requires specific bases at transcription initiation. For example, for an optimal transcription by the T7 promoter, the two primary transcripts of the nucleotide should be GG and for the U6 promoter must be G. Also, this software can design the primers to amplify the area in which the indel mutation is created by the CRISPR system. This software can identify the restriction enzymes that are at one or more points within the replication region through the primers. In the current study, *Herpes simplex virus type 1 KOS strain* and human including US6 (glycoprotein D), UL39 (ribonucleotide reductase subunit 1), UL23 (Thymidine kinase), ICP34.5 and ASS1 (argininosuccinate synthase 1) were respectively selected and included into CHOPCHOP.

Cloning of gRNA. Next step, sgRNAs should be cloned in pCas-Guide-GFP vector from now on as pCas-Guides. For cloning into this vector, several nucleotides (5-*GATCG*NNNNNNNNNNNNNNNNNNN*G*-3 and 5-*AAAAC*NNNNNNNNNNNNNNNNNNN*C*-3) are added to two sgRNA target ends complementary to the target region, and were ordered in two separate strands. When two oligo strands are annealed together, pre-cut sticky end of *BamHI* and *BsmBI* was established. Table 2 shows the protocol for annealing two proposed strands.

pCas-Guides CRISPR vector was cut by *BamHI* and *BsmBI* and followed by DNA clean up (Favorgen, Taiwan). Moreover, this tool can show the molar ratio of insert: vector that of 5:1 was recommended in the current study. Ligation reaction of gRNAs into double digested *pCas-Guides*

Table 2. Oligo annealing protocol used in the study

PCR program for oligo annealing		Add and mix the material in a PCR tube
Temperature	Time	5 μl forward oligo (10 μM) 5 μl reverse oligo (10 μM) 40 μl DNase free water
95°C	5 min.	
90°C	30 sec.	
80°C	30 sec.	
70°C	30 sec.	
60°C	30 sec.	
50°C	30 sec	

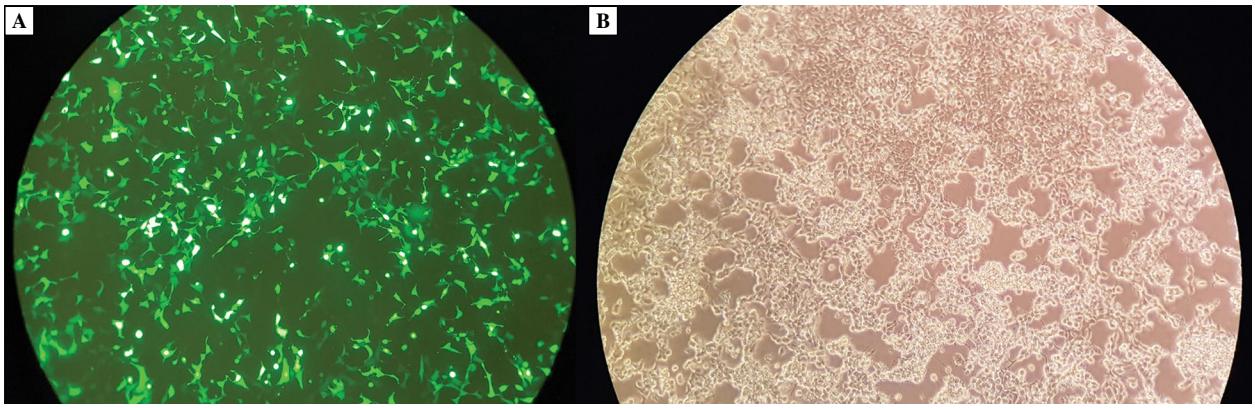

Figure 1. GFP expression of *pCas-guides* in HEK293-AD cells. **A.** Observation at 48 h post-transfected HEK293-AD cells. **B.** Control cells using an inverted fluorescent microscopy.

CRISPR vector was prepared in a 10 μl volume including 2 ng of gRNA, 150 ng of vector, 0.5 μl of T4 ligase, and 1 μl of 10× ligation buffer.
1 μL of 10× ligation buffer, 150 ng precut *pCas-Guide* vector (10 ng/μL), 5 ng annealed double-stranded oligo (diluted), 0.5 μL ligase (0.5 μL), and 6.5 μL dH_2o were mixed incubated for 2 hours at 22°C. Of this, 5 μL of the ligation mixture was added to competent cells.

Transfection of pCas-guide-Ef1-GFP. HEK293-AD, a derivative of the HEK293 cell line [14], was grown in a 24-well plate which contained Dulbecco's modified Eagle's medium (DMEM) (Gibco, Gaithersburg, MD, USA) supplemented with 10% fetal bovine serum (FBS) (Gibco, USA) and 100 IU/mL penicillin and 100 μg/mL streptomycin (Sigma-Aldrich, St. Louis, MO, USA) at 37°C in a humidified atmosphere containing 5% CO_2 for 48 hours. For transfection efficiency, *pCas-guides* were transfected using the *PolyFect* reagent (Qiagen, Germany). For each well, both DNA (1, 1.5, and 2 μg) and *PolyFect* (2, 4, and 6 μl) were diluted in DMEM to the final volume 100 μl. The complex solution was mixed and incubated for 15 min at room temperature, and then dropped into wells. After 5 hours, the supernatant was removed and fresh complete media was added into each well. At 24–48 hours post-transfection, expression of GFP reporter *pCas-guide* was examined by an inverted fluorescent microscope (Fig. 1) [15].

Virus production assay. HSV-1 genomic DNA in the supernatants from HSV-1 infected or transfected with gD gRNA was extracted by the DNA extraction kit according to the kit instructions (Favorgen, Taiwan). Relative quantitative real-time PCR for DNA of the virus was used and 2-ΔΔCt (CtHSV-1CtHSV-1 with gRNA treated) was applied.

The reaction contained 2 μL template, 1 μL ROX as a reference dye, 0.2 μM probe, 0.4 μM of each primer, 10 μL Qiagen Taqman Master Mix (2×), and 5 μL water. The amplification was carried out as follows: initial incubation at 95°C for 2 min, 35 cycles of 10 s at 95°C, and 15 s at 60°C. The standard curve was drawn using ten-fold serial dilutions of HSV-1 DNA for determining the reaction efficiency. Viral DNA was amplified using a QuantiNova Probe PCR Mix kit (Qiagen, Germany). The HSV-1 primers and probe (Metabion, GmbH, Germany) were designed to target the UL27 gene which encodes the glycoprotein B (gB) of the virus. For checking primer specificity, NCBI primer BLAST was used. The sequence and characteristics of the used oligonucleotides in this study are shown in Table 3.

To determine the virus titer, a plaque assay was performed. Vero cell monolayers in a six-well plate were infected with a serial ten-fold dilution of supernatants collected from HSV-1 infected or gRNA transfected HEK293-AD cells. After incubation for 1 hour at 37° C, 5% CO_2, the inoculum was replaced by 2X DMEM with agarose 1.5% in equal volume as an overlay. Nearly 48h later, cells were fixed in 4% formaldehyde and stained with 1% crystal violet (in 20% ethanol). The titer of a virus stock can be measured in plaque-forming units which is calculated by the number of plaques multiplied by dilution factor and the virus amount.

Statistical analysis. Data from the study are described as means or means ± SD. Effects were evaluated by one-way ANOVA and Turkey's *post hoc* test.

Results

In the current study, g-RNA was selected based on the updated CHOPCHOP software [16], along with top rank, high cutting efficiency, minimum self-complementary, and least off-target. Furthermore, among selected g-RNAs, the low cutting efficiency g-RNA

Table 3. The sequence and characteristics of the used oligonucleotides

Oligonucleotide	Sequence	Region in gB gene	Amplicon Size
Probe	5'-6-FAM-ATCACCACCGTCAGCACCTTCATCG-B00HQ-1-3'	702-726	96 bp
Sense primer	5'-TCCAGCATGGTGATGTTGAG-3'	680-996	
Antisense primer	5'-CGTGTACTTCGAGGAGTACG-3'	756-775	

Table 4. The gRNA sequences used in the current study

g-RNA	g-RNA Forward (5'-3')	g-RNA Reverse (5'-3')
UL39.1	GATCG***GTTGTTCCTGTCGCGACACA***G	AAAAC***TGTGTCGCGACAGGAACAAC***C
TK.1	GATCG***GGCTGCTTGCCAATACGGTG***G	AAAAC***CACCGTATTGGCAAGCAGCC***C
ICP34.5	GATCG***GTCGTCGTCGGACGCGGACT***G	AAAAC***AGTCCGCGTCCGACGACGAC***C
ASS1.1	GATCG***ACGGCGCCACAGGAAAGGTG***G	AAAAC***CACCTTTCCTGTGGCGCCGT***C
gD	GATCG***GCTCCTAAACGCACCGTCGG***G	AAAAC***CCGACGGTGCGTTTAGGAGC***C

(< 30) with each rank and off-target was eliminated. Two or three gRNAs were selected over a span of 100 to 200 nucleotides of a target gene and primers were designed up and downstream of the target gRNA position to identify any deletion or insertion. One candidate gRNA is represented in Table 4.

The used methods in this protocol were based on the creation of an single gRNA expression vectors. In fact, these vectors can be created by ligation of pre-digesting the vector backbone (Fig. 2) and annealing short oligonucleotides in a single reaction. Successful cloning using these protocols resulted in significantly more number of clones with an appropriate insert DNA as compared to no-insert control.

Clones were screened by colony PCR and confirmed by Sanger sequencing. To perform colony PCR, the forward primer was designed based on upstream of g-RNA site, and reverse g-RNA was used as a reverse primer. The forward primer is used as a common primer. Finally, the sequencing of the clones was performed to eliminate of false-positive PCR results (Fig. 3).

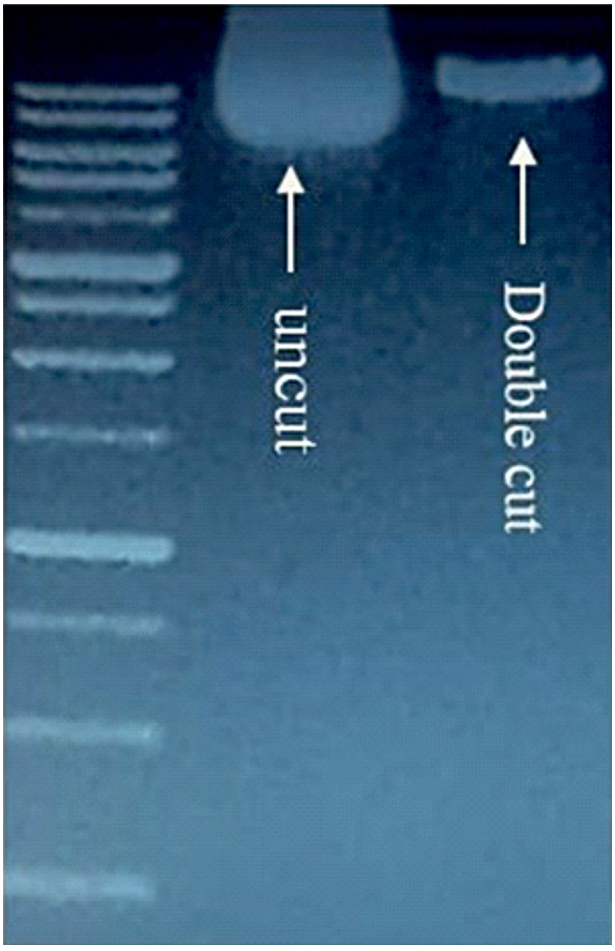

Figure 2. The digestion of a pCas-guides expression vector. 1% agarose gel was used. Lane 1: uncut pCas-guide EF1-GFP. Lane 2: pCas-guide cut with *Bam*HI and *Bsm*BI.

Virus production assay

At first, we selected the HSV-1 KOS strain for evaluating whether the HSV-1 genome could be effectively cleaved via the CRISPR/Cas9 system. Among designed gRNAs, we selected gD gRNA to survey effect of the CRISPR-Cas9 system on the HSV-1 replication. Twenty-four hours after transfection, HEK-AD cells were infected with HSV-1 at different multiplicities of infections (MOIs), and when cyto-

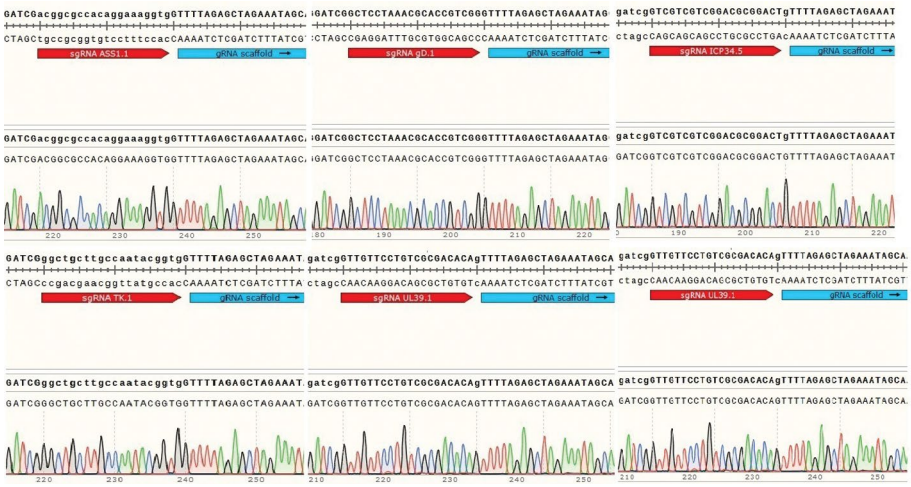

Figure 3. Sequencing of a pCas-guides g-RNA expression vector. Chromatograms corresponding to cloned g-RNA.

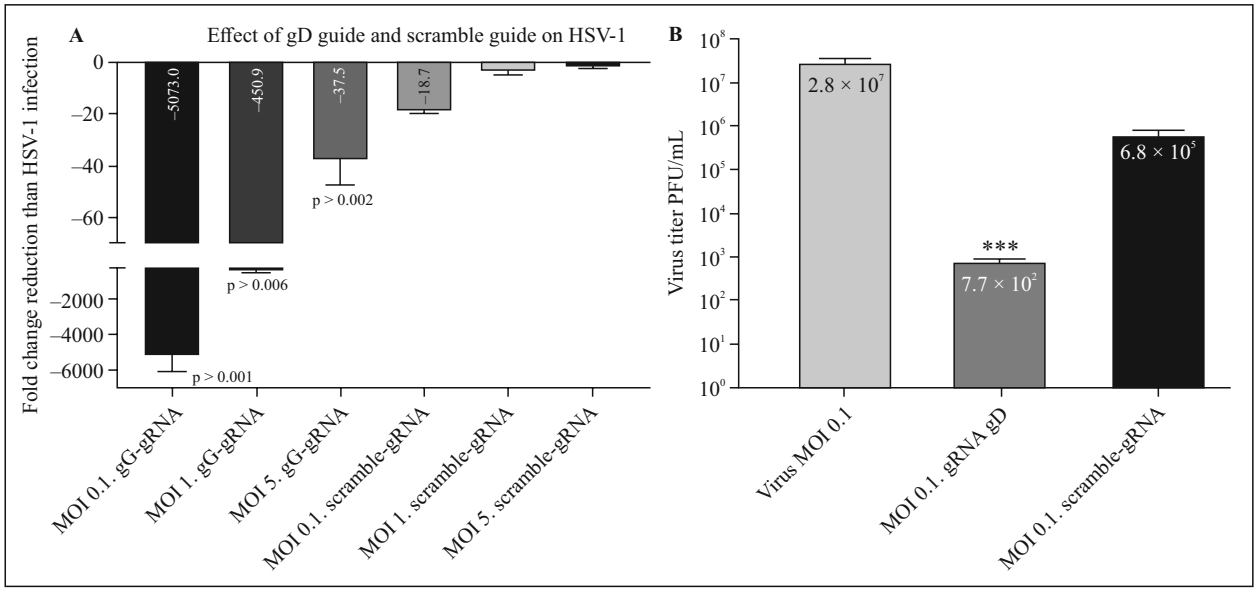

Figure. 4. The effect of gD guide on HSV-1 replication. **A**: by plaque assay. **B**: by Real Time PCR test (PFU: plaque-forming unit).

pathic effects were seen, the cells were harvested. Cytopathic effects were identified based on changes in the morphology of virus-infected HEK-AD cells after 24–48 hours. After performing a plaque assay, the CRISPR/Cas9 mediated reduction in HSV-1 infection was observed at MOI 0.1. The reduction of viral titer in this assay was computed 7.7×10^2 PFU/mL (plaque-forming unit/mL) that there was a statistically significant difference. Next, we checked the efficiency of the CRISPR/Cas9 system on the effect of viral infectious dose using real-time PCR. We found an increase of CRISPR-Cas9 (gD-gRNA) efficiency with decreasing viral infectious dose from MOI 5, 1, and 0.1 PFU/cell (Fig. 4A). In this method as in plaque assay, the decrease of HSV-1 infection was detected that there was a statistically significant difference.

The results showed that the gD gene was successfully knocked out at the infected HSV-1 into HEK-AD cells (Fig. 4B). Overall, our results showed that the CRISPR/Cas9-mediated cleavage was efficient.

Discussion

Recently, CRISPR/Cas9 technology has been used as a powerful tool in gene therapy, genetics, and genom-

ics. In this study, we used the *pCas-Guide-EF1a-GFP CRISPR* vector to create a fast and efficient method for gD gRNA cloning by restriction enzymes (*Esp3I* (*BsmBI*) and *BamHI*). We demonstrated that the CRISPR/Cas9 system could efficiently knockdown the gD locus, resulting in different sequence mutations and disrupted gD expression.

Karpof *et al.* determined that the CRISPR/Cas9 system targeted against UL52 and UL29 genes efficiently suppressed HSV-1 reproduction in Vero cells [17]. In recent years, the CRISPR/Cas9 technology has attracted much attention due to the simplicity and cost-effectiveness of gRNA design. Nevertheless, high-throughput genomic research by this method has increased the target of many viral and cellular genes with a single vector [18].

The gD is an HSV-1 envelope glycoprotein that binds to several cell receptor including HVEM, NECTIN1, and 3-O-sulfated heparan sulfate [17–19]. Mutations in gD can reduce physical interactions with some of the HSV entry receptors and also prevent cell fusion with its receptors. gD acts to block the fusion of lysosomes with the endocytic vesicles [20]. Nevertheless, it has been described that the deletion of gD produces a marked reduction in HSV-1 secondary envelopment [21].

The expression of one g-RNA is gained using oligonucleotides comprising of the forward and reverse g-RNA target sequences (each of them has 20 nt) contain extra bases (gatcg) at the 5' end of the forward sequence as a *Bam*HI overhang and 'G' at its 3' end.

The pCas-guide contains promoter RNA pol III, including U6 and H1 which have been used to express these small RNAs as gRNAs. It is believed that U6 promoter transcription starts at the +1 position, with G as the preferred initiation nucleotide [19]. To increase the efficiency of transcription site, 'aaaac' was added to the 5' end of reverse g-RNA as an *Esp3*I (*Bsm*BI) cleavage site and 'c' to its 3'end as a complementary of G in forward g-RNA.

*Esp*3I is one of the Class-IIS restriction enzymes which has an asymmetric recognition site and cleavage site separately [20]. The "aaaac" sequence also as a part of g-RNA scaffold ensures the compatibility of oligo for cloning into the *Esp*3I (*Bsm*BI)-digested pCas-guide vector. The gD gRNA among designed gRNAs was selected and the effect of the CRISPR-Cas9 system was surveyed on HSV-1 replication.

To survey results of the CRISPR-Cas9 system, plaque assay and real-time PCR were performed and the outcomes of these methods confirmed the decrease in HSV-1 infection as if they had a statistically significant difference. Nevertheless, it has been revealed that insert false-positive results were obtained when the derived primers from the insert alone or span on vector in colony PCR. The probable reason can be the amplification of the unligated insert DNA or untransformed ligated present in the bacterial plate [21]. To summarize, sequencing of the p-Cas-guide vector cloned with positive colony PCR is unavoidable. These findings provide us insights for future research, and more studies are needed to better understand the CRISPR technology.

Acknowledgment

The source of data used in this paper was from the research study of Ms. Nastaran Khodadad, a student of Ahvaz Jundishapur University of Medical Sciences. This work was registered by the Ethics Committee of the Ahvaz Jundishapur University (IR.AJUMS.REC.1395.292) and financially supported by the Cancer Research Center, Ahvaz Jundishapur University of Medical Sciences, Ahvaz, Iran.

Ethical Guidelines

This article does not contain any studies with human participants or animals performed by any of the authors.

Conflict of interest

The authors declare that they have no conflict of interest.

References

1. Chen YC, Sheng J, Trang P, et al. Potential Application of the CRISPR/Cas9 System against Herpesvirus Infections. Viruses. 2018; 10(6), doi: 10.3390/v10060291, indexed in Pubmed: 29844277.
2. Fani M, Khodadad N, Ebrahimi S, et al. Zinc Sulfate in Narrow Range as an In Vitro Anti-HSV-1 Assay. Biol Trace Elem Res. 2020; 193(2): 410–413, doi: 10.1007/s12011-019-01728-0, indexed in Pubmed: 31028520.
3. Liu G, Hai R, Liu F. Detection of congenital cytomegalovirus in newborns using nucleic acid amplification techniques and its public health implications. Virol Sin. 2017; 32(5): 376–386, doi: 10.1007/s12250-017-4055-y, indexed in Pubmed: 29116590.
4. Komor AC, Kim YB, Packer MS, et al. Programmable editing of a target base in genomic DNA without double-stranded DNA cleavage. Nature. 2016; 533(7603): 420–424, doi: 10.1038/nature17946, indexed in Pubmed: 27096365.
5. Long C, McAnally JR, Shelton JM, et al. Prevention of muscular dystrophy in mice by CRISPR/Cas9-mediated editing of germline DNA. Science. 2014; 345(6201): 1184–1188, doi: 10.1126/science.1254445, indexed in Pubmed: 25123483.
6. Jinek M, Chylinski K, Fonfara I, et al. A programmable dual-RNA-guided DNA endonuclease in adaptive bacterial immunity. Science. 2012; 337(6096): 816–821, doi: 10.1126/science.1225829, indexed in Pubmed: 22745249.

7. Barrangou R, Marraffini LA. CRISPR-Cas systems: Prokaryotes upgrade to adaptive immunity. Mol Cell. 2014; 54(2): 234–244, doi: 10.1016/j.molcel.2014.03.011, indexed in Pubmed: 24766887.
8. Jansen R, Embden JD, Gaastra W, et al. Identification of genes that are associated with DNA repeats in prokaryotes. Mol Microbiol. 2002; 43(6): 1565–1575, doi: 10.1046/j.1365-2958.2002.02839.x, indexed in Pubmed: 11952905.
9. Makarova K, Koonin E. Annotation and Classification of CRISPR-Cas Systems. CRISPR. 2015: 47–75, doi: 10.1007/978-1-4939-2687-9_4.
10. Chylinski K, Makarova K, Charpentier E, et al. Classification and evolution of type II CRISPR-Cas systems. Nucleic Acids Research. 2014; 42(10): 6091–6105, doi: 10.1093/nar/gku241, indexed in Pubmed: 24728998.
11. Ran FA, Hsu PD, Wright J, et al. Genome engineering using the CRISPR-Cas9 system. Nat Protoc. 2013; 8(11): 2281–2308, doi: 10.1038/nprot.2013.143, indexed in Pubmed: 24157548.
12. Chang HHY, Pannunzio NR, Adachi N, et al. Non-homologous DNA end joining and alternative pathways to double-strand break repair. Nat Rev Mol Cell Biol. 2017; 18(8): 495–506, doi: 10.1038/nrm.2017.48, indexed in Pubmed: 28512351.
13. Chen C, Fenk LA, de Bono M. Efficient genome editing in Caenorhabditis elegans by CRISPR-targeted homologous recombination. Nucleic Acids Res. 2013; 41(20): e193, doi: 10.1093/nar/gkt805, indexed in Pubmed: 24013562.
14. Graham FL, Smiley J, Russell WC, et al. Characteristics of a human cell line transformed by DNA from human adenovirus type 5. J Gen Virol. 1977; 36(1): 59–74, doi: 10.1099/0022-1317-36-1-59, indexed in Pubmed: 886304.
15. Wang T, Wei JJ, Sabatini DM, et al. Genetic screens in human cells using the CRISPR-Cas9 system. Science. 2014; 343(6166): 80–84, doi: 10.1126/science.1246981, indexed in Pubmed: 24336569.
16. Labun K, Montague TG, Krause M, et al. CHOPCHOP v3: expanding the CRISPR web toolbox beyond genome editing. Nucleic Acids Res. 2019; 47(W1): W171–W174, doi: 10.1093/nar/gkz365, indexed in Pubmed: 31106371.
17. Karpov DS, Karpov VL, Klimova RR, et al. A Plasmid-Expressed CRISPR/Cas9 System Suppresses Replication of HSV Type I in a Vero Cell Culture. Molecular Biology. 2019; 53(1): 70–78, doi: 10.1134/s0026893319010059.
18. Kabadi AM, Ousterout DG, Hilton IB, et al. Multiplex CRISPR/Cas9-based genome engineering from a single lentiviral vector. Nucleic Acids Res. 2014; 42(19): e147, doi: 10.1093/nar/gku749, indexed in Pubmed: 25122746.
19. Kunkel GR, Maser RL, Calvet JP, et al. U6 small nuclear RNA is transcribed by RNA polymerase III. Proc Natl Acad Sci U S A. 1986; 83(22): 8575–8579, doi: 10.1073/pnas.83.22.8575, indexed in Pubmed: 3464970.
20. Szybalski W, Kim SC, Hasan N, et al. Class-IIS restriction enzymes--a review. Gene. 1991; 100: 13–26, doi: 10.1016/0378-1119(91)90345-c, indexed in Pubmed: 2055464.
21. Zon LI, Dorfman DM, Orkin SH. The polymerase chain reaction colony miniprep. Biotechniques. 1989; 7(7): 696–698, indexed in Pubmed: 2631784.
22. Doench JG, Hartenian E, Graham DB, et al. Rational design of highly active sgRNAs for CRISPR-Cas9-mediated gene inactivation. Nat Biotechnol. 2014; 32(12): 1262–1267, doi: 10.1038/nbt.3026, indexed in Pubmed: 25184501.
23. Doench JG, Fusi N, Sullender M, et al. Optimized sgRNA design to maximize activity and minimize off-target effects of CRISPR-Cas9. Nat Biotechnol. 2016; 34(2): 184–191, doi: 10.1038/nbt.3437, indexed in Pubmed: 26780180.
24. Xu H, Xiao T, Chen CH, et al. Sequence determinants of improved CRISPR sgRNA design. Genome Res. 2015; 25(8): 1147–1157, doi: 10.1101/gr.191452.115, indexed in Pubmed: 26063738.
25. Moreno-Mateos MA, Vejnar CE, Beaudoin JD, et al. CRISPRscan: designing highly efficient sgRNAs for CRISPR-Cas9 targeting in vivo. Nat Methods. 2015; 12(10): 982–988, doi: 10.1038/nmeth.3543, indexed in Pubmed: 26322839.
26. Shen B, Zhang W, Zhang J, et al. Efficient genome modification by CRISPR-Cas9 nickase with minimal off-target effects. Nat Methods. 2014; 11(4): 399–402, doi: 10.1038/nmeth.2857, indexed in Pubmed: 24584192.
27. Sanson KR, Hanna RE, Hegde M, et al. Optimized libraries for CRISPR-Cas9 genetic screens with multiple modalities. Nat Commun. 2018; 9(1): 5416, doi: 10.1038/s41467-018-07901-8, indexed in Pubmed: 30575746.
28. Kim HK, Min S, Song M, et al. Deep learning improves prediction of CRISPR-Cpf1 guide RNA activity. Nat Biotechnol. 2018; 36(3): 239–241, doi: 10.1038/nbt.4061, indexed in Pubmed: 29431740.
29. Hsu PD, Scott DA, Weinstein JA, et al. DNA targeting specificity of RNA-guided Cas9 nucleases. Nat Biotechnol. 2013; 31(9): 827–832, doi: 10.1038/nbt.2647, indexed in Pubmed: 23873081.
30. Bae S, Park J, Kim JS. Cas-OFFinder: a fast and versatile algorithm that searches for potential off-target sites of Cas9 RNA-guided endonucleases. Bioinformatics. 2014; 30(10): 1473–1475, doi: 10.1093/bioinformatics/btu048, indexed in Pubmed: 24463181.

Submitted: 29 June, 2020
Accepted after reviews: 8 September, 2020
Available as AoP: 16 September, 2020

FOLIA HISTOCHEMICA ET CYTOBIOLOGICA
Vol. 58, No. 3, 2020
pp. 182–197

ORIGINAL PAPER

VIA MEDICA

The Light/Dark cycle disruption affects hepatic function both in metabolic parameters and tissue structure in a nocturnal desert rodent: *Gerbillus tarabuli*

Amina Derbouz Rouibate[1, 2], Nadir Benhafri[1, 2], Saliha Ouali-Hassenaoui[1], Aicha Dekar-Madoui[1]

[1]USTHB, Faculty of Biological Sciences, Laboratory of Biology and Physiology of Organisms, Neurobiology Team, BP 32, El Alia, 16111 Bab Ezzouar, Algiers, Algeria
[2]Dr Yahia Fares University of Medea, Faculty of Sciences, Algeria

Abstract

Introduction. Biological rhythms, such as Light/Dark (LD) cycles, are an integral component of virtually all aspects of life. These rhythms are controlled in large part by circadian clocks, allowing the organism to adapt its internal rhythmic metabolism to changes in the external environment created by daily fluctuations in the LD cycle. Therefore, changes in the daily duration of the lighting could lead to adverse health consequences. The aim of the study was to investigate, in a nocturnal desert rodent, *Gerbillus tarabuli,* the effects of the LD cycle disruption on the structure of the hepatic tissue and the content of carbohydrate and lipid parameters as indicators of metabolic state.

Material and methods. The present study was conducted on two gerbil groups: control group was exposed to a standard lighting cycle (LD: 12:12), and the shifted group was subjected to a chronic disrupted LD cycle, alternating a standard cycle (LD: 12:12) with a modified cycle (LD: 20:4), *i.e.*, the light phase of 24-h cycle was prolonged by 8 h on every second day during a period of 12 weeks. We used: (i) routine histology and histochemical staining for tissue analysis; (ii) immunohistochemistry (IHC) for MPO detection; (iii) biochemical methods for hepatic glycogen and lipids extraction and quantification. Blood metabolic parameters were assessed by enzymatic methods.

Results. Our structural results indicate in the shifted group an alteration of tissue architecture, showing widely scattered inflammatory *foci* with many dilated sinusoids and prominent leukocyte infiltration with connective fibrotic extension. IHC revealed also increased hepatic myeloperoxidase (MPO) expression confirming neutrophils' presence. In parallel, the histochemical study revealed a strong depletion of hepatocytic glycogen and lipid inclusions; these observations were also supported by the measurements of glycogen and total lipids in extracted tissue indicating a reduction in liver content. These results were accompanied by a decrease in body weight relative to the reduction of food intake, as well as hyperglycemia and some alterations in serum lipid parameters (triglycerides and cholesterol) suggesting a metabolic disturbance.

Conclusion. We conclude that a phase difference between the endogenous activity rhythm of the species and the daily cycle of illumination has a strong impact on the liver morphology as well as on the metabolic activity of liver cells. *(Folia Histochemica et Cytobiologica 2020, Vol. 58, No. 3, 182–197)*

Key words: *Gerbillus tarabuli*; liver, photic desynchronization; liver structure; metabolism; myeloperoxidase

Correspondence address: Amina Derbouz Rouibate,
Aicha Dekar-Madoui,
USTHB, Faculty of Biological Sciences,
Laboratory of Biology and Physiology of Organisms,
Neurobiology Team, BP 32, El Alia, 16111 Bab Ezzouar, Algiers, Algeria
e-mails: mounader@hotmail.com (A. Derbouz Rouibate), adekar@usthb.dz (A. Dekar-Madoui)

Introduction

Most living species have an internal circadian clock, which allows coordinating their physiology and behavior to the alternation of day and night.

The internal clock is synchronized by environmental factors. In mammals, light-dark alternation is the main environmental signal used by the central circadian oscillator to synchronize its endogenous rhythm with the environmental rhythm [1–3]. Thus, changes in the daily duration of the exposure to light will have a strong impact on body's physiology [4]. The diurnal physiology is therefore cyclical and organized in a coordinated way so that the period of natural light corresponds to that of awakening, food intake, and energy storage while the night period is associated with sleep, fasting and the use of energy reserves in the short term. This temporal coordination which is opposite in phase in nocturnal animals, is ensured, to a very large extent, by the main circadian clock, located in the suprachiasmatic nuclei (SCN) of the hypothalamus [5] and in the peripheral clocks identified in the majority of peripheral organs, including the liver [6].

The liver was among the first peripheral organs in which molecular oscillations of clock genes were demonstrated [7]. It is interesting to note that circadian regulation plays a large role in liver metabolism. Indeed, glucose, bile acids, lipids, and cholesterol are all subject to timed circadian control [8].

Recent studies suggest that changes in circadian rhythm would have adverse health consequences, causing metabolic dysfunction. These shifts in peripheral tissues result in asynchrony between the master clock and the peripheral clocks [9].

However, the advents of artificial lighting and current lifestyles have led to significant, sometimes extreme, changes in our diurnal habits. Thus, many people working at night or performing rotating shifts, such as the police, doctors and emergency medical technicians have profoundly disturbed daily rhythms [10, 11]. They represent a significant portion of the population that must work at a time when humans have evolved to sleep, and are required to sleep when the suprachiasmatic nuclei promotes awakening. In addition, epidemiological studies from shift workers suggest that prolonged exposure to light at night increases the risk of breast cancer [12], sleep disturbances [13], cardiovascular disorders [10, 14], and mood disorders [15]. Additionally, the increase in exposure to light at night parallels the global increase in the prevalence of metabolic syndrome and obesity [16, 17].

Several different animal models are used to model shift work and study the mechanism responsible for the observed correlation between shift work and metabolic dysfunctions.

This study was conducted on *Gerbillus tarabuli* a nocturnal species from Algerian Sahara. This area is undergoing an urban expansion causing the invasion of the ecological niches of wild species adapted to the nocturnal environment and necessarily suffering from growing light pollution, these lighting effects undeniably have effects on the biodiversity, and it would be naïve to believe that one can illuminate the night environment without causing impacts. For this reason, this rodent seems a useful model to study the metabolic effects of shiftwork in humans. We want to explore the effect of artificial and irregular light schedules on the morphofunctional aspects of the gerbil's liver.

Material and methods

Animals. The current study was performed on a nocturnal desert animal: *Gerbillus tarabuli.* These animals were captured in April, in the desert region of Béni-Abbès (240 km south-east of Béchar and located 1200 km southwest of Algiers, 30°07'N 2°10'W). It is a region characterized by an arid climate. We have used 19 mature animals, of both sexes of mean body weight 42 g. The animals were cared for according to the recommendations of the Association Algérienne des Sciences en Expérimentation Animale (AASEA) (http://www.aasea.asso.dz/).

Experimental design. In captivity, for 4 weeks, all animals were housed individually in 12h light-12h dark cycle (lights on at 00:00 and lights off at 12:00), and temperature-controlled cages (22 ± 2°C), fed on barley grains *ad libitum* without water. Then, the animals were randomly separated into two groups and placed in chronobiotic rooms. The first group (control; n = 9) was maintained in standard circadian cycle (LD: 12:12), and the second one (shifted; n = 10) was subjected to a chronic disrupted Light/Dark cycle, alternating a standard cycle (LD: 12:12) with a modified cycle (LD: 20:4), *i.e.*, the light phase of the 24-h cycle was prolonged by 8 hours every second day during a period of 12 weeks (Fig. 1).

The sacrifice of anesthetized animals was performed at the end of the experiment between 9–12 h when the LD cycle of control and shifted groups came together.

The study targeted the body mass, food intake, plasma parameters, histological and immunohistochemical features, which were performed on 5 gerbils of the control group and 6 gerbils of the shifted group.

The biochemical tissue analysis requiring the use of the whole fresh liver was performed on 4 other gerbils of each group.

Body mass and food intake. The body mass and the food intake were measured by weekly individual weighing. In

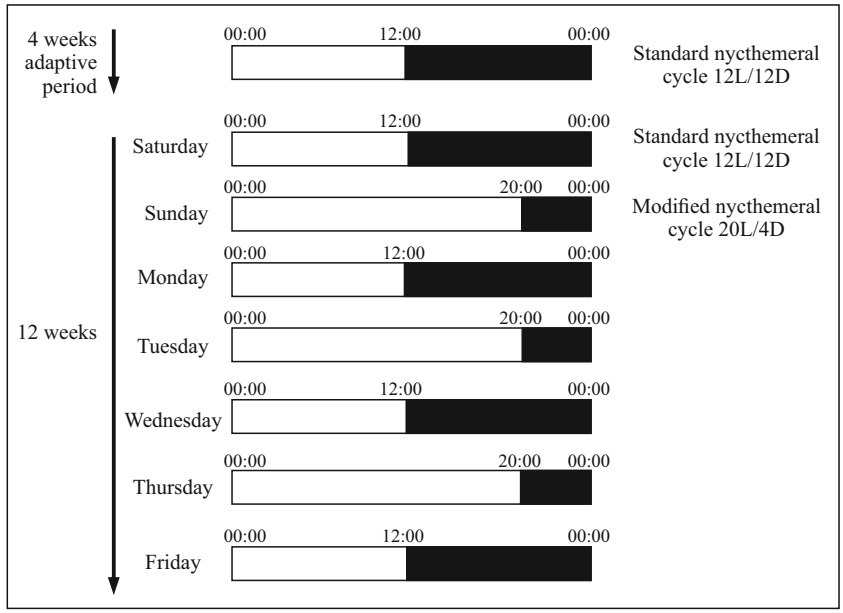

Figure 1. Time schedule of lighting conditions over 16 weeks, including 4 weeks of adaptive period and 12 weeks of experimental conditions. A daily period of darkness is indicated by black bars.

order to estimate food consumption, we gave 50 g of barley each week.

Blood metabolic parameters. Blood was collected by retro-orbital puncture into heparin tubes and kept on ice, and subsequently centrifuged for 10 min at 2500 rpm at room temperature (RT); the plasma was recovered and stored at –20°C until measurements.

Blood glucose was measured at 10:00 am using a Glucometer (One Touch Ultra 2, LifeScan, Zug, Switzerland) by retro-orbital bleeding.

Cholesterol and triglycerides were assayed by the enzymatic method using test kits from SPINREACT (S.A./S.A.U. Ctra. Santa Coloma, Spain).

Hepatic glycogen content. Gerbils were euthanized (zeitgeber time: ZT 9–12), the whole liver was removed and glycogen content was assessed according to the method of Hassid and Abraham [18]. In short, liver portions weighing between 300–400 mg were boiled in a 30% potassium hydroxide solution (KOH) for 30 minutes to hydrolyze the glycogen. Total glycogen was precipitated by addition of 95% alcohol and then recovered by centrifugation at 2500 rpm for 15 min; hydrolyses of glycogen into glucose was performed by adding 2.5N H_2SO_4 solution. The solution obtained was neutralized with 2M NaOH to pH 7.4 and the hydrolyzed free glucose concentration was evaluated using the enzymatic colorimetric glucose oxidase method according to Trinder (1969) [19].

Hepatic total lipids content. Livers were harvested (ZT 9–12), and total lipids were quantified by the Folch method [20].

To this aim, a weighed fresh liver fragment was ground cold with a Potter-type homogenizer in the chloroform-methanol mixture (2: 1, v/v), for 24 hours, the chloroform has the property of completely dissolving protein-bound lipids, which are then precipitated by methanol.

The ground material was filtered under defatted filter paper. The extract obtained was recovered in flasks, adjusted to 25 mL of Folch, sealed and placed at 4 °C. An aliquot of the filtrate (5 mL) was washed with distilled water. After stirring and centrifugation at 2500 rpm, the upper phase was removed; the lower phase was collected in previously weighed tubes, and allowed to evaporate in a ventilated oven at 60° C. After evaporation, the tubes were reweighed. The amount of total lipids was determined by the difference between the two values.

Morphological studies

Histochemical analysis. Liver pieces of both groups of animals were immersed in Bouin's and Ciaccio's fluids [21] and, after typical procedure, embedded in paraffin. Sections of 4 μm, obtained on a microtome, were stained with Masson's trichrome method as topographic stain, Periodic acid-Schiff (PAS) was used to stain for glycogen and Sudan Black B was used to detect lipids in the samples fixed in Ciaccio's fluid [21].

Structural analysis. Livers of both groups of animals were fixed by intracardiac perfusion with 4% paraformaldehyde

and 2.5% glutaraldehyde in a 0.1 M phosphate buffer (pH 7.2–7.4) and subsequently post fixed in 1% osmium tetroxide (OsO_4) for two hours and embedded in epoxy resin blocks. Semithin sections of 1 μm were cut with an ultramicrotome (8800 Ultratome III LKB, Bromma, Sweden) and these semithin sections were stained with Toluidine Blue.

The analyses were performed on two sections per animal with a total of 80 images for controls and 96 images for shifted group.

All histological samples were examined by Zeiss Axoplan microscope (Zeiss, Jena, Germany) and photographed with High-Resolution Optics Microscope Camera (MA88-500/ /Premiere®, 5.0 Megapixels with a 1280 × 1024 resolution) using TSView version 6.2.4.5 (Tucsen. Imaging Technology Co. Limited, Fuzhou, China). None of the images collected were digitally manipulated.

Immunohistochemistry. Fixed in 4% paraformaldehyde for 48 h, paraffin-embedded liver samples were cut into 2 μm-thick tissue sections and mounted on Silanized Slides. Tissue sections were deparaffinized and heat induced epitope retrieval was carried out in EnVision™ FLEX Target Retrieval Solution (TRS), high pH (Dako K8004, Glostrup, Denmark) for 40 min at 95–99°C using the Dako PTLink apparatus, followed by a 20 min cool down and rinse in phosphate-buffered saline (PBS). Endogenous peroxidase activity was blocked by incubation in 3% H_2O_2 for 10 min. Primary antibodies, polyclonal rabbit anti-human myeloperoxidase (MPO, ready-to-use prediluted primary antibody, Dako code IR511) were applied for 30 min on the tissue slides.

Sections were washed in PBS solution before incubation with the secondary antibody (EnVision FLEX/HRP SM802, K8000; Dako UK Ltd) for 30 min at room temperature, washed and revealed with 3,3'-diaminobenzidine peroxidase substrate (Envision™ FLEX DAB + Chromogen DM827, Dako) solution to yield an insoluble brown deposit. Tissue sections were counterstained with Groat's hematoxylin for few seconds. The immunostaining was observed with Zeiss light microscope.

Reactivity for MPO was tested by the omission of primary antibodies and incubation in normal rabbit serum or with irrelevant secondary antibodies. These sections did not show any labeling.

The MPO immunoexpression was quantified using Image J software (NIH, Bethesda, MD, USA) that measures the average darkness of the image due to DAB signal. The image was inverted to clean out the white noise, then the regions of interest were drawn to define the stain color, the background and the counterstaining with hematoxylin were subtracted. The labeling was measured for two sections per animal with a total of 80 images for controls and 96 images for shifted group using a 40× objective.

Statistical analysis. Statistical analysis was performed by testing first the distribution of all variables for normality. Two-way analysis of variance on ranks with repeated measures was used to test the effect of time and desynchronization in addition to the interaction between factors on body weight, food intake or metabolic parameters. One-way analysis of variance was used to test the effect of desynchronization on hepatic glycogen and total lipid content between the two groups at the end of experimentation. The two analyses were followed by Tukey *post-hoc* test.

One-way ANOVA was used to quantify the intensity of the immunostaining of hepatic cells.

All data are expressed as the means ± SEM, with a statistically significant difference defined as a value of $P < 0.05$ (R software version 3.5.1).

Results

Photic desynchronization effects on body weight and food intake

Comparative change in body weight for 12 weeks

Body weight, body weight loss, and food intake curves of control group (n = 5) and shifted group (n = 6) are shown in Fig. 2. The body weight in both groups was comparable at the beginning of the study (48.14 ± 4.05 g *vs*. 44.61 ± 3.15 g) and throughout experimental light conditions.

The analysis of the body weight evolution reveals in the control group a slight decrease of -2.83% with a final body weight of 44.18 ± 3.14 g. In the shifted group this decrease is greater and achieves a loss of 12.63% with a final weight of 38.98 ± 4.38 g (Fig. 2A).

We observed a significant effect of desynchronization on the evolution of body weight and body weight loss ($p < 0.001$; two-way repeated measures of ANOVA on ranks). Tukey post hoc test showed a significant effect of circadian rhythm disruption on body weight loss ($P < 0.05$) in respect to the first week in the shifted group. In addition, the post hoc contrast function indicates a significant difference between the two groups for body weight loss during experiment ([week (1–3) – week 10], $P < 0.05$, Fig. 2C).

Comparative change in food intake for 12 weeks

The shifted group displayed a 9.20% decrease in the amount ingested. Conversely, compared to the control group (12:12: LD), experimental disruption (12:12/ 20:4: LD) showed higher ingested amounts during the whole period of shifting with significant effect of desynchronization on the evolution of food consumption ($P < 0.01$). Nevertheless, Tukey post-hoc test didn't show significant differences between the two groups (Fig. 2B).

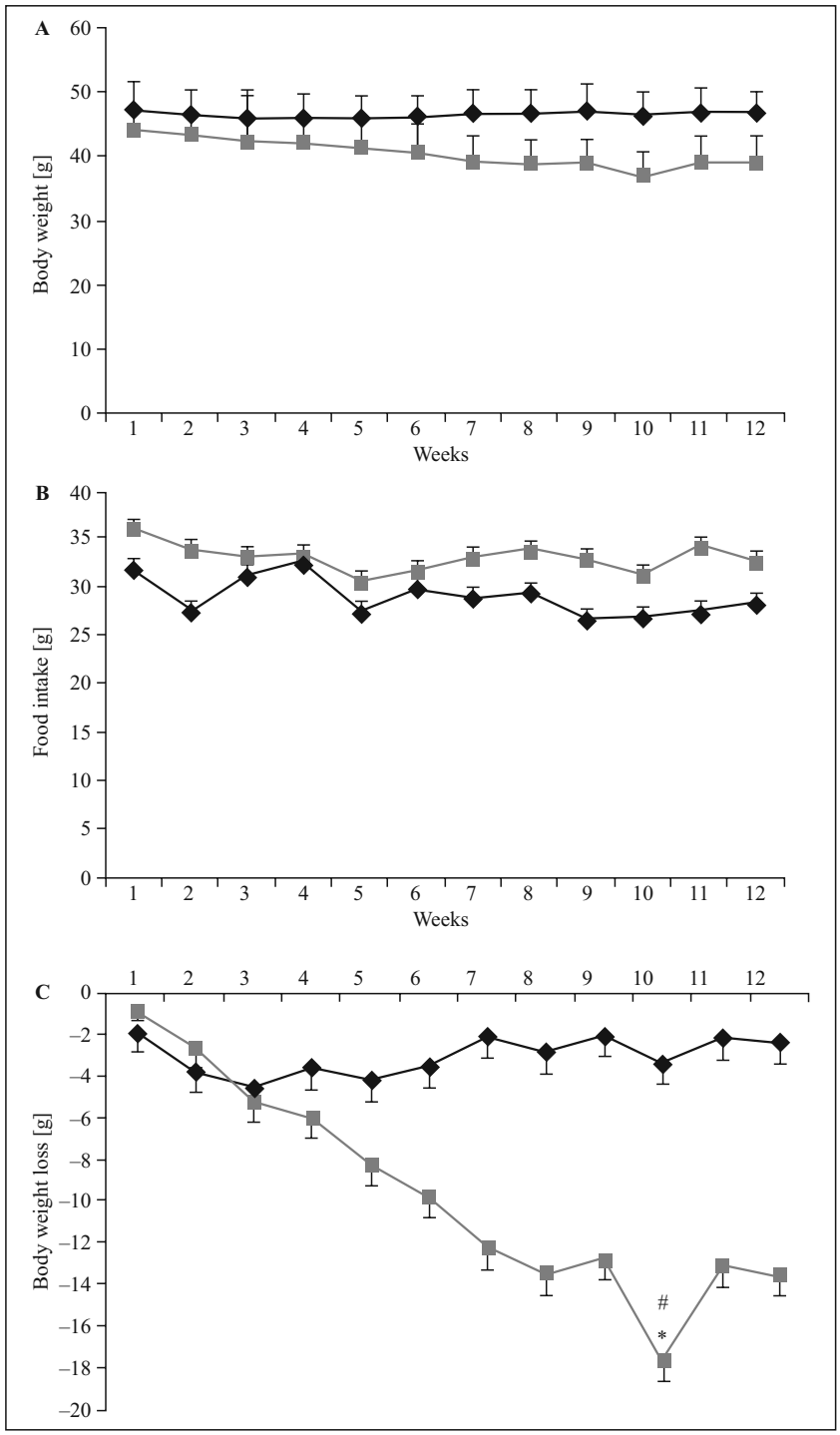

Figure 2. Changes in body weight **(A)**, food intake **(B)** and body weight loss **(C)** in control group (dark line, n = 5), and shifted group (gray line, n = 6). Profiles were measured during 12 weeks. Values are expressed as mean ± SEM, *P < 0.05 *vs*. week 1 in the shifted group (Two-way repeated measures ANOVA on ranks), # P < 0.05 *vs*. control group during experiment [week (1–3) – week 10] (*post hoc* contrast function).

Photic desynchronization effects on blood glucose, cholesterol, and triglycerides levels

Blood glucose, cholesterol, and triglycerides curves of control group (n = 5) and shifted group (n = 6) are presented in Fig. 3. Two-way ANOVA on ranks (Aligned Rank Transform) indicates a significant effect of desynchronization only for triglyceride levels (P < 0.05). However, no time effect is observed on all metabolic parameters (P > 0.05).

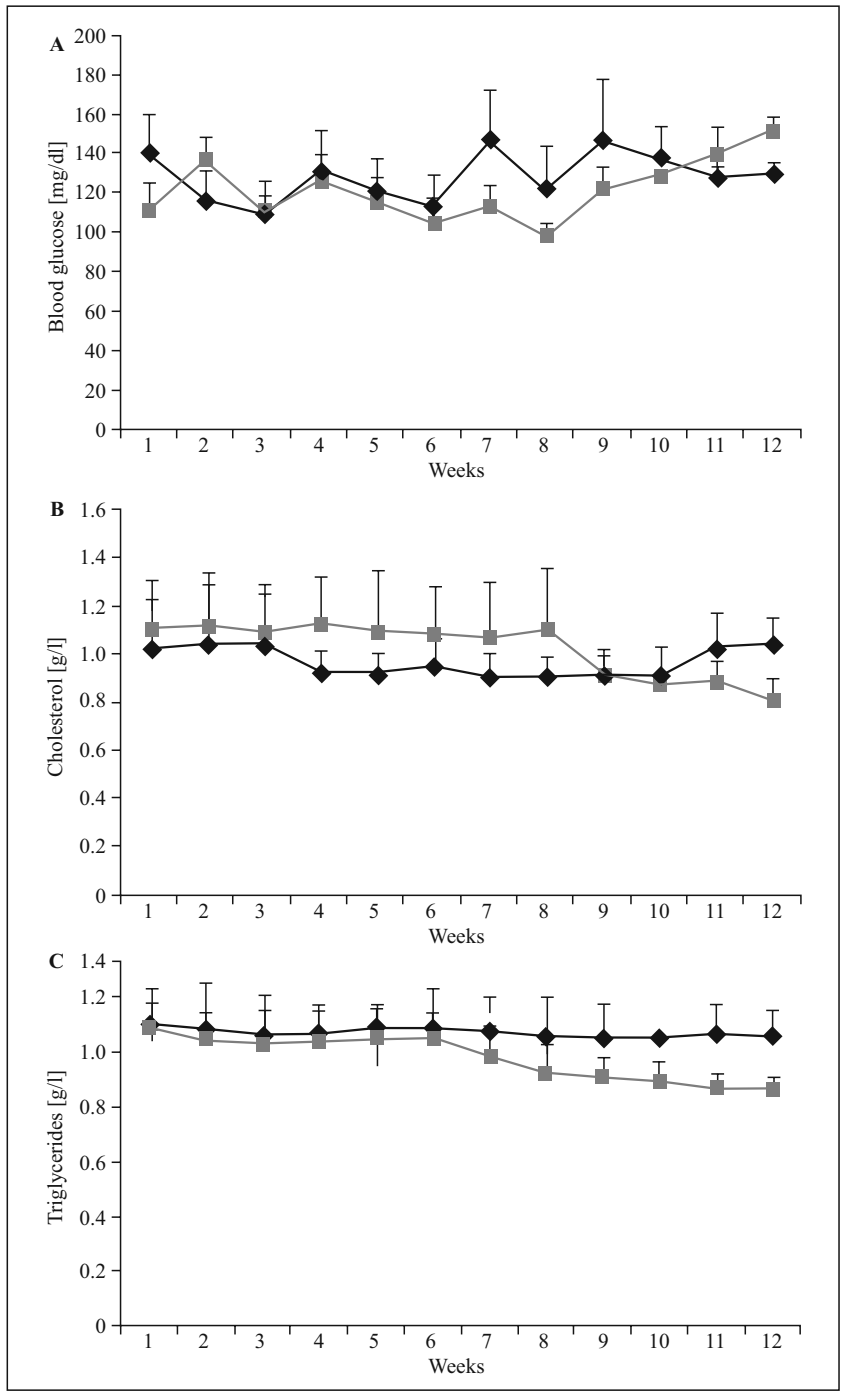

Figure 3. Effect of 12 weeks of photic desynchronization on blood metabolic parameters in control group (dark line, n = 5), and shifted group (gray line, n = 6). Glucose **(A)**, cholesterol **(B)** and triglyceride **(C)** plasma concentrations were measured as described in Methods. Profiles were measured during 12 weeks. (Values are expressed as mean ± SEM, two-way repeated measures ANOVA on ranks).

The evolution of blood glucose levels in the two groups of gerbils, obtained after 12 weeks of experiments, was fluctuating. While blood glucose values of controls seemed stable (began at 140 ± 20.29 mg/dL and achieved 129.8 ± 5.54 mg/dL), in the shifted group, blood glucose levels fluctuated until 8th week. Then, blood glucose elevated progressively to reach 151.33 ± 8.07 *vs.* 111.16 ± 13.86 mg/dL at the beginning, indicating a hyperglycemic state (Fig. 3A).

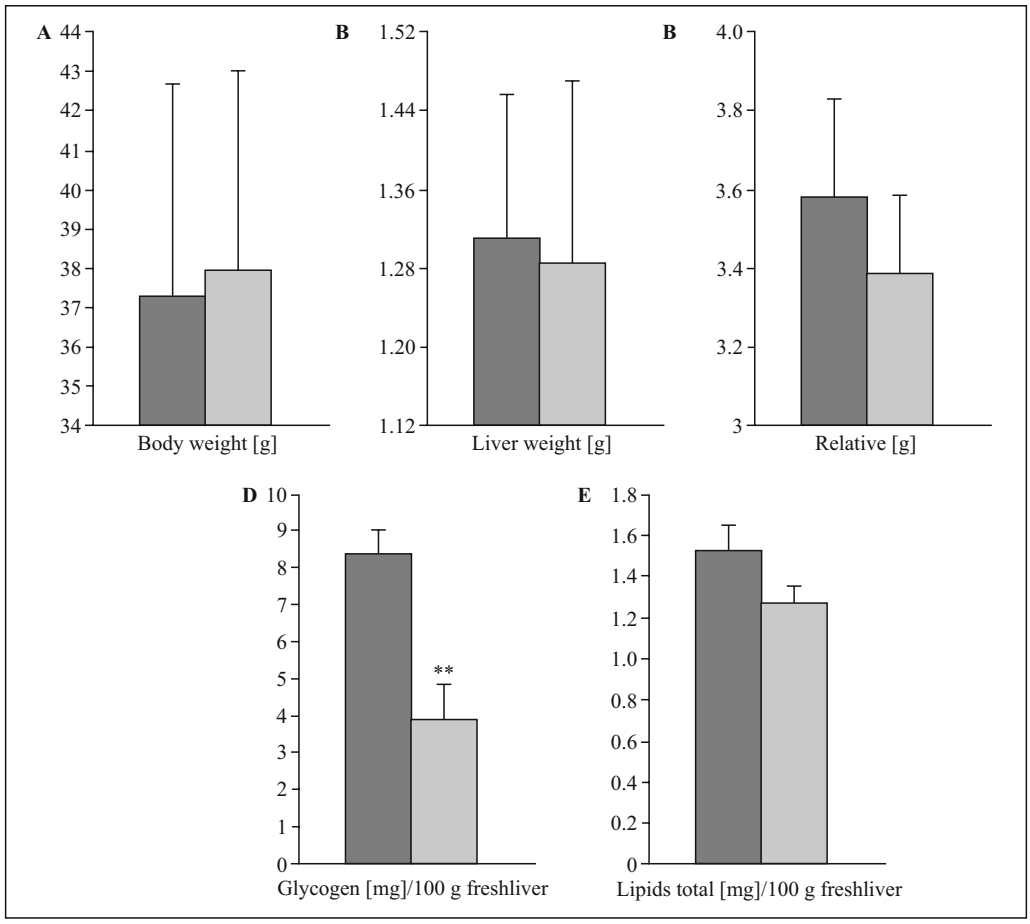

Figure 4. Effect of 12 weeks of photic desynchronization on the content of glycogen and total lipids in gerbil's liver. **A.** The body weights of control group (dark bars, n = 4) and shifted group (gray bars, n = 4) were 37.27 ± 5.39 and 37.95 ± 5.10 g ($P > 0.05$). **B.** The absolute weights of shifted gerbil's liver compared with controls were 1.28 ± 0.18 and 1.31 ± 0.14 g ($P > 0.05$) showing little variation. **C.** The relative mean value of liver weights of control group and shifted group were 3.58 ± 0.25% and 3.38 ± 0.20% ($P > 0.05$). **D**, **E.** Hepatic glycogen and total lipids levels in gerbils of both batches ($^{**}P < 0.01$). Values are expressed as mean ± SEM, One-way ANOVA.

For plasma cholesterol, compared to the control group which showed a stability (1.02 ± 0.20 g/L at the beginning of the experiment and 1.04 ± 0.10 g/L at the end of 12 weeks), the shifted group showed a reduction (1.11 ± 0.20 g /L at the beginning of the experiment to 0.81 ± 0.08 g/L at the end) thus achieving a decrease of 27% (Fig. 3B).

The shifted group showed a progressive decrease in triglyceride levels (from 1.09 ± 0.09 g/L at the beginning to 0.86 ± 0.04 g/L at the end of the experiment), giving a percentage decline of 21.11% compared to controls (1.10 ± 0.12 to 1.05 ± 0.10 g/L) (Fig. 3C).

However, Tukey *post-hoc* test didn't show any significant differences between the two groups for all metabolic parameters.

Hepatic glycogen and total lipids content

The relative and absolute weights of the liver of shifted gerbils showed no significant difference compared to controls (Fig. 4B and C).

After extraction at the end of the 12 weeks of experimentation, we observed a significant effect of desynchronization on hepatic glycogen content ($P < 0.01$; one-way ANOVA). Indeed, lower glycogen values were found in the shifted group (3.89 ± 0.98 mg/100 g fresh liver), representing a decrease of 53.49%, compared to control group (8.36 ± 0.67 mg /100 g fresh liver). Tukey's *post hoc* test showed a very significant difference between the two groups.

In addition, one-way ANOVA showed no significant effect of desynchronization on hepatic total lipids

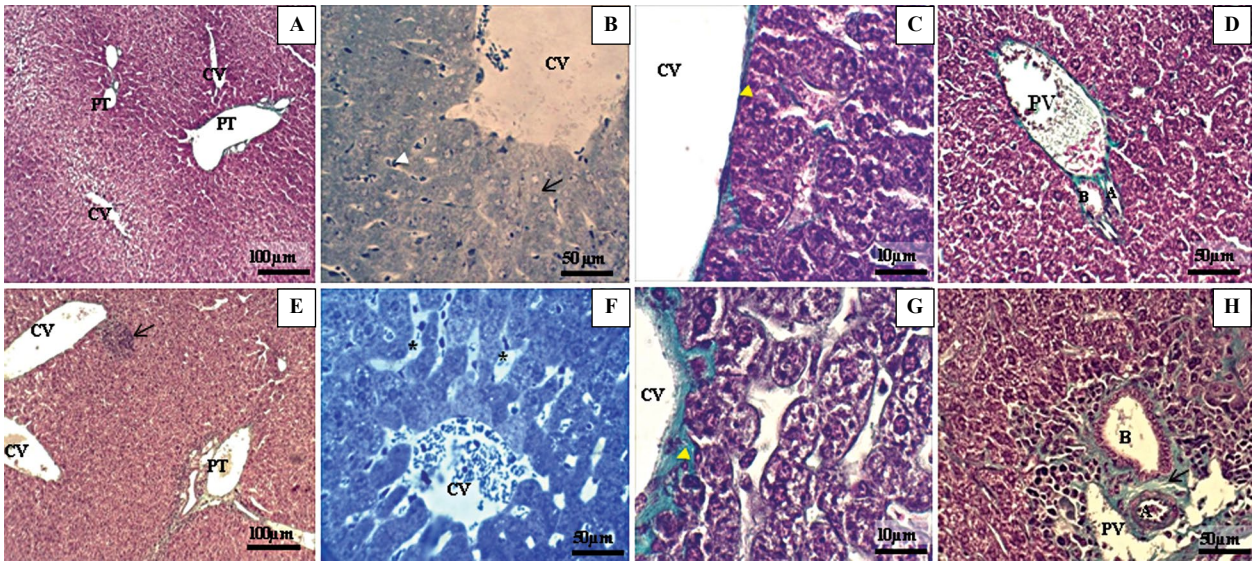

Figure 5. The structure of the hepatic parenchyma in control (upper row) and shifted (lower row) gerbils. **Control gerbils**. **A.** The overview of the hepatic tissue showed a classical lobular organization with central veins (CV) in the middle of the lobules and peripherally located portal triads (PT). **B.** At higher magnification, in the hepatic lobule and from the central vein (CV) radiate the hepatocytic cords (arrow) separated by thin sinusoid capillaries (arrowhead). **C.** The light of the central vein (CV) is lined by a regular endothelium with minimal presence of connective tissue (arrowhead). **D.** Only small amount of connective tissue is present in the portal triad that contains portal vein (PV), artery (A), and bile duct (B).

Shifted gerbils. E. The hepatic tissue architecture is strongly altered by numerous inflammatory *foci* (arrow). **F.** At higher magnification dilations of the sinusoidal capillaries are clearly visible (asterisks). **G.** Dilations of sinusoids and disorganization of central vein's endothelial layer (arrowhead) underlined by an abnormally thick connective layer. **H.** The abundance of connective tissue around the portal triad (arrow) indicates fibrosis installation. Stainings: A, C, D, E, G, and H: Masson's trichrome; B and F: toluidine blue. Scale bars: 100 μm (A and E); 50 μm (B, D, F and H); 10 μm (C and G).

content ($P > 0.05$) at the end of experimentation (control group: 1.525 ± 0.13 mg/100g of fresh liver *vs*. shifted group: 1.265 ± 0.09 mg /100g of fresh liver). After the analysis of these results, we note that in shifted gerbils, the hepatic total lipids level decreased by 17.04%, though the difference with the controls was not significant ($P > 0.05$; Fig. 4).

Morphological alterations of the liver structure

Control animals showed the typical hepatic structure with lobules (Functional Units) centered by a central vein accompanying the portal triads (Fig. 5A). Hepatic cells are arranged in anastomosed and radial cords separated by fine vascular spaces: sinusoid capillaries, which carry blood from the portal spaces and lead into the central vein (Fig. 5B). The lobules are limited by portal spaces that contain the branches of the portal veins, hepatic arteries, and bile ducts (Fig. 5D). At the highest magnification, the lumen of the central vein was lined by a thin layer of endothelial cells (Fig. 5C).

After 12 weeks shifting, the hepatic parenchyma displayed a strong alteration evidenced by the appearance of inflammatory *foci* (Fig. 5E). Hepatocyte cords appeared separated by very dilated sinusoid capillaries (Fig. 5F). Marked contingent of inflammatory cells was observed at portal triads suggesting phagocytic activity. The high magnification showed disorganization of the endothelial layer of the central vein which became bordered by an abnormally thick connective tissue layer (Fig. 5G), a pattern not seen in the controls. We also noted an extension of the connective tissue that would indicate fibrosis (Fig. 5H).

Inflammatory *foci* showed significant perivascular and intra-lobular leukocyte infiltration (Fig. 6A) and numerous Kupffer cells in dilated sinusoidal capillaries (Fig. 6B). We also noted marked foldings of the sinusoidal endothelium indicating an increased communication surface between the central vein and the sinusoids (Fig. 6C). The number of hypertrophied cells had increased (Fig. 6D).

On semithin sections hepatocytes displayed a very basophilic cytoplasm rich in heteromorphic granulations (Fig. 6E). Several binuclear cells showed perinuclear dilation extended to the cytoplasm that may probably be an extension of the endoplasmic reticulum (ER). Stellate cells are recognizable by their star-shape with dense nucleus and fat-rich cytoplasm (Fig. 6F).

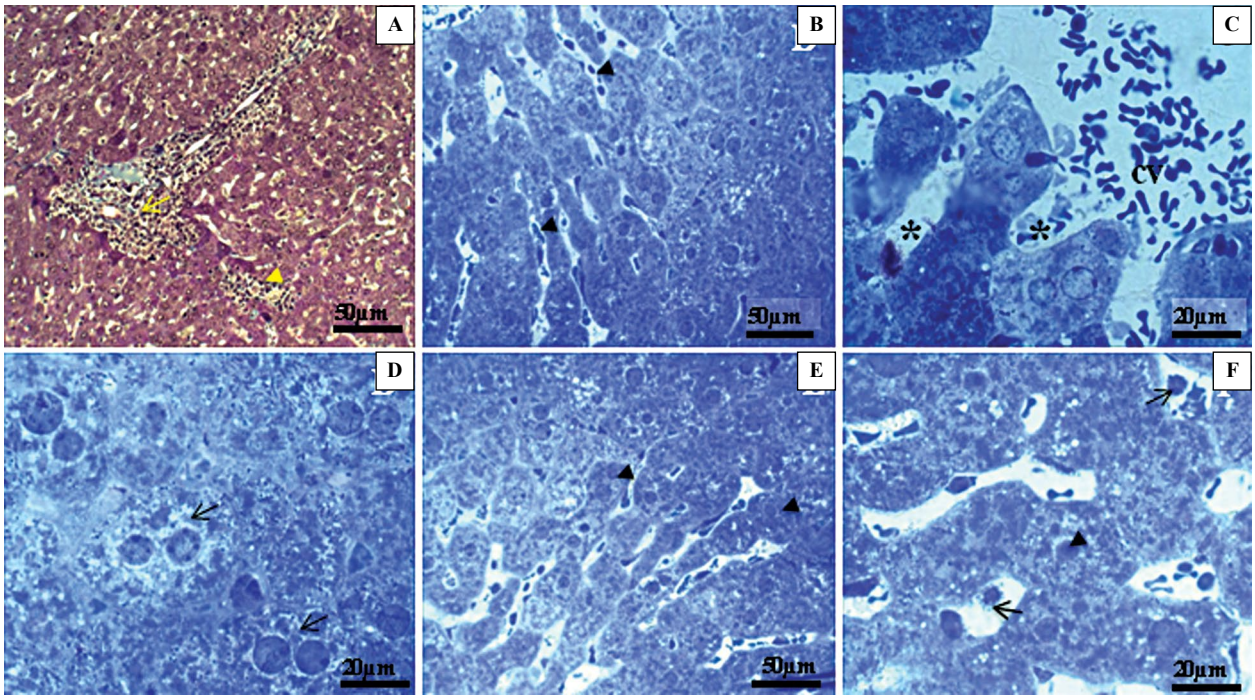

Figure 6. Histological and semithin sections showing the effect of circadian rhythm disruption on the structure of liver tissue in shifted gerbils. **A.** Microphotographs show large inflammatory *foci* with perivascular (arrows) and intralobular (arrowhead) infiltrated leukocyte clusters. **B.** Abundance of Kupffer cells (arrowhead). **C.** Great communication surface between a large central vein (CV) and sinusoids (asterisks). **D.** The abundance of hypertrophied cells binucleated or with hypertrophied nuclei (arrows). **E.** Semithin sections showed very basophilic hepatocytes's cytoplasm (arrowheads) due to the abundance of ribosomes. Note the centrifugal chromophilia in the acinus. **F.** The high magnification reveals perisinusoidal stellate cells (arrows). Chromophilic hepatocytes are rich in organelles; their nuclei are surrounded by a granulated cytoplasm (arrowhead) which reflects the heterogeneity of its content. Stainings: A: Masson's trichrome; B, C, D, E, and F: toluidine blue. Scale bar: 100 μm (A); 50 μm (B and E); 20 μm (C, D and F).

Histochemical analysis by PAS staining revealed important purplish red granular inclusions corresponding to glycogenic deposits in the control gerbils (Fig. 7A, B). In contrast, in shifted gerbils only few fine cytoplasmic granulations were detected indicating a glycogenic depletion (Fig. 7E, F). In addition, the intensity of the Sudan Black B reaction was more pronounced in control gerbils (Fig.7C, D), compared to shifted gerbils (Fig.7G, H) that showed fine lipid inclusions dispersed in the cytoplasm.

Immunohistochemical hepatic expression of myeloperoxidase

The immunohistochemical labeling of myeloperoxidase in both groups revealed a significantly increased number of MPO positive neutrophils and hepatocytes (173.03 ± 2.26 and 115.12 ± 2.24 respectively, Fig. 8B and C; $P < 0.001$) expressed by a positive brown cytoplasm in the shifted group compared to the control group that showed MPO negative expression in neutrophils and hepatocytes (159.70 ± 3.10 and 102.76 ± 0.98 respectively, Fig. 8A). Also MPO immunoreactivity increased with progression of hepatic fibrosis in shifted group.

Discussion

Circadian rhythms are biological events that are constantly repeated over a 24-hour period and are generated by an endogenous mechanism. This mechanism is managed by circadian clocks, located both at the central level (SCN) and at the peripheral organs. This system allows the body to adapt to predictable changes in its environment [22]. Indeed, the central clock is synchronized to make its periodic activities coincide with the environmental cycles, in particular the light/dark cycle [23]. This central adjustment also makes it possible to coordinate peripheral biological functions. In this study, we explored the effect of alternating a standard cycle (12L/12D) and an artificial cycle (20L/4D) for 12 weeks on the morpho-functional characteristics of gerbil's liver. The obtained results showed signs of disruption at both structural and metabolic levels.

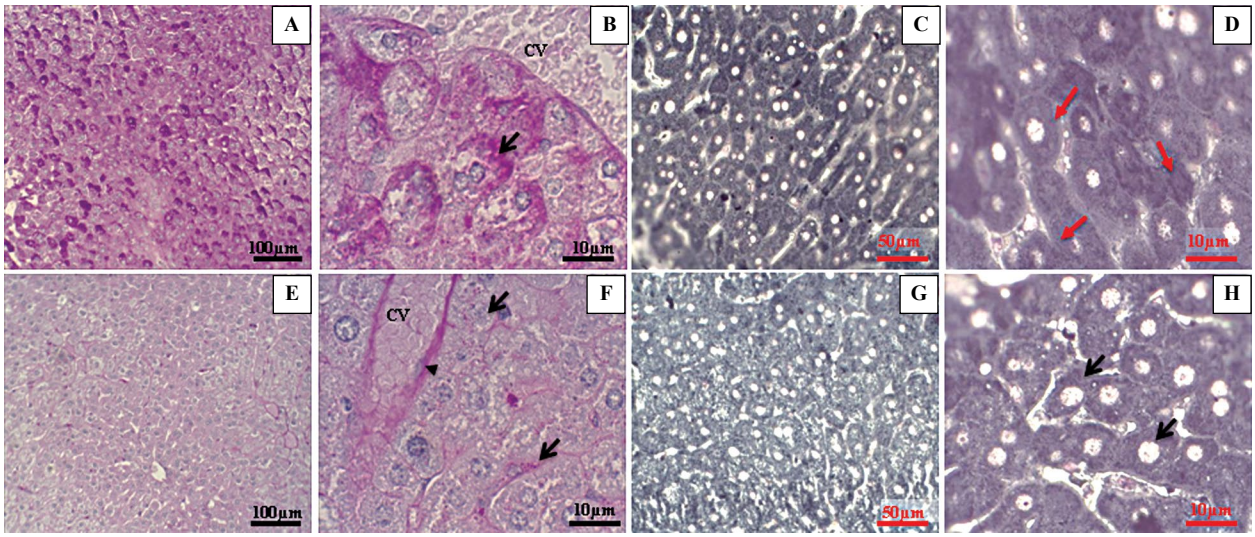

Figure 7. Histochemical photographs showing the reaction of liver tissue to PAS and Sudan Black B staining in control (upper row) and shifted (lower row) gerbils. **Control gerbils. A.** The overview of hepatic tissue showing the presence of important glycogen deposits. **B.** At higher magnification the glycogen granules sometimes occupy the whole hepatocyte (arrow). **C.** The overview of hepatic tissue after Sudan Black B staining showed a strong Sudanophilia. **D.** At higher magnification abundance of lipid inclusions completely obscure the cytoplasm (red arrows).

Shifted gerbils. E, F. We note a marked depletion of glycogen (arrows). **F.** PAS positivity is important in the intercellular space reflecting the abundance of extracellular matrix elements (arrowhead). **G, H.** Conversely, Sudan Black B staining revealed thinly positive dispersed lipid inclusions (arrows).

Stainings: A, B, E, and F: Periodic Acid Schiff (PAS); C, D, G and H: Sudan Black B. Scale bars: 100 μm (A and E); 50 μm (C and G); 10 μm (B, F, D and H).

Experimental disruption of circadian rhythms disrupts weight

In our study gerbils subjected to disturbed circadian rhythms show a loss of 12.62% of their body mass. This result is similar to that obtained in male Siberian hamsters subjected to a short day (8L/16D) for 12 weeks; these animals lose up to 22% of their body weight [24]. Our result is also reported in a mouse model with Amyotrophic Lateral Sclerosis (ALS) maintained under a 20L/4D cycle for 120 days [25]. Likewise, the aging rats maintained with constant dim light showed a rapid body weight loss [26]. In addition, another study showed that mice habituated to an ultradian 6 meals schedule lose > 10% body mass (hypocaloric group) [27]. Otherwise, in Webster mice, a 10L/10D cycle resulted in a body weight gain [28] as in Wistar rats subjected to an ultradian feeding schedule [29]. In addition, exposure to continuous light (4–8 weeks) led to body weight gain in mice [30, 31], and resulted in increased body fat [32] and more food consumption during the subjective day [30, 31]. Conversely, a study using exposure to continuous bright light for 6–10 weeks in Sprague Dawley rats reports no change in body weight [33]. We also observed increased food intake in shifted gerbils compared to the control group; a similar result is reported after long-term exposure (90 weeks) to a Light/Dark cycle (20L/4D) [34].

Altogether these results indicate that disruption of the environmental cycle has changed the feeding behavior of gerbils. This may indicate that the response of nocturnal species to desynchronization depends on the species and the phase shift protocol applied but generally reflects changes in feeding habits. According to Challet [35], the periodic supply of nutrients follows a rhythm of food intake, specific to each species, in close relation to its sleep-wake cycle.

Several studies report that altering the feeding pattern can desynchronize metabolic rhythms and potentially disrupt energy homeostasis. Indeed, a standard diet during the day alters the energy balance in mice (nocturnal species) compared to those fed only at night [9], likewise, central and peripheral clocks tick in opposite phases [36, 37].

The shifted gerbils in our experiment had a shortened awakening phase (4 h) probably limiting their feeding time and showed intense physical activity (personal observations) which implies excessive energy expenditure that could explain the decrease in body weight despite the increase in the amount of barley

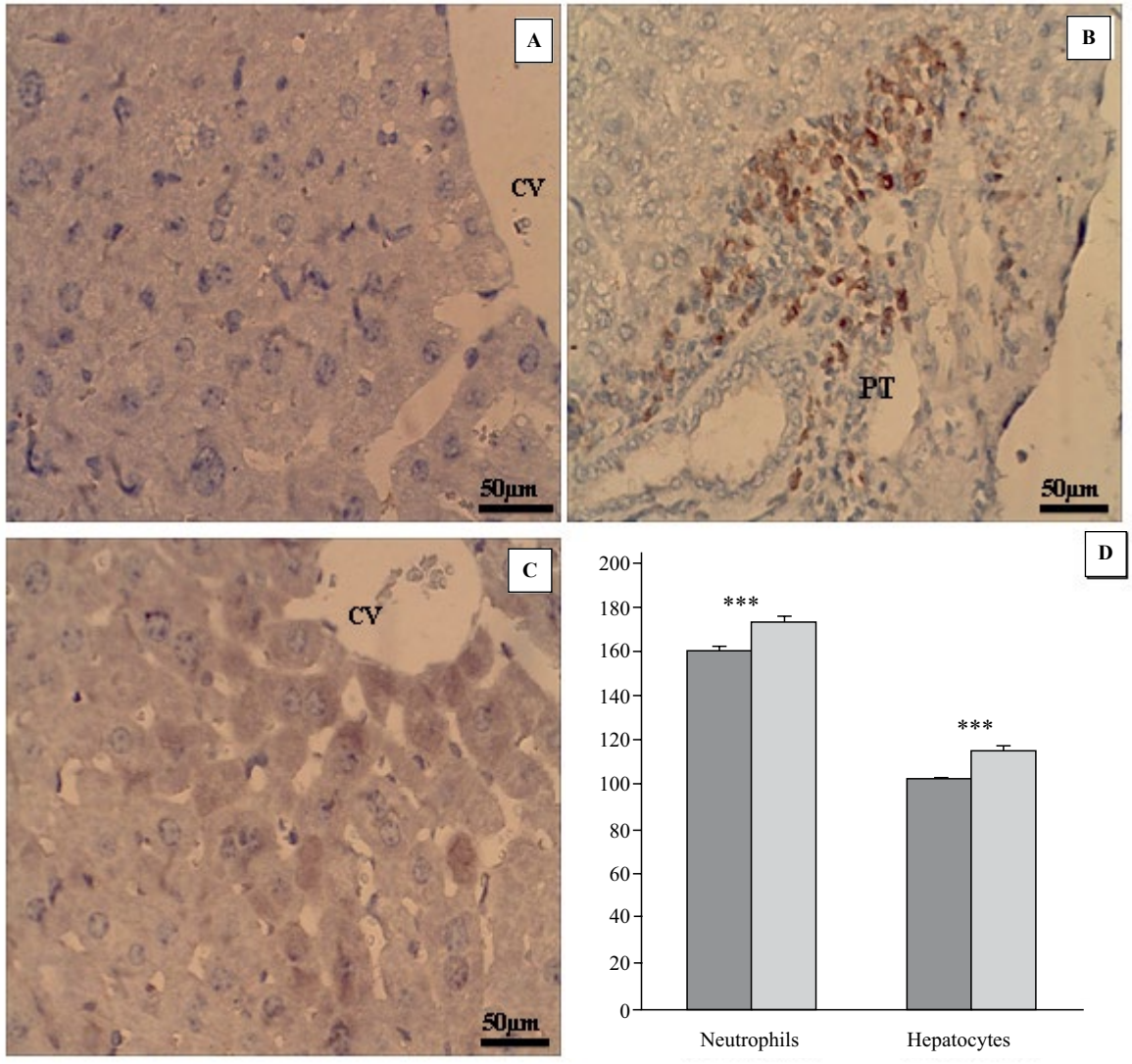

Figure 8. Representative immunohistochemical staining for myeloperoxidase in the liver tissue of two gerbils' groups. Compared to the control group **(A)**, intense immunoreactivity of MPO was identified in the shifted gerbils' in neutrophils infiltrating portal tracts and the periphery of hepatic lobules **(B).** Moreover, the immunolabeling is also detectable in some centrolobular hepatocytes (arrow) **(C).** MPO cells intensity in control group (dark bars) and shifted group (gray bars) **(D).** Values are expressed as mean ± SEM, One-way ANOVA, (***$P < 0.001$).

ingested. Indeed, it was shown that a reduction in the period of food access (< 6 h) does not allow the animals to eat an equivalent amount of food as their ad lib feed (ALF) counterparts [38].

It would, therefore, appear that the circadian time of food intake is an important factor in regulating metabolic activity probably by interaction with molecules that control diurnal liver clock. Indeed, it was reported that eating during the sleep period leads to a disruption of peripheral clocks in nocturnal mice [39].

Photic desynchronization induced metabolic disturbances

In gerbils subjected to a disturbance of the light/dark cycle, blood glucose values show a fluctuating rate during the first 8 weeks, and then tended to increase gradually to exceed the values observed in control gerbils, until the 12th week. Indeed, it has been reported that the plasma glucose in nocturnal rats is increased by exposure to light at different times of

the day [40]. In addition, diabetes-prone (HIP) rats develop hyperglycemia in response to a 6h light advance or under constant light conditions [41].

Interestingly, the work of the Nagai group [42] was the first to show the direct involvement of SCNs in the control of glucose homeostasis, suggesting that the recorded hyperglycemia reflected a disturbance of the central clock. Indeed, mutant mice for *Clock* and *Bmal1* genes in the SCN show hyperphagia as well as hyperglycemia [43].

The presence of peripheral clocks outside the suprachiasmatic nuclei is now well established. Accordingly, the liver is one of the first peripheral organs in which molecular oscillations of clock genes have been demonstrated [7]. Nevertheless, maintaining their rhythmicity in the liver seems less robust than that of the central clock [44]. Thus, we believe that the hyperglycemia found in desynchronized gerbils may also result from a disturbance of the liver clock. Indeed, it has been shown in Wistar rats that the LD cycle mimicking the rotating shift-work with 8-h phase delay affects the expression of 'metabolic' genes (*Per2*, *Bmal1*, *Rev-erba*, *Pparα*, and *Pdk4*) in the liver [45].

The hyperglycemia obtained indicates also a disruption of carbohydrate metabolism. Histochemical analysis with PAS staining revealed hepatocytic glycogen depletion confirmed by the biochemical tissue assay, with 53% reduction suggesting an association between hyperglycemia and glycogen depletion. This result could reflect either activation of the glycogenolytic pathway or an inhibition of the glycogenogenesis pathway.

Doi *et al.* found that mutation of the *Clock* gene or disruption of *Per2* gene expression leads to attenuated oscillations of hepatic glycogen and expression of glycogen synthase 2 (Gys2), the glycogenogenesis limiting enzyme [46]. In addition, disruption of *Per2* gene expression alters glycogen accumulation in the liver and gluconeogenesis [47–49].

Hyperglycemia observed in shifted gerbils implies a preponderant action of glucagon. It is well known that stimulation of glycogenolysis in the liver increases glycemia [50]. Since the action of glucagon is observed under conditions of pressing energy needs [51], we believe that as feeding time is shortened, shifted gerbils are unable to synthesize enough glycogen. In this case, glycogen depletion could be due to insufficient amounts of ingested glucose and not to glycogenolysis. However, the shifted group ingested larger amounts of barley than control animals, which cannot explain the decrease in liver glycogen. Therefore, we suggest that because of *Gerbillus tarabuli* nocturnal habits, the short duration of the dark phase is not sufficient for the activation of glycogenogenesis enzymes. Indeed, it was reported that several genes encoding key enzymes of the carbohydrate metabolism display circadian variations in the liver [52–55].

We found that the disrupted circadian cycle has led to a decrease in triglyceride and cholesterol plasma levels. Liver is a central organ of lipid metabolism so that the histochemical Sudan Black B staining revealed only discrete cytoplasmic dispersed lipid inclusions and the lipid extractions assay showed decreased total hepatic lipids in shifted gerbils compared to controls.

Human studies showed that plasma triglyceride levels are increased in shift workers [56–58]. In mice kept in constant lighting conditions plasma lipid rhythm is abolished indicating the regulation of this metabolism by light signals [59]. Plasma triglycerides and cholesterol exhibit a diurnal rhythm with high levels at midnight in rats maintained in 12 h LD cycle [60]. Also in DD (constant darkness) conditions, several works indicate that mice lipid metabolism is rhythmically coordinated by the endogenous circadian clock [52]. Therefore, it seems that the phase shifting applied to gerbils has also affected their endogenous lipid metabolism rhythm. Indeed, *Clock* or *Bmal1* mutant mice, develop hypertriglyceridemia and hypercholesterolemia [43, 61]. Similarly, mice lacking the *Per2* gene have dyslipidemia [62].

In addition, the decrease in plasma lipid in shifted gerbils may be due to changes in the daily rhythm of eating behavior. Thus, it was found that a daily feeding rhythm is essential for maintaining the daily rhythm in TG secretion [63]. This proposal is consistent with the work of other authors [60, 64–66] who showed that changes in the daily rhythm of eating behavior modified or suppressed the daily rhythm of plasma triglycerides. Also, gene expression of enzymes such as adipose triglyceride lipase (ATGL), medium-chain acyl-CoA dehydrogenase [67] and lipoprotein lipase (LPL) (an enzyme that clears the circulation of TGs and releases free fatty acids for cellular absorption) [68] have been shown to exhibit circadian oscillations in various tissues. Moreover, it was reported that lipid and cholesterol absorption rates are higher during the active period and lower during the rest period in nocturnal mice [59].

Furthermore, synthesized cholesterol combines with apolipoproteins to be secreted and transported as HDLs or VLDLs [35, 59, 69]. Experiments on rats and mice suggest that the increase in nocturnal cholesterol in plasma is caused by changes in lipoproteins [60]. The liver is also involved in lipid metabolism by regulating lipoprotein synthesis, lipid uptake and conversion, besides *de novo* synthesis and oxidation of fatty acids [70].

Altogether this, and our data, may indicate that prolonged light phase caused a decrease in liver activity. The biochemical determination of total tissue lipids and the Sudan Black B staining revealed a lipid decrease in hepatocytes of shifted gerbils. This suggests that plasma lipid alterations might have been caused by changes in hepatic lipid metabolism.

Impact of light/dark cycle disruption on the liver structure

At the structural level, compared to the standard 12L/12D cycle, the shifted cycle led to a loss of the hepatic parenchyma architecture by the appearance of several lesional *foci*. These sites of inflammatory process combine sinusoid capillary dilation, Kupffer cells proliferation and leukocytes infiltration. The most probably causes of such structural alterations may be the activation of Kupffer cells which chemoatract neutrophils.

Kupffer cells and leukocytes secrete several inflammatory mediators, including cytokines [71]. These molecules play an active role in the tissue recruitment of neutrophils from circulation [72] and in the activation of Kupffer cells themselves [73]. The activation of Kupffer cells also leads to the release of reactive oxygen species (ROS) [74] that are important for normal functioning of the liver [75].

We also show in the shifted group an intense immunoreactivity of MPO essentially located in leukocytes and centrolobular hepatocytes. It is well known that MPO is a marker of neutrophil activation and tissue infiltration. Also many authors suggest that MPO expression is a reliable indicator of inflammation [76, 77] more sensitive than histopathological examination of tissues [78]. Indeed, local degranulation of neutrophils would induce the release of MPO into the extracellular matrix [79–81]. This proteolytic enzyme is responsible for the acidification of the environment [82] so that it adheres to cell membranes and produces hypochlorous acid (HOCl) which easily passes the plasma membrane. That could explain the positive immunoreactivity of MPO in hepatocytes. Finally, HOCl exhaust intracellular glutathione [83] an important biological antioxidant [84].

Our observations also showed in the shifted gerbils an expansion of stellate cells and an increase in connective tissue within the hepatic parenchyma that may lead to hepatic fibrosis. This accumulation of connective tissue components may be caused by an imbalance between an increased synthesis of matrix components and a decrease in their degradation. Some studies proved that myeloperoxidase can stimulate the production of extracellular matrix proteins by Kupffer cells. Also matrix alteration has been linked to the activation of stellate liver cells, a critical step in the development of liver fibrosis [85–88]. Indeed, stellate cells become the primary source of extracellular matrix accumulation in the liver during injury [89, 90].

Conclusions

As a whole, it appears that a chronic phase shifting (12 weeks) in *Gerbillus tarabuli* not only affects metabolic parameters, but it also alters liver architecture. The short duration of the nocturnal phase in our model lead to the accelerated development of hyperglycemia, some perturbations in serum lipid parameters (triglycerides and cholesterol) and a depletion of hepatocytic glycogen and lipid inclusions suggesting interference with the regulation of lipid and glucose hepatic metabolism. Interestingly, our morphological observations clearly implicate the effects of shifted LD cycle on the structure of liver tissue. Further studies should clarify the effect of a long-lasting disrupted LD cycle on the expression profiles of liver's clock genes under the same conditions in this species.

Acknowledgments

We are grateful to the Center Pierre and Marie Curie (CPMC) for hosting us to carry out the immunohistochemistry in particular Professor N. Chaher.

A special thank for Dr J. Falcon (UPMC and CNRS) for proofreading the manuscript, H. Touati for her help in statistical analysis part.

The authors wish to thank the participating members especially R. Hammi, as well as the Neurobiology Team (Faculty of Biological Sciences, Laboratory of Biology and Physiology of Organisms, USTHB, Algeria). We also thank all the personnel who helped directly and indirectly to the establishment of this work particularly A. Ben Saad.

Contributors

A. Derbouz Rouibate conducted the experimental part, the collection, the interpretation of data and wrote the first draft of the manuscript. N. Benhafri helped in the experimental part of the work. A. Dekar-Madoui contributed to the conception and design of the study, supervised the experimental part of the work, and participated in data analysis and the correction of the paper. S. Ouali-Hassenaoui participated in analyzing data and drafting the final version of manuscript. All authors contributed to manuscript revision, read and approved the submitted final version.

Funding

This research was performed at the level of the Laboratory of Biology and Physiology of Organisms (LBPO), Faculty of Biological Sciences, USTHB, (Algiers, Algeria).

This work was supported by the General Direction of Scientific Research and Development of Technology (Ministry of Higher Education and Scientific Research, DGRSDT-MESRS), Algeria.

Conflicts of interest

The authors declare no conflict of interest.

References

1. Rosa RR, Bonnet MH, Bootzin RR, et al. Intervention factors for promoting adjustment to nightwork and shiftwork. Occup Med. 1990; 5(2):391–415. , indexed in Pubmed: 2203163.
2. Esseveldt Lv, Lehman M, Boer G. The suprachiasmatic nucleus and the circadian time-keeping system revisited. Brain Res Rev. 2000; 33(1): 34–77, doi: 10.1016/s0165-0173(00)00025-4.
3. Chou T, Scammell T, Gooley J, et al. Critical Role of Dorsomedial Hypothalamic Nucleus in a Wide Range of Behavioral Circadian Rhythms. J Neurosci. 2003; 23(33): 10691–10702, doi: 10.1523/jneurosci.23-33-10691.2003, indexed in Pubmed: 14627654.
4. Challet E. Horloges circadiennes, troubles métaboliques et chronobésité. Obésité. 2009; 4(1): 73–85, doi: 10.1007/s11690-009-0172-6.
5. Ralph MR, Foster RG, Davis FC, et al. Transplanted suprachiasmatic nucleus determines circadian period. Science. 1990; 247(4945): 975–978, doi: 10.1126/science.2305266, indexed in Pubmed: 2305266.
6. Schibler U, Ripperger J, Brown SA. Peripheral circadian oscillators in mammals: time and food. J Biol Rhythms. 2003; 18(3): 250–260, doi: 10.1177/0748730403018003007, indexed in Pubmed: 12828282.
7. Balsalobre A, Damiola F, Schibler U. A Serum Shock Induces Circadian Gene Expression in Mammalian Tissue Culture Cells. Cell. 1998; 93(6): 929–937, doi: 10.1016/s0092-8674(00)81199-x.
8. Kumar Jha P, Challet E, Kalsbeek A. Circadian rhythms in glucose and lipid metabolism in nocturnal and diurnal mammals. Mol Cell Endocrinol. 2015; 418 Pt 1: 74–88, doi: 10.1016/j.mce.2015.01.024, indexed in Pubmed: 25662277.
9. Bray MS, Ratcliffe WF, Grenett MH, et al. Quantitative analysis of light-phase restricted feeding reveals metabolic dyssynchrony in mice. Int J Obes (Lond). 2013; 37(6): 843–852, doi: 10.1038/ijo.2012.137, indexed in Pubmed: 22907695.
10. Puttonen S, Härmä M, Hublin C. Shift work and cardiovascular disease - pathways from circadian stress to morbidity. Scand J Work Environ Health. 2010; 36(2): 96–108, doi: 10.5271/sjweh.2894, indexed in Pubmed: 20087536.
11. Fritschi L, Glass DC, Heyworth JS, et al. Hypotheses for mechanisms linking shiftwork and cancer. Med Hypotheses. 2011; 77(3): 430–436, doi: 10.1016/j.mehy.2011.06.002, indexed in Pubmed: 21723672.
12. Stevens RG. Light-at-night, circadian disruption and breast cancer: assessment of existing evidence. Int J Epidemiol. 2009; 38(4): 963–970, doi: 10.1093/ije/dyp178, indexed in Pubmed: 19380369.
13. Kohyama J. A newly proposed disease condition produced by light exposure during night: asynchronization. Brain Dev. 2009; 31(4): 255–273, doi: 10.1016/j.braindev.2008.07.006, indexed in Pubmed: 18757146.
14. Scheer FA, Hilton MF, Mantzoros CS, et al. Adverse metabolic and cardiovascular consequences of circadian misalignment. Proc Natl Acad Sci U S A. 2009; 106(11): 4453–4458, doi: 10.1073/pnas.0808180106, indexed in Pubmed: 19255424.
15. Bedrosian TA, Nelson RJ. Influence of the modern light environment on mood. Mol Psychiatry. 2013; 18(7): 751–757, doi: 10.1038/mp.2013.70, indexed in Pubmed: 23711982.
16. Karlsson B, Knutsson A, Lindahl B. Is there an association between shift work and having a metabolic syndrome? Results from a population based study of 27,485 people. Occup Environ Med. 2001; 58(11): 747–752, doi: 10.1136/oem.58.11.747, indexed in Pubmed: 11600731.
17. Knutsson A. Health disorders of shift workers. Occup Med (Lond). 2003; 53(2): 103–108, doi: 10.1093/occmed/kqg048, indexed in Pubmed: 12637594.
18. Hassid WZ, Abraham S. [7] Chemical procedures for analysis of polysaccharides. Methods Enzymol. 1957: 34–50, doi: 10.1016/s0076-6879(57)03345-5.
19. Trinder P. Determination of Glucose in Blood Using Glucose Oxidase with an Alternative Oxygen Acceptor. Ann Clin Biochem. 1969; 6(1): 24–27, doi: 10.1177/000456326900600108.
20. Folch J, Lees M SGHS. A simple method for the isolation on purification of total lipids from animal tissues. J Biol Chem. 1957; 226(1):497–235. , doi: 10.0000/www.jbc.org/226/1/497.
21. Martoja R, Martoja-Pierson M. Initiation aux techniques de l'histologie animale. Elsevier Masson.; 1967.
22. Albrecht U, Eichele G. The mammalian circadian clock. Curr Opin Genet Dev. 2003; 13(3): 271–277, doi: 10.1016/s0959-437x(03)00055-8.
23. Reppert SM, Weaver DR. Molecular analysis of mammalian circadian rhythms. Annu Rev Physiol. 2001; 63: 647–676, doi: 10.1146/annurev.physiol.63.1.647, indexed in Pubmed: 11181971.
24. Mercer JG, Moar KM, Logie TJ, et al. Seasonally inappropriate body weight induced by food restriction: effect on hypothalamic gene expression in male Siberian hamsters. Endocrinology. 2001; 142(10): 4173–4181, doi: 10.1210/endo.142.10.8454, indexed in Pubmed: 11564670.
25. Huang Z, Liu Q, Peng Yu, et al. Circadian Rhythm Dysfunction Accelerates Disease Progression in a Mouse Model With Amyotrophic Lateral Sclerosis. Front Neurol. 2018; 9: 218, doi: 10.3389/fneur.2018.00218, indexed in Pubmed: 29740382.
26. McDonald RB, Hoban-Higgins TM, Ruhe RC, et al. Alterations in endogenous circadian rhythm of core temperature in senescent Fischer 344 rats. Am J Physiol. 1999; 276(3 Pt 2): R824–R830, doi: 10.1152/ajpregu.1999.276.3.r824, indexed in Pubmed: 10070144.
27. Sen S, Raingard H, Dumont S, et al. Ultradian feeding in mice not only affects the peripheral clock in the liver, but also the master clock in the brain. Chronobiol Int. 2017; 34(1): 17–36, doi: 10.1080/07420528.2016.1231689, indexed in Pubmed: 27668547.
28. Karatsoreos IN, Bhagat S, Bloss EB, et al. Disruption of circadian clocks has ramifications for metabolism, brain, and behavior. Proc Natl Acad Sci U S A. 2011; 108(4): 1657–1662, doi: 10.1073/pnas.1018375108, indexed in Pubmed: 21220317.
29. de Goede P, Sen S, Su Y, et al. An Ultradian Feeding Schedule in Rats Affects Metabolic Gene Expression in Liver, Brown Adipose Tissue and Skeletal Muscle with Only Mild Effects on Circadian Clocks. Int J Mol Sci. 2018; 19(10), doi: 10.3390/ijms19103171, indexed in Pubmed: 30326619.

30. Fonken LK, Workman JL, Walton JC, et al. Light at night increases body mass by shifting the time of food intake. Proc Natl Acad Sci U S A. 2010; 107(43): 18664–18669, doi: 10.1073/pnas.1008734107, indexed in Pubmed: 20937863.
31. Coomans CP, van den Berg SAA, Houben T, et al. Detrimental effects of constant light exposure and high-fat diet on circadian energy metabolism and insulin sensitivity. FASEB J. 2013; 27(4): 1721–1732, doi: 10.1096/fj.12-210898, indexed in Pubmed: 23303208.
32. Shi Sq, Ansari TS, McGuinness OP, et al. Circadian disruption leads to insulin resistance and obesity. Curr Biol. 2013; 23(5): 372–381, doi: 10.1016/j.cub.2013.01.048, indexed in Pubmed: 23434278.
33. Dauchy RT, Dauchy EM, Tirrell RP, et al. Dark-phase light contamination disrupts circadian rhythms in plasma measures of endocrine physiology and metabolism in rats. Comp Med. 2010; 60(5):348–356. , indexed in Pubmed: 21262119.
34. Kettner NM, Voicu H, Finegold MJ, et al. Circadian Homeostasis of Liver Metabolism Suppresses Hepatocarcinogenesis. Cancer Cell. 2016; 30(6): 909–924, doi: 10.1016/j.ccell.2016.10.007, indexed in Pubmed: 27889186.
35. Challet E. Circadian clocks, food intake, and metabolism. Prog Mol Biol Transl Sci. 2013; 119: 105–135, doi: 10.1016/B978-0-12-396971-2.00005-1, indexed in Pubmed: 23899596.
36. Stokkan KA, Yamazaki S, Tei H, et al. Entrainment of the circadian clock in the liver by feeding. Science. 2001; 291(5503): 490–493, doi: 10.1126/science.291.5503.490, indexed in Pubmed: 11161204.
37. Tarquini R, Mazzoccoli G. Clock Genes, Metabolism, and Cardiovascular Risk. Heart Fail Clin. 2017; 13(4): 645–655, doi: 10.1016/j.hfc.2017.05.001, indexed in Pubmed: 28865774.
38. Manoogian ENC, Panda S. Circadian rhythms, time-restricted feeding, and healthy aging. Ageing Res Rev. 2017; 39: 59–67, doi: 10.1016/j.arr.2016.12.006, indexed in Pubmed: 28017879.
39. Damiola F, Le Minh N, Preitner N, et al. Restricted feeding uncouples circadian oscillators in peripheral tissues from the central pacemaker in the suprachiasmatic nucleus. Genes Dev. 2000; 14(23): 2950–2961, doi: 10.1101/gad.183500, indexed in Pubmed: 11114885.
40. Challet E, Malan A, Turek FW, et al. Daily variations of blood glucose, acid-base state and PCO2 in rats: effect of light exposure. Neurosci Lett. 2004; 355(1-2): 131–135, doi: 10.1016/j.neulet.2003.10.041, indexed in Pubmed: 14729252.
41. Gale JE, Cox HI, Qian J, et al. Disruption of circadian rhythms accelerates development of diabetes through pancreatic beta-cell loss and dysfunction. J Biol Rhythms. 2011; 26(5): 423–433, doi: 10.1177/0748730411416341, indexed in Pubmed: 21921296.
42. Nagai K, Nagai N, Sugahara K, et al. Circadian rhythms and energy metabolism with special reference to the suprachiasmatic nucleus. Neurosci Biobehav Rev. 1994; 18(4): 579–584, doi: 10.1016/0149-7634(94)90014-0.
43. Turek FW, Joshu C, Kohsaka A, et al. Obesity and metabolic syndrome in circadian Clock mutant mice. Science. 2005; 308(5724): 1043–1045, doi: 10.1126/science.1108750, indexed in Pubmed: 15845877.
44. Yamazaki S, Numano R, Abe M, et al. Resetting central and peripheral circadian oscillators in transgenic rats. Science. 2000; 288(5466): 682–685, doi: 10.1126/science.288.5466.682, indexed in Pubmed: 10784453.
45. Szántóová K, Zeman M, Veselá A, et al. Effect of phase delay lighting rotation schedule on daily expression of per2, bmal1, rev-erbα, pparα, and pdk4 genes in the heart and liver of Wistar rats. Mol Cell Biochem. 2011; 348(1-2): 53–60, doi: 10.1007/s11010-010-0636-x, indexed in Pubmed: 21076970.
46. Doi R, Oishi K, Ishida N. CLOCK regulates circadian rhythms of hepatic glycogen synthesis through transcriptional activation of Gys2. J Biol Chem. 2010; 285(29): 22114–22121, doi: 10.1074/jbc.M110.110361, indexed in Pubmed: 20430893.
47. Schmutz I, Ripperger JA, Baeriswyl-Aebischer S, et al. The mammalian clock component PERIOD2 coordinates circadian output by interaction with nuclear receptors. Genes Dev. 2010; 24(4): 345–357, doi: 10.1101/gad.564110, indexed in Pubmed: 20159955.
48. Zhao Y, Zhang Y, Zhou M, et al. Loss of mPer2 increases plasma insulin levels by enhanced glucose-stimulated insulin secretion and impaired insulin clearance in mice. FEBS Lett. 2012; 586(9): 1306–1311, doi: 10.1016/j.febslet.2012.03.034, indexed in Pubmed: 22504074.
49. Zani F, Breasson L, Becattini B, et al. PER2 promotes glucose storage to liver glycogen during feeding and acute fasting by inducing Gys2 PTG and G L expression. Mol Metab. 2013; 2(3): 292–305, doi: 10.1016/j.molmet.2013.06.006, indexed in Pubmed: 24049741.
50. Voet D, Voet JG, Pratt CW. Principles of Biochemistry. John Wiley & Sons. ; 2008.
51. Pearson MJ, Unger RH, Holland WL. Clinical Trials, Triumphs, and Tribulations of Glucagon Receptor Antagonists. Diabetes Care. 2016; 39(7): 1075–1077, doi: 10.2337/dci15-0033, indexed in Pubmed: 27330122.
52. Panda S, Antoch M, Miller B, et al. Coordinated Transcription of Key Pathways in the Mouse by the Circadian Clock. Cell. 2002; 109(3): 307–320, doi: 10.1016/s0092-8674(02)00722-5.
53. Storch K-F, Lipan O, Leykin I, et al. Extensive and divergent circadian gene expression in liver and heart. Nature. 2002; 417(6884):78–83. , doi: 10.1038/nature744, indexed in Pubmed: 11967526.
54. Lamia KA, Storch KF, Weitz CJ. Physiological significance of a peripheral tissue circadian clock. Proc Natl Acad Sci U S A. 2008; 105(39): 15172–15177, doi: 10.1073/pnas.0806717105, indexed in Pubmed: 18779586.
55. Reinke H, Asher G. Circadian Clock Control of Liver Metabolic Functions. Gastroenterology. 2016; 150(3): 574–580, doi: 10.1053/j.gastro.2015.11.043, indexed in Pubmed: 26657326.
56. Romon M, Nuttens MC, Fievet C, et al. Increased triglyceride levels in shift workers. Am J Med. 1992; 93(3): 259–262, doi: 10.1016/0002-9343(92)90230-9.
57. Itani O, Kaneita Y, Tokiya M, et al. Short sleep duration, shift work, and actual days taken off work are predictive life-style risk factors for new-onset metabolic syndrome: a seven-year cohort study of 40,000 male workers. Sleep Med. 2017; 39: 87–94, doi: 10.1016/j.sleep.2017.07.027, indexed in Pubmed: 29157594.
58. Lu YC, Wang CP, Yu TH, et al. Shift work is associated with metabolic syndrome in male steel workers-the role of resistin and WBC count-related metabolic derangements. Diabetol Metab Syndr. 2017; 9: 83, doi: 10.1186/s13098-017-0283-4, indexed in Pubmed: 29075331.
59. Pan X, Hussain MM. Clock is important for food and circadian regulation of macronutrient absorption in mice. J Lipid Res. 2009; 50(9): 1800–1813, doi: 10.1194/jlr.M900085-JLR200, indexed in Pubmed: 19387090.
60. Pan X, Hussain MM. Diurnal regulation of microsomal triglyceride transfer protein and plasma lipid levels. J Biol Chem. 2007; 282(34): 24707–24719, doi: 10.1074/jbc.M701305200, indexed in Pubmed: 17575276.
61. Rudic RD, McNamara P, Curtis AM, et al. BMAL1 and CLOCK, two essential components of the circadian clock, are involved in glucose homeostasis. PLoS Biol. 2004; 2(11): e377, doi: 10.1371/journal.pbio.0020377, indexed in Pubmed: 15523558.

62. Grimaldi B, Bellet MM, Katada S, et al. PER2 controls lipid metabolism by direct regulation of PPARγ. Cell Metab. 2010; 12(5): 509–520, doi: 10.1016/j.cmet.2010.10.005, indexed in Pubmed: 21035761.
63. Su Y, Foppen E, Mansur Machado FS, et al. The role of the daily feeding rhythm in the regulation of the day/night rhythm in triglyceride secretion in rats. Chronobiol Int. 2018; 35(7): 885–895, doi: 10.1080/07420528.2018.1438456, indexed in Pubmed: 29446660.
64. Pan X, Munshi MK, Iqbal J, et al. Circadian regulation of intestinal lipid absorption by apolipoprotein AIV involves forkhead transcription factors A2 and O1 and microsomal triglyceride transfer protein. J Biol Chem. 2013; 288(28): 20464–20476, doi: 10.1074/jbc.M113.473454, indexed in Pubmed: 23729668.
65. Shamsi NA, Salkeld MD, Rattanatray L, et al. Metabolic consequences of timed feeding in mice. Physiol Behav. 2014; 128: 188–201, doi: 10.1016/j.physbeh.2014.02.021, indexed in Pubmed: 24534172.
66. Yasumoto Y, Hashimoto C, Nakao R, et al. Short-term feeding at the wrong time is sufficient to desynchronize peripheral clocks and induce obesity with hyperphagia, physical inactivity and metabolic disorders in mice. Metabolism. 2016; 65(5): 714–727, doi: 10.1016/j.metabol.2016.02.003, indexed in Pubmed: 27085778.
67. Bailey SM, Udoh US, Young ME. Circadian regulation of metabolism. J Endocrinol. 2014; 222(2): R75–R96, doi: 10.1530/JOE-14-0200, indexed in Pubmed: 24928941.
68. Gimble JM, Floyd ZE. Fat circadian biology. J Appl Physiol (1985). 2009; 107(5): 1629–1637, doi: 10.1152/japplphysiol.00090.2009, indexed in Pubmed: 19470701.
69. Sassolas A, Cartier R. Hypocholesterolemias: causes and diagnosis. Ann Biol Clin. 1999; 57(5):555–60. , indexed in Pubmed: 10518057.
70. Adamovich Y, Aviram R, Asher G. The emerging roles of lipids in circadian control. Biochim Biophys Acta. 2015; 1851(8): 1017–1025, doi: 10.1016/j.bbalip.2014.11.013, indexed in Pubmed: 25483623.
71. Mathurin P, Poynard T. Pharmacological treatment for alcoholic hepatitis and cirrhosis. Ethanol and the Liver. 2013: 592–613, doi: 10.3109/9780203301388-31.
72. SAWADOGO A, DIB N, CALES P. Physiopathologie de la cirrhose et de ses complications. Réanimation. 2007; 16(7-8): 557–562, doi: 10.1016/j.reaurg.2007.09.001.
73. Suffredini A, Fantuzzi G, Badolato R, et al. New insights into the biology of the acute phase response. J Clin Immunol. 1999; 19(4): 203–214, doi: 10.1023/a:1020563913045.
74. Gregory SH, Wing EJ. Neutrophil-Kupffer cell interaction: a critical component of host defenses to systemic bacterial infections. J Leukoc Biol. 2002; 72(2):239–248. , doi: 10.1189/jlb.72.2.239.
75. Wick M, Leithauser F, Reimann J. The Hepatic Immune System. Crit Rev Immunol. 2002; 22(1): 57, doi: 10.1615/critrevimmunol.v22.i1.30.
76. Jawhara S, Thuru X, Standaert-Vitse A, et al. Colonization of mice by Candida albicans is promoted by chemically induced colitis and augments inflammatory responses through galectin-3. J Infect Dis. 2008; 197(7): 972–980, doi: 10.1086/528990, indexed in Pubmed: 18419533.
77. Kim HW, Uh DK, Yoon SY, et al. Low-frequency electroacupuncture suppresses carrageenan-induced paw inflammation in mice via sympathetic post-ganglionic neurons, while high-frequency EA suppression is mediated by the sympathoadrenal medullary axis. Brain Res Bull. 2008; 75(5): 698–705, doi: 10.1016/j.brainresbull.2007.11.015, indexed in Pubmed: 18355649.
78. Faith M, Sukumaran A, Pulimood AB, et al. How reliable an indicator of inflammation is myeloperoxidase activity? Clin Chim Acta. 2008; 396(1-2): 23–25, doi: 10.1016/j.cca.2008.06.016, indexed in Pubmed: 18619953.
79. McConnico RS, Weinstock D, Poston ME, et al. Myeloperoxidase activity of the large intestine in an equine model of acute colitis. Am J Vet Res. 1999; 60(7): 807–813. , indexed in Pubmed: 10407471.
80. Zhang C, Patel R, Eiserich JP, et al. Endothelial dysfunction is induced by proinflammatory oxidant hypochlorous acid. Am J Physiol Heart Circ Physiol. 2001; 281(4): H1469––H1475, doi: 10.1152/ajpheart.2001.281.4.H1469, indexed in Pubmed: 11557534.
81. Hoy A, Leininger-Muller B, Kutter D, et al. Growing significance of myeloperoxidase in non-infectious diseases. Clin Chem Lab Med. 2002; 40(1): 2–8, doi: 10.1515/CCLM.2002.002, indexed in Pubmed: 11916266.
82. Heinecke J. Mechanisms of oxidative damage by myeloperoxidase in atherosclerosis and other inflammatory disorders. J Lab Clin Med. 1999; 133(4): 321–325, doi: 10.1016/s0022-2143(99)90061-6.
83. Nahon P, Sutton A, Rufat P, et al. Myeloperoxidase and superoxide dismutase 2 polymorphisms comodulate the risk of hepatocellular carcinoma and death in alcoholic cirrhosis. Hepatology. 2009; 50(5): 1484–1493, doi: 10.1002/hep.23187, indexed in Pubmed: 19731237.
84. Winterbourn CC, Brennan SO. Characterization of the oxidation products of the reaction between reduced glutathione and hypochlorous acid. Biochem J. 1997; 326 (Pt 1): 87–92, doi: 10.1042/bj3260087, indexed in Pubmed: 9337854.
85. Jarnagin WR, Rockey DC, Koteliansky VE, et al. Expression of variant fibronectins in wound healing: cellular source and biological activity of the EIIIA segment in rat hepatic fibrogenesis. J Cell Biol. 1994; 127(6 Pt 2): 2037–2048, doi: 10.1083/jcb.127.6.2037, indexed in Pubmed: 7806580.
86. Gressner AM, Bachem MG. Molecular mechanisms of liver fibrogenesis--a homage to the role of activated fat-storing cells. Digestion. 1995; 56(5): 335–346, doi: 10.1159/000201257, indexed in Pubmed: 8549875.
87. Bekheet IW, Madkour ME, Ghaffar N, et al. The Role of Myeloperoxidase in Hepatitis C Virus Infection and Associated Liver Cirrhosis. Open Trop Med J. 2009; 2(1): 1–7, doi: 10.2174/1874315300902010001.
88. Abdel-Hamid M, Nada O, Ellakwa DS, et al. Role of Myeloperoxidase in hepatitis C virus related hepatocellular carcinoma. Meta Gene. 2018; 18: 1–8, doi: 10.1016/j.mgene.2018.07.008.
89. Friedman SL. Hepatic stellate cells: protean, multifunctional, and enigmatic cells of the liver. Physiol Rev. 2008; 88(1): 125–172, doi: 10.1152/physrev.00013.2007, indexed in Pubmed: 18195085.
90. DeLeve LD, Jaeschke H, Kalra VK, et al. 15th International Symposium on Cells of the Hepatic Sinusoid, 2010. Liver Int. 2011; 31(6): 762–772, doi: 10.1111/j.1478-3231.2011.02527.x, indexed in Pubmed: 21645207.

Submitted: 3 February, 2020
Accepted after reviews: 13 September, 2020
Available as AoP: 22 September, 2020

FOLIA HISTOCHEMICA ET CYTOBIOLOGICA
Vol. 58, No. 3, 2020
pp. 198–207

ORIGINAL PAPER

VIA MEDICA

Wilms' tumor 1 antigen immunoreactivity in epithelial ovarian cancer — diagnostic and prognostic value

Elzbieta Zarychta[1], Katarzyna Lepinay[1], Sebastian Szubert[1], Jakub Jozwicki[2], Jan Misiak[3], Anna A. Brozyna[4], Katarzyna Kosinska-Kaczynska[1], Agnieszka Lewandowska[1], Ewa Malicka[1], Adrianna Makarewicz[5], Piotr Rhone[6], Wojciech Jozwicki[3]

[1]Second Department of Obstetrics and Gynecology, Centre of Postgraduate Medical Education, Warsaw, Poland
[2]Department of Clinical Pathomorphology, Faculty of Medicine, Ludwik Rydygier Collegium Medicum in Bydgoszcz, Nicolaus Copernicus University, Torun, Poland
[3]Department of Tumor Pathology and Pathomorphology, Department of Oncology, Faculty of Health Sciences, Ludwik Rydygier Collegium Medicum in Bydgoszcz, Nicolaus Copernicus University, Torun, Poland
[4]Department of Human Biology, Institute of Biology, Faculty of Biological and Veterinary Sciences, Nicolaus Copernicus University, Torun, Poland
[5]Department of Oncology, The Franciszek Lukaszczyk Oncological Center, Bydgoszcz, Poland
[6]Department of Clinical Breast Cancer and Reconstructive Surgery, The Franciszek Lukaszczyk Oncological Center, Bydgoszcz, Poland

Abstract

Objectives. Ovarian cancer is a heterogeneous disease, with a number of different histological subtypes with various responses to treatment. Wilms' tumor 1 (WT1) immunoreactivity is used to distinguish between OC's various subtypes. However, little is known about the protein's role as a prognostic factor. Thus, the main aim of our study was to evaluate the relationship between WT1 expression and patient overall survival (OS) and lymph node metastases.

Materials and methods. Study group consisted of 164 women aged 22–84, diagnosed with epithelial ovarian cancer (EOC). WT1 expression in histological slides was assessed by immunohistochemistry.

Results. Serous tumors were the most common subtype among EOC (n = 126; 76.8%), followed by endometrioid (n = 20; 12.2%), clear-cell (n = 14; 8.5%) and mucinous cancer (n = 4; 2.4%). Of all serous EOC, WT1-positive tumors accounted for 75.6% of cases and this number was significantly higher than in other histological subtypes ($p < 0.0001$). Patients with lymph node metastases were more likely to have WT1-positive than WT1-negative tumors ($p = 0.006$). There was no significant correlation between WT1 immunoreactivity and OS across the whole study group of EOC patients ($p = 0.6$); however, in the group of non-serous (mucinous, endometrioid and clear-cell) EOC subjects, WT1 immunoreactivity was associated with shorter OS ($p = 0.046$).

Conclusions. WT1 immunoreactivity may be helpful in differentiating primary epithelial serous carcinomas from non-serous ovarian cancers; however, its prognostic role in EOC is rather uncertain. *(Folia Histochemica et Cytobiologica 2020, Vol. 58, No. 3, 198–207)*

Key words: epithelial ovarian cancer; WT1; Wilms' tumor antigen 1; lymph node metastases

Correspondence address: Prof. Wojciech Jozwicki, MD., PhD
Department of Tumor Pathology and Pathomorphology,
Department of Oncology, Faculty of Health Sciences,
Ludwik Rydygier Collegium Medicum in Bydgoszcz, Nicolaus Copernicus University in Torun, Torun, Poland
2 Romanowska St., Bydgoszcz 85–796, Poland
e-mail: jozwickiw@co.bydgoszcz.pl

Introduction

In 2018 over 295 000 women worldwide were diagnosed with ovarian cancer (OC) and almost 185 000 women died because of this malignancy, making it the eight most common cause of cancer death in females [1]. Well-established risk factors of ovarian cancer are a family history of ovarian or breast cancer, BRCA1 and BRCA2 mutations, Lynch syndrome, hereditary non-polyposis colon cancer (HNPCC), nulliparity or low parity, use of hormone replacement therapy, menarche at an early age, greater height, being overweight, tobacco smoking and diagnosis of endometriosis [2, 3]. Ovarian cancer is a highly heterogeneous disease that involves malignancies with various histological features, site of origin, grade, risk factors, prognoses and treatment. According to tumor cell histology, the main types of epithelial ovarian cancer are serous (52%), endometrioid (10%), mucinous (6%) and clear-cell (6%). About one quarter of epithelial ovarian cancers are classified as either unspecified or rarer subtypes of ovarian cancer. Non-epithelial cancers make up approximately 10% of all ovarian neoplasms and are of secondary importance [4].

Wilms' tumor 1 (WT1) is a transcription factor involved in the regulation of genes such as growth factors, regulators of cell cycle and apoptosis. Primarily regarded as a tumor suppressor gene, it is now considered to have oncogenic functions. WT1 is located on chromosome 11 and its expression is found in normal human tissues such as the kidney, ovary, testis, spleen, peritoneal mesothelium and fallopian tube epithelium, as well as in leukemias (where WT1 mRNA expression levels increase along with progression of the disease) and various types of solid tumors, including ovarian cancer. WT1 gene expression levels in many tumors may serve as a prognostic factor. Previous studies demonstrated that in leukemias, as well as in solid cancer cells, induction of WT1 expression promoted cell growth and motility together with suppression of apoptosis [5–10].

Most patients with epithelial ovarian cancer (EOC) present with advanced stage disease. Prognosis is strongly associated with the disease stage at the time of diagnosis, and the prognosis also differs largely according to epithelial subtype. Serous carcinomas are diagnosed mostly at stage III (51%) or IV (29%), while more than half (58−64%) of endometroid, mucinous, and clear cell carcinomas are diagnosed at stage I. Apart from stage, other factors associated with poor prognosis are high histological grade, patient age of 65 years or older, large volume of the residual tumor, and low global quality-of-life score. However, while WT1's role in distinguishing serous EOC from other subtypes of ovarian cancer seems to be established, there are still discrepancies regarding its role in prognosis in both serous and non-serous EOC [4, 11–14].

The aims of this study were to establish whether the presence of WT1 immunoreactivity in ovarian cancer cells varies between particular histological subtypes of the malignancy, to determine whether it is associated with lymph node metastases, and to assess its prognostic value.

Material and methods

Patient samples and clinical data. Our study group comprised 164 women aged 22 to 84 (age 59.45 ± 11.27; mean ± SD) diagnosed with EOC. All patients were operated on between March 2010 and March 2018 in the Clinical Department of Gynecological Oncology, The Franciszek Lukaszczyk Oncological Center Bydgoszcz, Poland; and each patient underwent a comprehensive histopathological confirmation of the diagnosis along with an analysis of WT1 immunoreactivity in cancer cells. Disease stage was assigned in accordance with the International Federation of Gynecology and Obstetrics (FIGO) surgical staging criteria. The histologic grade was categorized as either high or low. The clinicopathological characteristics of the study group are shown in Table 1.

Patients underwent longitudinal laparotomy extending from the xiphoid process to the pubic bone. All of the patients underwent bilateral/unilateral salpingoophorectomy and pelvic peritonectomy with retroperitoneal hysterectomy or, in the case of previous hysterectomy, vaginal vault resection. Additionally, total omentectomy was performed. Appendectomy was performed in cases of tumor infiltration or where there was suspicion of the mucinous type of ovarian cancer. Lymphadenectomy was always performed in cases where enlarged or suspicious lymph nodes were found. In cases where the lymph nodes were unchanged, the primary surgeon decided whether to perform lymphadenectomy. The resection of other organs was performed when necessary, depending on the degree of tumor infiltration, in order to remove all macroscopic lesions. All surgeries were performed by accredited gynecological oncologists (in most cases, L.W.). The extent of post-surgery residual disease was described according to Sugarbaker score [15]. All patients had received first-line chemotherapy consisting of intravenous carboplatin and paclitaxel.

The present study was approved by the Human Research Ethics Committee of Centre of Postgraduate Medical Education in Warsaw (8/PB/2020). The study was conducted in accordance with the ethical standards and principles embodied in the Declaration of Helsinki. All subjects provided written informed consent to participate in this study after receiving a full explanation of the aim of the study.

Table 1. Clinicopathological characteristics of the study group

Type of EOC	Serous N	Mucinous N	Endometrioid N	Clear cell N	Total N
Number of patients	126	4	14	20	164
Mean age	59.56	54	60.15	59.42	59.45
Lymph nodes:					
Positive	29	0	1	2	32
Negative	97	4	13	18	132
Grade					
Low grade	1	1	0	3	2
High grade (G2, G3)	125	3	14	17	162
FIGO stage					
I	14	0	1	4	19
II	11	0	4	6	21
III	91	3	9	10	113
IV	10	1	0	0	11
CC					
0	75	2	8	16	101
1	15	0	2	0	17
2	22	1	3	3	29
3	14	1	1	1	17

Abbreviations: EOC — epithelial ovarian cancer; CC — completeness of cytoreduction according to Sugarbaker score [15].

Immunohistochemistry. Immunohistochemistry staining was performed with mouse monoclonal WT1 antibody (Roche/Ventana, Oro Valley, AZ, USA, 6F-H2 clone, #760-4397) and an ultraView Universal DAB Detection Kit chromogen (Roche/Ventana, #760-500) using a Benchmark Ultra instrument (Roche/Ventana).

Staining of all samples was done on 4 μm tissue sections which were obtained from tumor samples fixed in 4% buffered formaldehyde and embedded in paraffin blocks according to a standard protocol. Paraffin block sections were placed on adhesive slides (Knittel Glass) and incubated for 2 h at 60°C in a thermostatic chamber.

All the steps of the IHC staining were automated using a Benchmark Ultra instrument (Roche/Ventana). The final step involved dehydration in a series of ethanol concentrations and xylene followed by a coverslip mounting medium (Consul Mount Shandon, Thermo Scientific, Kalamazoo, MI, USA). Each patient sample series included a control sample as recommended by the manufacturer. In each case, the level of WT1 expression was assessed as either negative or positive (see Figs. 1B, 1D, and 1F, 1H respectively). WT1 expression was assessed independently by two pathologists. The histological classification of the tumors was performed according to the WHO Classification of Tumors.

Microscopic assessment was performed with the use of a Nikon Eclipse 80i microscope (Nikon, Tokyo, Japan). Pictures were taken with a Nikon Digital Sight DS Fi1-U2 camera and with NISElements BR 3.0 software (Nikon Instruments Europe B.V., Badhoevedorp, The Netherlands).

Statistical analysis. Categorical data were analyzed using the Fisher's exact test, and with the Freeman-Halton extension when appropriate. We performed multiple-regression model with stepwise entering method to evaluate the relationship between WT1 immunoreactivity and clinicopathological features of EOC disease. Survival analysis was conducted using Kaplan-Meier survival curves. The log-rank test was used for the comparing survival distributions between the analyzed subgroups. P-values < 0.05 were considered significant.

Results

WT1 immunoreactivity in EOC

A total of 164 subjects were included in our study. The most common type of ovarian epithelial cancer in the study group was serous (n = 126; 76.8%), followed by endometrioid (n = 20; 12.2%), clear cell (n = 14; 8.5%) and mucinous (n = 4; 2.4%). The number of WT1-positive and negative tumors varied significantly between the particular types of EOC and the data are shown in Table 2 ($p < 0.0001$).When we compared serous and non-serous EOC, we have found

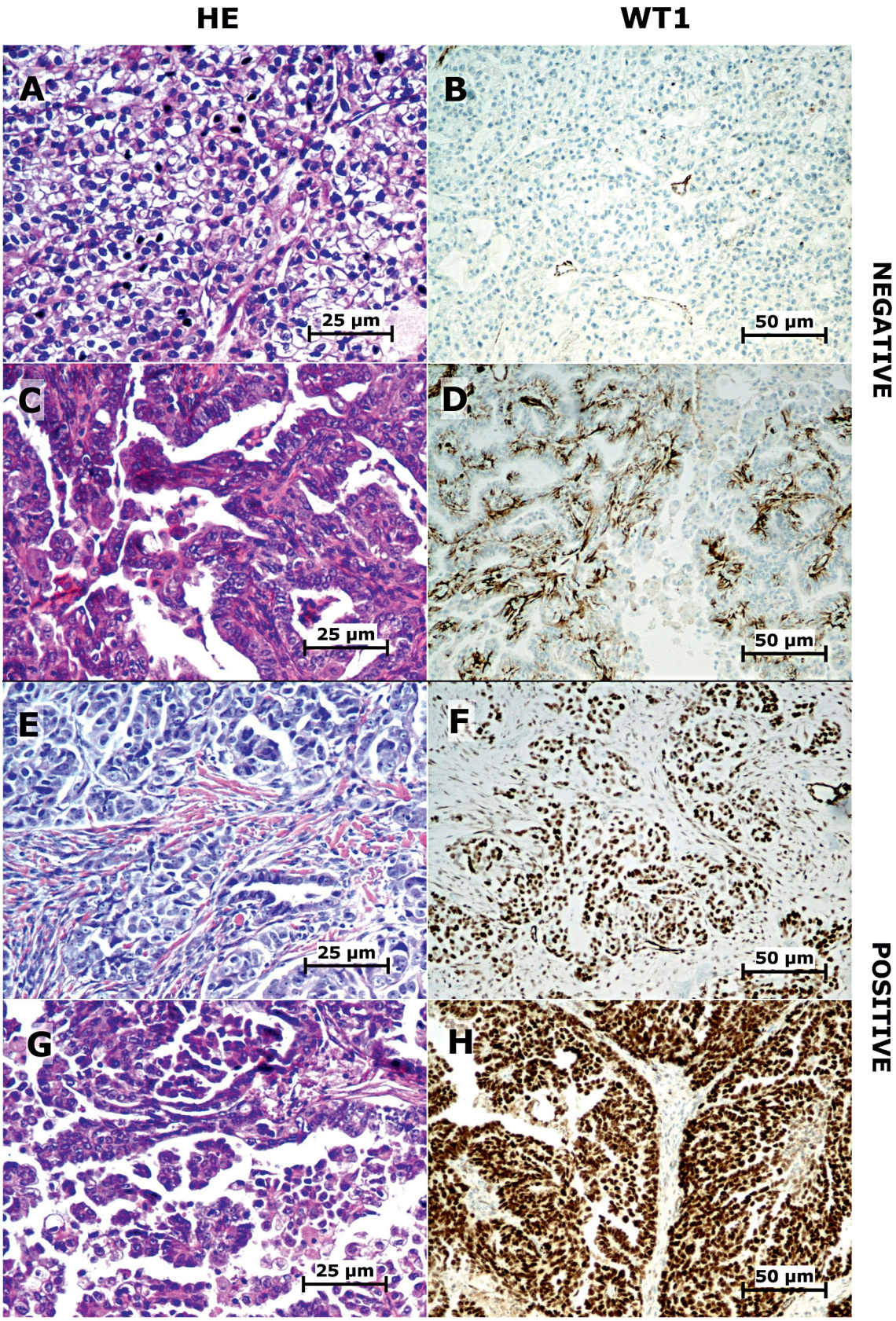

Figure 1. Representative staining intensity of WT1 in ovarian cancer (OC) cells, defined as either negative (no cellular expression **(B)** or with membrane reactivity but without nuclear expression **(D)**), or positive (low and mediate **(F)** or high **(H)** expression), regardless of the histological type of cancer (A — clear-cell type, C — endometrioid type, E and G — serous type).

Table 2. WT1 immunoreactivity in different histological types of EOC

Type of EOC	Serous N (%)	Mucinous N (%)	Clear-cell N (%)	Endometrioid N (%)	Total N (%)	p-value
WT1 (+)	106	0	9	9	124	P < 0.0001
WT1 (–)	20	4	5	11	40	
Total	126 (76.83)	4 (2.44)	14 (8.54)	20 (12.19)	164 (100)	

Abbreviations: WT1 — Wilms' tumor; EOC — epithelial ovarian cancer.

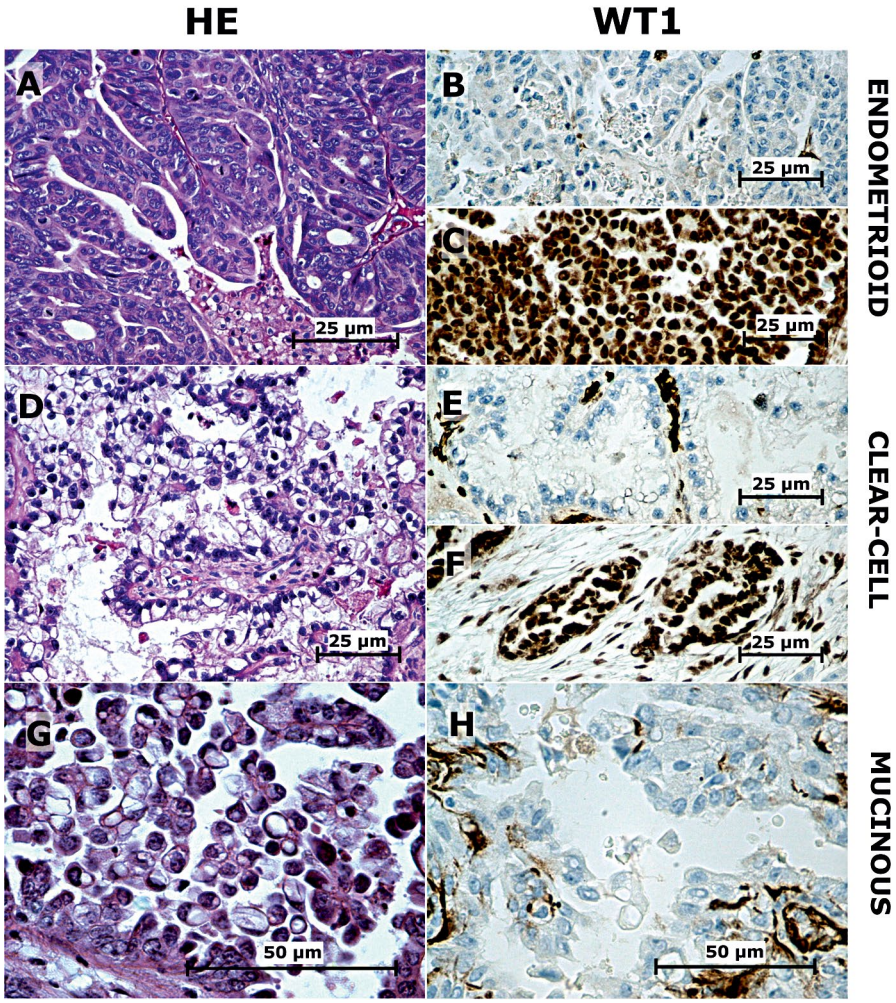

Figure 2. The complete absence of WT1 nuclear expression was observed in mucinous ovarian cancers **(G–H).** In contrast, endometrioid **(A)** and clear cell **(D)** carcinomas varied in terms of the intensity of WT1 expression (B *vs.* C and E *vs.* F).

significantly higher WT1 immunoreactivity in serous EOC (84% *vs.* 47%, P < 0.0001). In the multiple regression model including the following independent variables: histopathological type of the tumor (serous *vs.* non-serous), post-surgery residual disease, lymph node metastases; only the tumor histopathological type (P < 0.0001) was significantly associated with WT1 immunoreactivity.

The presence or absence of expression was observed in all non-serous ovarian cancers except mucinous (Fig. 2).

WT1 immunoreactivity and lymph nodes metastases

Furthermore, we analyzed the histological types of ovarian cancer and WT1 immunoreactivity in patients with lymph node metastases. In general, metastatic

Table 3. Different histological types of EOC in WT1-positive and WT1-negative patients with lymph node metastases

Type of EOC	Serous N	Non-serous N	Total N	p-value
WT1-positive	28	2	30	P = 0.2
WT1-negative	1	1	2	

Abbreviations as for table 2.

Table 4. Presence of lymph node metastases in WT1-positive patients *vs.* WT1-negative patients

Presence of lymph nodes metastases	LN (+) N (%)	LN (–) N (%)	Total N (%)	p-value
WT1-positive	30 (24.19)	94 (75.81)	124 (100)	P = 0.006
WT1-negative	2 (5.0)	38 (95.00)	40 (100)	

Abbreviations: WT1 — Wilms' tumor; LN — lymph nodes.

lymph nodes were confirmed in 32 (19.5%) patients. In the serous tumors, the metastatic spread of the disease was found in 23% of the cases; in the clear cell cancers in 14.3% of the cases; in the endometrioid in 5% of the cases; and in the mucinous ovarian cancers there were no cases of metastatic lymph nodes. In the group of both WT1-positive and WT1-negative patients with metastatic lymph nodes, the presence of lymph node metastases did not differ significantly according to the type of cancer, whether serous or non-serous, p = 0.2). The results are shown in Table 3.

Subsequently, statistical calculations were made on the study group data based on the presence of lymph node metastases and WT1 immunoreactivity. Patients with WT1-positive tumors were more likely to have lymph node metastases; specifically, 30 out of 124 (24.2%) WT1-positive patients had affected LN compared with 2 out of 40 (5%) WT1-negative patients (Table 4). The differences between these groups were statistically significant (p = 0.006).

Survival analysis

The correlation between WT1 immunoreactivity and overall survival (OS) in patients with epithelial ovarian cancer was evaluated *via* Kaplan-Meier curves. Survival analysis included 164 EOC patients: 124 women with WT1 immunoreactivity and 40 without WT1 immunoreactivity. The median OS for the first group was 1084 days, while the median OS in second group was not reached. The presence of WT1 immunoreactivity in the tumor cells did not correlate with a shorter OS (HR (95% CI) = 1.2594 (0.7746–2.0477), p = 0.4) in members of the group comprising all ovarian cancer patients (Fig. 3A).

Finally, the prognostic value of WT1 in ovarian cancer with different histological subtypes was assessed. Patients were divided into two subgroups: serous and non-serous (mucinous, endometrioid and clear-cell). Among serous ovarian cancer patients with the presence of WT1 in cancer cells, OS was shorter than among WT1-negative patients; however, the difference was not statistically significant (HR (95%CI) = 0.8643 (0.4389–1.7020), P = 0.6)] (Fig. 3B). On the other hand, in the non-serous group, WT1-positive patients presented with a significantly shorter OS than the WT1-negative patients (HR (95%CI) = 2.6400 (1.0042–6.9404), P = 0.046) (Fig. 3C).

Discussion

In our study, we investigated WT1 immunoreactivity in different histological subtypes of ovarian cancer as well as its association with the presence of lymph node metastases. We analyzed the overall survival rates of the whole study group of WT1-positive and WT1-negative patients as well as considering the OS rates for serous and non-serous tumors.

Various studies have found WT1-positivity in serous ovarian tumors to range between 61 and 97% [16–21]. The percentage of ovarian serous carcinoma expressing WT1 in our study (84%) fell within the range of values reported in those studies. Furthermore, in our study we found no WT1-positive mucinous tumors, which was a similar result to those of other authors [18, 19, 21]. However, there were discrepancies between our study and others' concerning endometrioid and clear-cell EOCs. We found WT1 immunoreactivity in 64% of clear-cell ovarian carcinomas, which diverges from the results obtained by Hylander *et al.* (20% of WT1-positive clear-cell carcinomas) [16] and Acs *et al.* (22% of WT1-positive

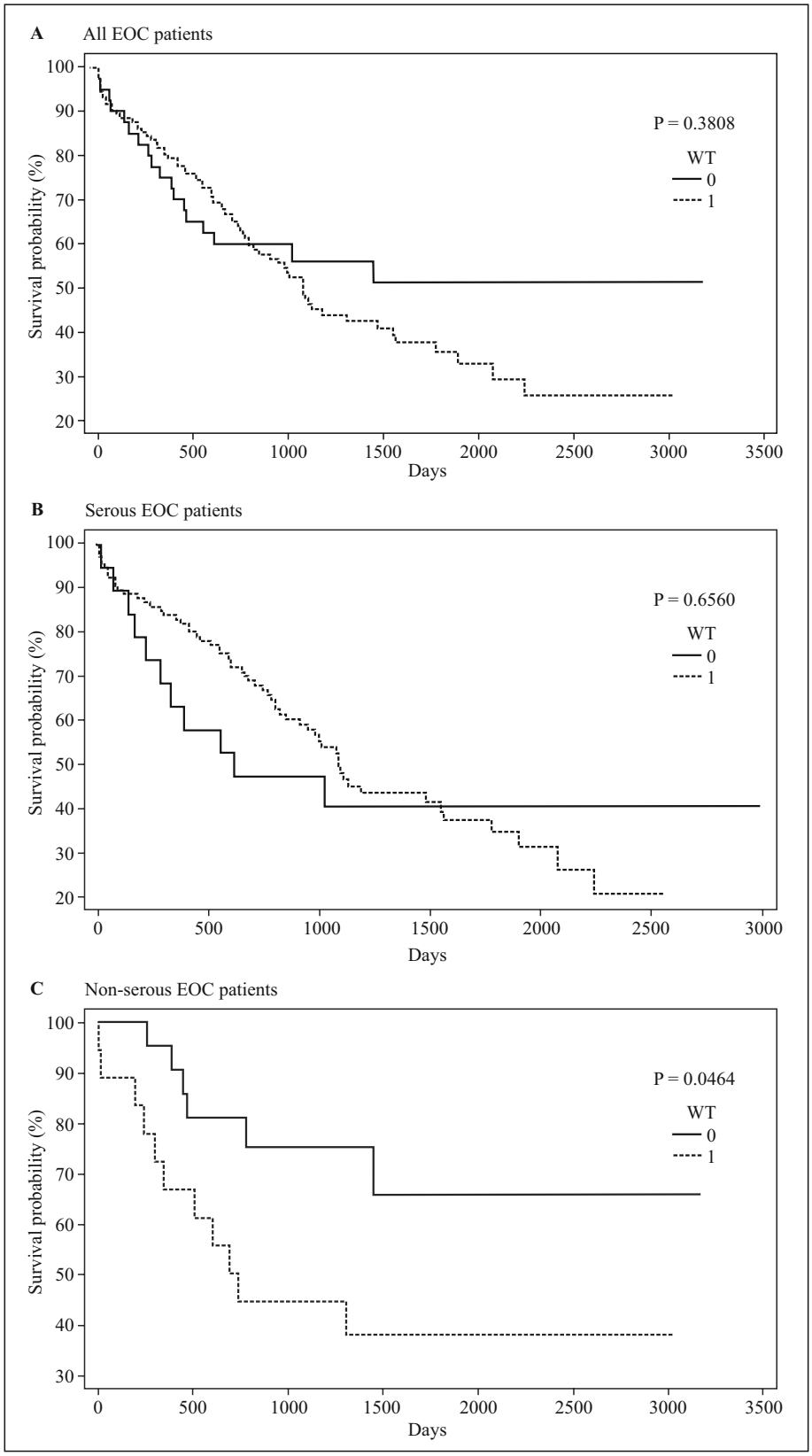

Figure 3. Kaplan-Meier survival analysis in epithelial ovarian cancer (EOC) in relation to Wilms' tumor (WT1) immunoreactivity. **A.** Overall survival of the all EOC patients: WT1 (–) group (n = 40, median overall survival (mOS) was not reached) *vs.* WT1 (+) group (n = 124, mOS 1084 days), P = 0.4. **B.** Overall survival profile of the serous EOC patients: WT1 (–) group (n = 19, mOS 614 days) *vs.* WT1 (+) group (n = 106, mOS 1084 days), P = 0.7. **C.** Overall survival profile of the non-serous EOC patients: WT1 (–) group (n = 21, mOS was not reached) *vs.* WT1 (+) group (n = 18, mOS 697 days), P = 0.046.

clear-cell carcinomas) [18]. Also, in studies by Rekhi *et al*. and Høgdall *et al*., both with larger groups of clear-cell carcinoma patients (55 and 46, respectively), there were no cases of WT1-positive clear-cell ovarian cancer [17, 21]. There was also a divergence between our results and other authors' regarding the percentages of endometrioid ovarian tumors expressing WT1. We reported WT1 immunoreactivity in 45% of these carcinomas, and similar results were obtained by Cathro *et al*. (36% of endometrioid EOCs). However, Hylander *et al*. [16] and Acs *et al*. [18] found no WT1-positive endometrioid tumors, while Høgdall *et al*. [21] reported WT1 immunoreactivity in only 5% of endometrioid EOCs. Reasons for these divergent results may lie in the sizes of study population in the reported studies, which had relatively small groups of patients with non-serous tumors; the use of differing immunohistochemical analysis protocols or antibodies, and the lack of a consistent definition of positive WT1 immunoreactivity. However, our findings concur with other authors when we postulate that serous EOCs are mainly WT1-positive tumors, while mucinous carcinomas present with either no or minor WT1 immunoreactivity.

Subsequently, we showed that WT1-positive patients were more likely to have lymph node metastases than WT1-negative patients (24.2% *vs.* 5%, respectively). Several earlier published studies concur with our finding that the presence of WT1 immunoreactivity is associated with metastatic lymph nodes, and that it correlates with an advanced stage of the disease [17, 22–25]. In a study by Liu *et al.*, WT1 expression was associated with an aggressive phenotype of ovarian cancer [22]. In a pilot project directed by the US National Cancer Institute, WT1 was identified as one of the most important antigens for the production of cancer vaccines [26]. Clinical trials on vaccines against WT1 in ovarian cancer showed promising results and may lead to their use in future treatments [27, 28]. Furthermore, finding patients with more aggressive tumors (with positive WT1 immunoreactivity) may contribute to an improved selection of patients for immunotherapy.

Although the prognostic and immunotherapeutic roles of WT1 have been demonstrated in a variety of non-gynecological cancer types [8, 9], the prognostic value of WT1 immunoreactivity in ovarian cancer remains unclear. We evaluated the prognostic value of WT1 in various histopathological types of EOC, and we found improved OS in patients with WT1-negative tumors; however, the finding was not statistically significant; and this finding is in line with those of several other studies [11, 16, 21]. However, in the subgroup of non-serous EOCs, we found that WT1 immunoreactivity was associated with significantly shortened OS. In a study by Hylander *et al.*, patients with WT1-positive tumors had a shorter median OS than patients with WT1-negative tumors, but this difference was not statistically significant [16]. The authors suggested that the lack of a significant correlation between WT1 and survival may reflect the fact that most patients (85%) were in an advanced stage of the disease [16]. This may also apply to our study, where over 80% of the WT1-positive patients were diagnosed at either FIGO stage III or IV of the disease. On the other hand, the large Danish 'MALOVA' ovarian cancer study of 560 ovarian cancer patients didn't find any association between WT1 immunoreactivity and disease specific survival when analyzing the whole study group as well considering a subgroup of 214 patients with serous EOC stage III [21]. Similarly, we did not find any association between WT1 immunoreactivity and OS in those patients with serous EOC. Yamamoto *et al*. examined serous EOC and classified the WT1-positive tumor as having both low and high levels of immunoreactivity. Interestingly in that study, in a group with high-levels of WT1 immunoreactivity, the patient outcomes were significantly worse than those in a group with low-level WT1 immunoreactivity (5-year survival rates of 36.5% *vs.* 63.8%, respectively). In a large meta-analysis by Lu *et al.*, it was reported that WT1 overexpression did not have an unfavorable effect on overall survival in ovarian cancer, which is in line with our results [11].

We also found that in WT1-positive patients with non-serous EOC the OS was significantly shorter than in WT1-negative patients; however, the relatively small number of patients with these types of tumors in our study may be a limiting factor. Furthermore, the retrospective character of our study is another limitation. Of note, the treatment (surgery, chemotherapy) of our patients was not dependent on WT1 immunoreactivity, thus we conclude that the retrospective design did not influence the results. On the other hand, the experienced team of both pathologist and surgeons standardized and automated immunohistochemical staining and the evaluation of an established end-point (overall survival) are the main advantages of our study.

To the best of our knowledge, there is no study analyzing the association between WT1 immunoreactivity and patient survival in respect of various histopathological types of ovarian cancer; and this is important because these histopathological subtypes are molecularly and clinically different. The divergence of results regarding the prognostic role of WT1 across different studies may be partly explained by the fact that histological subtypes differ in their

rates of WT1 expression. However, this issue requires further study.

In summary, our study indicates that immunohistochemical staining for WT1 helps in typing primary epithelial serous carcinomas; however, expression of the WT1 protein is not only limited to serous ovarian carcinoma. The results are suggestive of an association between the presence of WT1 and an aggressive clinical condition in ovarian cancer, yet it cannot be considered as a prognostic factor in EOC. Moreover, further studies on the association between WT1 expression and non-serous types of EOCs are required. In future, the targeting of WT1 could have had therapeutic implications in the treatment of this disease.

Conflicts of interest

The authors declare that they have no conflicts of interest.

Financial disclosure

The study was supported by the grant from the Centre of Postgraduate Medical Education, Warsaw, Poland (No. 98/2020).

Acknowledgement

We would like also to thank Robert Garrett for his assistance with the manuscript.

References

1. Bray F, Ferlay J, Soerjomataram I, et al. Global cancer statistics 2018: GLOBOCAN estimates of incidence and mortality worldwide for 36 cancers in 185 countries. CA Cancer J Clin. 2018; 68(6): 394–424, doi: 10.3322/caac.21492, indexed in Pubmed: 30207593.
2. Vecchia CLa. Ovarian cancer. Eur J Cancer Prev. 2017; 26(1): 55–62, doi: 10.1097/cej.0000000000000217, indexed in Pubmed: 26731563.
3. Rizzuto I, Behrens RF, Smith LA, et al. Risk of ovarian cancer in women treated with ovarian stimulating drugs for infertility. Cochrane Database Syst Rev. 2013; 6(8): CD008215, doi: 10.1002/14651858.CD008215.pub2, indexed in Pubmed: 23943232.
4. Torre LA, Trabert B, DeSantis CE, et al. Ovarian cancer statistics, 2018. CA Cancer J Clin. 2018; 68(4): 284–296, doi: 10.3322/caac.21456, indexed in Pubmed: 29809280.
5. Şakirahmet Şen D, Gökmen Karasu AF, Özgün Geçer M, et al. Utilization of Wilms' tumor 1 antigen in a panel for differential diagnosis of ovarian carcinomas. Turk J Obstet Gynecol. 2016; 13(1): 37–41, doi: 10.4274/tjod.22220, indexed in Pubmed: 28913087.
6. Sugiyama H. Wilms' tumor gene WT1: its oncogenic function and clinical application. Int J Hematol. 2001; 73(2): 177–187, doi: 10.1007/BF02981935, indexed in Pubmed: 11372729.
7. Pritchard-Jones K, Fleming S, Davidson D, et al. The candidate Wilms' tumour gene is involved in genitourinary development. Nature. 1990; 346(6280): 194–197, doi: 10.1038/346194a0, indexed in Pubmed: 2164159.
8. Charles AK, Mall S, Watson J, et al. Expression of the Wilms' tumour gene WT1 in the developing human and in paediatric renal tumours: an immunohistochemical study. Mol Pathol. 1997; 50(3): 138–144, doi: 10.1136/mp.50.3.138, indexed in Pubmed: 9292148.
9. Sagiyama H. WT1 (Wilms' Tumor Gene 1): Biology and Cancer Immunotherapy. Jpn J ClinOncol. 2010; 40(5): 377–87.
10. Carter JH, Deddens JA, Mueller G, et al. Transcription factors WT1 and p53 combined: a prognostic biomarker in ovarian cancer. Br J Cancer. 2018; 119(4): 462–470, doi: 10.1038/s41416-018-0191-x, indexed in Pubmed: 30057405.
11. Lu J, Gu Y, Li Q, et al. Wilms' tumor 1 (WT1) as a prognosis factor in gynecological cancers: A meta-analysis. Medicine (Baltimore). 2018; 97(28): e11485, doi: 10.1097/MD.0000000000011485, indexed in Pubmed: 29995811.
12. Pecorrelli S, Creasman WT, Pettersson F, et al. FIGO annual report on the results of treatment in gynecologic cancer. J Epidemiol Biostat. 1998; 3: 75–102.
13. Seidman JD, Kurman RJ. Ovarian serous borderline tumors: a critical review of the literature with emphasis on prognostic indicators. Hum Pathol. 2000; 31(5): 539–557, doi: 10.1053/hp.2000.8048, indexed in Pubmed: 10836293.
14. Thigpen T, Brady MF, Omura GA, et al. Age as a prognostic factor in ovarian carcinoma. The Gynecologic Oncology Group experience. Cancer. 1993; 71(2 Suppl): 606–614, doi: 10.1002/cncr.2820710218, indexed in Pubmed: 8420683.
15. Harmon RL, Sugarbaker PH. Prognostic indicators in peritoneal carcinomatosis from gastrointestinal cancer. Int Semin Surg Oncol. 2005; 2(1): 3, doi: 10.1186/1477-7800-2-3, indexed in Pubmed: 15701175.
16. Hylander B, Repasky E, Shrikant P, et al. Expression of Wilms tumor gene (WT1) in epithelial ovarian cancer. Gynecol Oncol. 2006; 101(1): 12–17, doi: 10.1016/j.ygyno.2005.09.052, indexed in Pubmed: 16263157.
17. Rekhi B, Deodhar KK, Menon S, et al. Napsin A and WT 1 are useful immunohistochemical markers for differentiating clear cell carcinoma ovary from high-grade serous carcinoma. APMIS. 2018; 126(1): 45–55, doi: 10.1111/apm.12784, indexed in Pubmed: 29266433.
18. Acs G, Pasha T, Zhang PJ. WT1 is differentially expressed in serous, endometrioid, clear cell, and mucinous carcinomas of the peritoneum, fallopian tube, ovary, and endometrium. Int J Gynecol Pathol. 2004; 23(2): 110–118, doi: 10.1097/00004347-200404000-00004, indexed in Pubmed: 15084838.
19. Cathro HP, Stoler MH. The utility of calretinin, inhibin, and WT1 immunohistochemical staining in the differential diagnosis of ovarian tumors. Hum Pathol. 2005; 36(2): 195–201, doi: 10.1016/j.humpath.2004.11.011, indexed in Pubmed: 15754297.
20. Goldstein NS, Uzieblo A. WT1 immunoreactivity in uterine papillary serous carcinomas is different from ovarian serous carcinomas. Am J Clin Pathol. 2002; 117(4): 541–545, doi: 10.1309/K84K-005F-TCB8-FV4B, indexed in Pubmed: 11939727.
21. Høgdall EVS, Christensen L, Kjaer SK, et al. Expression level of Wilms tumor 1 (WT1) protein has limited prognostic value in epithelial ovarian cancer: from the Danish „MALOVA" ovarian cancer study. Gynecol Oncol. 2007; 106(2): 318–324, doi: 10.1016/j.ygyno.2007.03.043, indexed in Pubmed: 17540436.
22. Liu Z, Yamanouchi K, Ohtao T, et al. High levels of Wilms' tumor 1 (WT1) expression were associated with aggressive

clinical features in ovarian cancer. Anticancer Res. 2014; 34(5): 2331–2340, indexed in Pubmed: 24778040.
23. Rhodes A, Vallikkannu N, Jayalakshmi P. Expression of WT1 and PAX8 in the epithelial tumours of Malaysian women with ovarian cancer. Br J Biomed Sci. 2017; 74(2): 65–70, doi: 10.1080/09674845.2016.1220709, indexed in Pubmed: 28367736.
24. Yamamoto S, Tsuda H, Kita T, et al. Clinicopathological significance of WT1 expression in ovarian cancer: a possible accelerator of tumor progression in serous adenocarcinoma. Virchows Arch. 2007; 451(1): 27–35, doi: 10.1007/s00428-007-0433-4, indexed in Pubmed: 17594113.
25. Barbolina MV, Adley BP, Shea LD, et al. Wilms tumor gene protein 1 is associated with ovarian cancer metastasis and modulates cell invasion. Cancer. 2008; 112(7): 1632–1641, doi: 10.1002/cncr.23341, indexed in Pubmed: 18260155.
26. Cheever MA, Allison JP, Ferris AS, et al. The prioritization of cancer antigens: a national cancer institute pilot project for the acceleration of translational research. Clin Cancer Res. 2009; 15(17): 5323–5337, doi: 10.1158/1078-0432.CCR-09-0737, indexed in Pubmed: 19723653.
27. Vermeij R, Daemen T, de Bock GH, et al. Potential target antigens for a universal vaccine in epithelial ovarian cancer. Clin Dev Immunol. 2010; 2010, doi: 10.1155/2010/891505, indexed in Pubmed: 20885926.
28. Li G, Zeng Y, Chen X, et al. Human ovarian tumour-derived chaperone-rich cell lysate (CRCL) elicits T cell responses in vitro. Clin Exp Immunol. 2007; 148(1): 136–145, doi: 10.1111/j.1365-2249.2007.03323.x, indexed in Pubmed: 17349014.

Submitted: 19 March, 2020
Accepted after reviews: 13 September, 2020
Available as AoP: 22 September, 2020

FOLIA HISTOCHEMICA ET CYTOBIOLOGICA
Vol. 58, No. 3, 2020
pp. 208–218

ORIGINAL PAPER

VIA MEDICA

Suppression of the inflammation and fibrosis in Asherman syndrome rat model by mesenchymal stem cells: histological and immunohistochemical studies

Nagla Mohamed Salama[1], Somaia Saad Zaghlol[1], Hala Hassan Mohamed[1], Samaa Samir Kamar[1]

[1]Department of Histology and Cell Biology, Faculty of Medicine, Cairo University, Cairo, Egypt

Abstract

Introduction. Asherman syndrome (AS) is a symptomatic intrauterine adhesion caused by endometrial basal layer fibrosis as a result of either uterine cavity surgery or infection leading to many complications. There is a concern to repair the injured tissues by using bone marrow mesenchymal stem cells (BM-MSCs). We aimed in this study to develop an animal model of AS and evaluate the anti-inflammatory and anti-fibrotic effects of BM-MSCs in this model through histological, immunohistochemical, and morphometric studies.

Material and methods. Forty-two adult female adult albino rats were divided into (i) donor group composed of 2 rats used for isolation and propagation of BM-MSCs, and (ii) experimental groups: 40 rats equally divided into 4 groups: GpI (control), GpII (AS model), GpIII (BM-MSCs-treated AS rats), GpIV (untreated AS rats). Histological staining and immunohistochemical (IHC) detection of proliferating cell nuclear antigen (PCNA), vascular endothelial growth factor (VEGF), and nuclear factor-kappa beta (NF-κB) were performed. The results were evaluated by morphometric and statistical analysis.

Results. Significant endometrial thinning, fibrosis, and degeneration of the endometrial epithelium with a significant decrease in PCNA and VEGF immunoexpression and a significant increase in NF-κB immunoexpression were detected in GpII and GpIV groups. These changes were substantially reversed in BM-MSCs-treated animals.

Conclusions: BM-MSCs treatment resulted in substantial improvement of intrauterine adhesion in the rat model of Asherman syndrome. *(Folia Histochemica et Cytobiologica 2020, Vol. 58, No. 3, 208–218)*

Key words: BM-MSCs; intrauterine adhesions; NF-κB; PCNA; VEGF; IHC

Introduction

Asherman syndrome (AS) is a symptomatic intrauterine adhesion (IUA) caused by endometrial basal layer fibrosis as a result of either uterine cavity surgery or infection. This can lead to partial or complete obstruction of the uterine cavity with abnormal menstruation such as amenorrhea, hypomenorrhea, and menorrhagia [1]. Besides, it could potentially corrupt the blastocyst implantation and impede blood supply to the uterus and embryo, causing recurrent miscarriage or infertility [2]. The incidence of AS has been increasing over the last few decades because of the expanding frequency of cesarean sections and uterine medical procedures [3]. The main pathologic issue is the avascular fibrous connective tissue (CT) band with or without glandular tissue [4]. The current treatment strategy of AS includes dilatation and curettage, uterine balloon stent, and hormonal treatment to restore normal endometrium [5]. However, this strategy is characterized by a high failure rate due to the recurrence of the adhesion [6].

The use of bone marrow mesenchymal stem cells (BM-MSCs) opens a new era in repairing the tissue

Correspondence address: Samaa Samir Kamar,
Department of Histology and Cell Biology, Faculty of Medicine
Cairo University, Cairo, Egypt
phone: +02 01008909069
e-mail: Dr_samaakamar@yahoo.com

injury. BM-MSCs are adult stem cells that have the ability of self-renewal, transdifferentiation, and autotransplantation without stimulation of immune rejection [7]. Mesenchymal stem cells (MSCs) have provided a novel method in the treatment of fibrotic disease due to their ability to evade the immune detection and secretion of anti-inflammatory and anti-fibrotic mediators [8]. After autotransplantation, they can migrate and accumulate in the endometrial tissue. Thus, BM-MSCs treatment may be a promising therapy for AS [9].

The development of an animal model of AS is particularly essential for the study of AS phenotype, pathogenetic mechanisms, and the development of effective therapeutic strategies for the treatment of AS [2]. Trichloroacetic acid (TCA) is a topically applied chemical agent that is not absorbed systemically and denatures proteins, resulting in chemical cauterization. Uterine TCA installation is a chemical ablation technique that has been used previously in humans to treat dysfunctional menstrual bleeding [10]. It has been postulated that TCA could be used experimentally to develop a model of AS in rat [11].

The aim of this study was to evaluate the possible therapeutic anti-inflammatory and anti-fibrotic effects of BM-MSCs in experimentally induced AS model using histological, immunohistochemical and morphometric studies.

Materials and methods

Design of the experiment. This study included 42 adult female Wistar albino rats (aged about 12 weeks), with average body weight 200–220 g. Each group was kept in separate wire cages at room temperature (about 25°C) in 12:12 h light/dark cycle, fed *ad libitum* with free water access. All procedures of the study protocol were approved by the Institutional Animal Care and Use Committee of Cairo University (CU-IACUC) with an approval number (CU-III-F-28-18) and the principles of laboratory animal care. Animals were divided into donor group and experimental groups. The donor group included 2 rats used for stem cell isolation, culture, phenotyping, and labelling.

The rats of the experimental groups were cycle synchronized according to the vaginal smear examination. Daily morning vaginal smear was performed and analyzed to assess the estrous cycle. Rats with 4–5 days regular cycles were included in the experiment. 40 rats were included and equally divided into the following four groups (n = 10 each).

GpI (control): The animals were equally subdivided into 2 subgroups (n = 5 each):

— **subgroup Ia:** normal rats, not subjected to any surgical procedure;

— **subgroup Ib:** rats underwent a sham operation in which the right (Rt) uterine horn was installed with 0.3 ml saline.

GpII (AS model): the rats were anesthetized using an intraperitoneal injection of ketamine (50 mg/kg) and placed in a supine position. The inferior abdomen was shaved and disinfected, then a midline incision (about 3 cm) was made. For the trichloroacetic acid (TCA) injection (Istanbul Ilac Sanayive Ticaret AS, Turkey), each uterine horn was identified and clamped with hemostatic forceps. Rt uterine horn was injected with a single dose of 0.3 mL of 90% TCA using an insulin needle. The peritoneum was irrigated with Ringer solution and the abdominal wall was closed. Post-operative analgesics and prophylactic antibiotics were supplied. Rats were sacrificed in the estrus phase of the 3rd cycle (about 2 weeks) to assess the establishment of the model [10, 11].

GpIII (AS rats BMSCs-treated): after 2 weeks of the modeling as in **GpII**, 1×10^6 PKH26 labeled BM-MSCs suspended in 1 ml of phosphate-buffered saline (PBS) were injected into the tail vein of each rat. Then the animals were sacrificed in the estrus phase of the 3rd cycle [12].

GpIV (untreated AS): after 2 weeks of modeling, each rat was injected via tail vein with 1ml PBS (solvent of BM-MSCs). They were then sacrificed in the estrus phase of the 3rd cycle.

Isolation and characterization of BM-MSC. Under complete aseptic conditions, bone marrow was harvested from the tibia and femur of 8-week-old male white Wistar rats by flushing using low glucose Dulbecco's Modified Eagle's Medium (DMEM) [Gibco, Gainesville, MD, USA], supplemented with 10% fetal bovine serum [FBS, GIBCO/ /BRL]. The isolated cells were cultured in a growth medium containing 1% penicillin/streptomycin [GIBCO] and incubated in 5% humidified CO_2 at 37°C for about 2 weeks as a primary culture or when large colonies appeared. At 80% confluence, the cells were washed with PBS. The cells were trypsinized with 0.25% trypsin in 1mM ethylene-diaminetetraacetic acid for 5 min at 37°C. After centrifugation, cells were resuspended with serum-supplemented medium (10% FBS) and incubated in 50 cm^2 culture Falcon flask. The subculture passage was done till the 3rd passage to expand the cell population [13]. BM-MSCs were characterized by their adhesiveness and fusiform shape and with flow cytometry (CYTOMICS FC 500, Beckman Coulter, Champaign, IL, USA) identification of the mesenchymal stem cells surface markers [14]. The BM-MSCs were positive for CD90 and CD105 and negative for CD45 and CD34.

Labeling of BM-MSc with PKH26 fluorescent linker dye. The MSCs were harvested during the 3rd passage and labeled with PKH26, a lipophilic red fluorescent linker dye (Cat. # MINI26, Sigma Aldrich, St. Louis, MO, USA). It was used to localize the injected stem cells in the uterine tissue. The BM-MSCs were centrifuged and washed 2 times in serum-free medium and pelleted. Then, they were incubated for 1 h (5% CO_2 at 37°C) in a cocktail solution consisting of serum-free

DMEM (83.3% vol/vol) and 1.1% of PKH26 dye solution in diluent ad 100%. The staining was stopped according to the manufacturer's recommendations (SigmaAldrich). The PKH26-labeled BM-MSCs were examined using phase-contrast Olympus CKX53 fluorescent microscope (Olympus, Tokyo, Japan) and maintained in the growth medium for the following experiment to be injected intravenously into the rat tail vein [15] of the animals in the group **GpIII** of rats (AS rats BMSCs-treated).

Vaginal smear examination. Vaginal smears were obtained with a micropipette [16]. The tip of the micropipette was filled with a small amount of saline (1–2 drops), then inserted into the vagina of the female rat. The vagina was flushed 2–3 times with the saline and then the fluid was placed onto a glass slide. The fluid was equally distributed onto the slides and was spread out. Samples were left to dry without fixation and then stained with 1% crystal violet. Determination of the phases of the estrous cycle was made using a light microscope.

Biological samples' collection. The rats were euthanized using an intraperitoneal injection of thiopental sodium-500 (90 mg/kg; EPICO, 10th of Ramadan City, Egypt). Specimens of mid-portion of the Rt uterine horn were collected, fixed in 10% formol saline, and processed into paraffin blocks. Serial sections, 5–7 μm thickness, were obtained and subjected to fluorescent, histological and immunohistochemical studies. The stained sections were examined by expertized histologists using light microscope connected to Olympus camera (BX-50 f4, Olympus Optical Co. Ltd., Japan). To detect the homing of the PKH26-labeled BM-MSCs in the uterine tissue, a reflected light fluorescent microscope (Olympus) was used.

Histological studies. Hematoxylin and eosin (H&E) staining was used for general morphological analysis [17] and Masson's trichrome staining to elucidate collagen deposition [18].

Immunohistochemistry. Anti-PCNA mouse monoclonal antibody (Ab) (Cat. # MS106P Thermo Scientific Laboratories, Fermont, CA, USA) was used as a standard marker for the proliferating cells and anti-VEGF rabbit polyclonal Ab [Boster Biological Technology, Pleasanton, CA, USA, Cat. # PA1080] was applied to demonstrate neovascularization in the endometrium [19].

Anti-NF-κB rabbit polyclonal Ab (Cat. # PA1669; Boster Biological Technology) was used to detect this transcription factor that links the pathogenic signals and cellular danger signals.

Immunohistochemistry required pre-treatment by boiling the deparaffinized sections in 10 mM citrate buffer (Cat. # 005000) pH 6 for 10 min for the antigen retrieval. The sections were allowed to cool in RT for 20 min then endogenous peroxidase activity was blocked by hydrogen peroxide and the sections were then rinsed in PBS. Incubation with the primary Ab was performed for 1 h. The biotinylated secondary Ab (Cat. # 62-9520; Life Technologies) was applied. Immunostaining was completed by the use of Ultravision One Detection System (Cat. # TL-060-HLJ; Life Technologies). Adding of diaminobenzidine (DAB) solution resulted in a brown-colored precipitate. Counter-staining was performed using Meyer's hematoxylin (Cat. # TA-060-MH; Life Technologies) to visualize the nuclei. Negative controls were prepared using the same steps with omitting the primary Ab.

Morphometry. Data were obtained using "Leica Qwin-500 C" image analyzer (Cambridge, England) in the Histology Department, Faculty of Medicine, Cairo University. The slides were examined under the light microscope and ten non-overlapping randomly selected low power fields (×100)/ /slide were examined to measure: (i) the thickness of endometrium and number of uterine glands in the H&E stained sections (using interactive measuring menu); (ii) relative area of collagen deposition in Masson's trichrome stained sections (measured using the color detect menu with a standard measuring frame with an area 116946.91 μm^2); (iii) the number of PCNA positive (+ve) immunostained cells; (iv) relative area of VEGF and NF-κB immunostained cells (areas of positivity were measured using the color detect menu with a standard measuring frame with an area 116946.91 μm^2).

Statistical analysis. The obtained measurements were analyzed using the SPSS software version 16 (SPSS Inc., Chicago, IL, USA). Comparisons between different groups were done using one-way analysis of variance (ANOVA) test followed by a *post-hoc* Tukey test. Quantitative data were summarized as means and standard deviations (SD). The p-value of less than 0.05 was considered statistically significant.

Results

Clinical observation

No death was registered in the experimental animals nor changes in their conduct of the water and food consumption.

Vaginal smear morphology

The estrous cycle was assessed by the daily morning vaginal smears examination. The estrus phase was identified by the presence of predominant cornified squamous epithelial cells with no apparent nuclei. Cells had an angular appearance and present in densely packed clusters (Fig. 1).

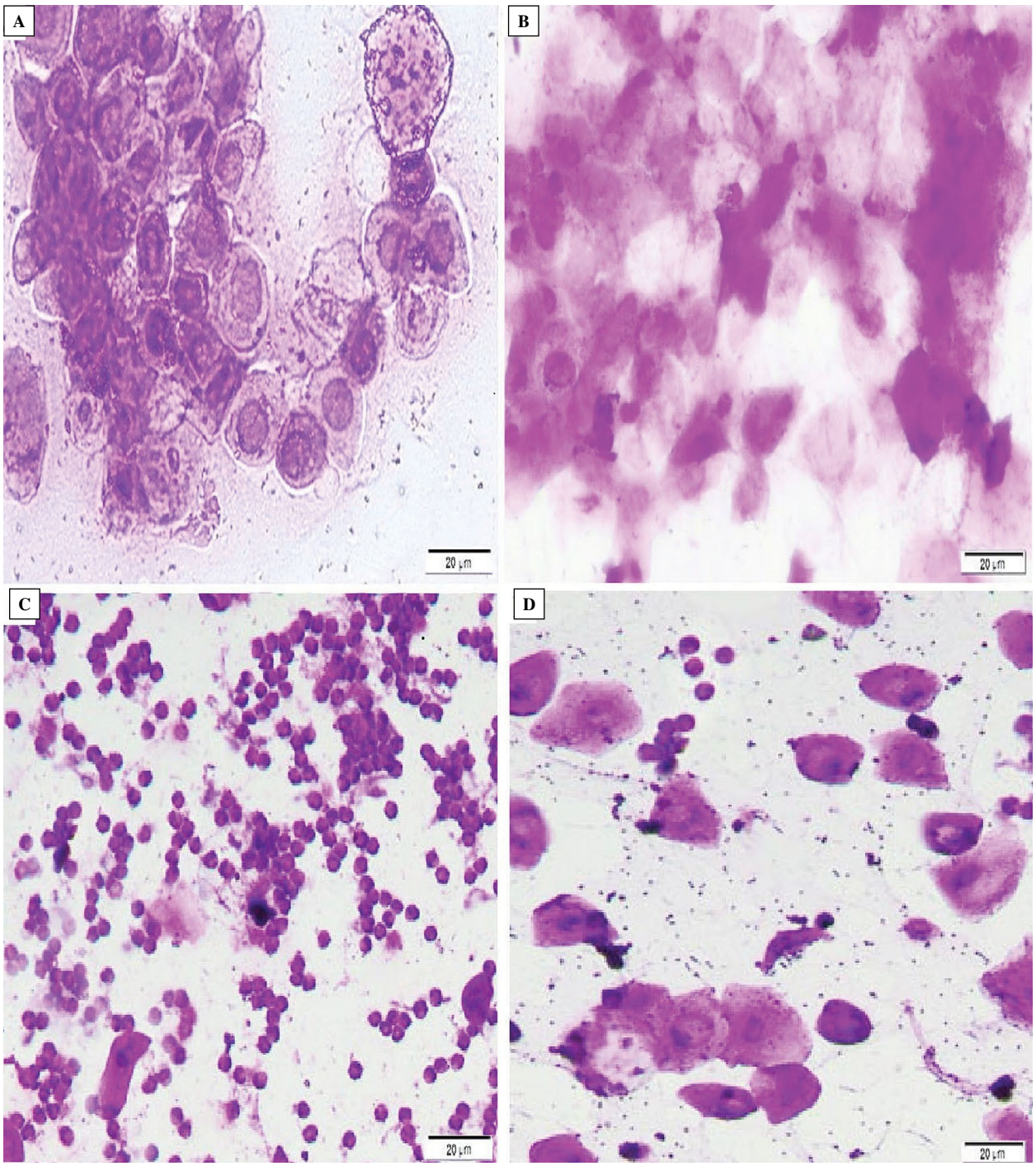

Figure 1. Photomicrographs of crystal violet stained vaginal smear showing different phases of estrous cycle of the rat. **A.** Proestrus phase: rounded, well-formed nucleated epithelial cells with darkly stained nuclei present in clusters. **B.** Estrus phase: predominant cornified squamous epithelial cells with no apparent nuclei, present in densely packed clusters. **C.** Metestrus phase: the predominant cells are small darkly stained leukocytes with few scattered cornified squamous epithelial cells. **D.** Diestrus phase: the predominant cells are leukocytes. Nucleated epithelial cells also present. Magnification: 400×.

Characteristics of the BM-MSCs

Fluorescent microscopic examination of the unstained uterine sections of GpIII (AS rats BM-SCs-treated group) revealed red fluorescent cells distributed within the regenerated endometrium (Fig. 2), thus confirming that injected BM-MSCs labeled with PKH26 fluorescent dye homed into the uterus.

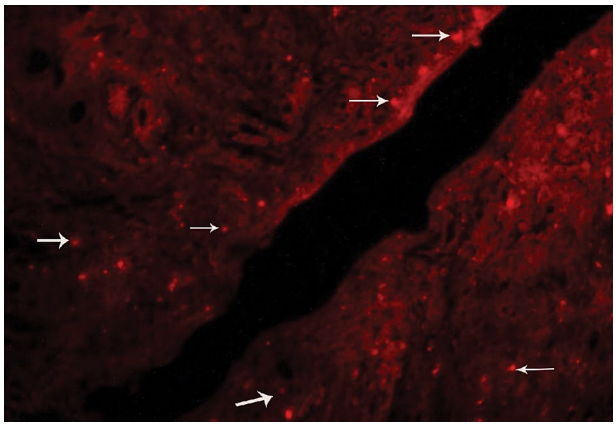

Figure 2. Photomicrograph of a section rat uterus of GpIII group. (White-arrows): red fluorescent cells. (PKH26 fluorescence, 200×).

Morphological observations

Effects of TCA instillation on the morphology of rat uterus

Uteri of the control rats in the estrous cycle showed thick endometrium harboring numerous uterine glands, intact surface, and glandular epithelium with highly cellular CT stroma containing numerous blood vessels (Fig. 3A). These uterine changes define the onset of the estrus phase. The model group exhibited thin endometrium, few distorted glands, and little cellularity of the fibrous stroma**.** In GpIV, the endometrium was thin with few glands and discontinuous surface epithelium (Fig. 3B). Masson's trichrome-stained uterine sections of GpI showed fine collagen fibers (Fig. 4A). In GpII, marked collagen deposition in the lamina propria of the thin endometrium was observed

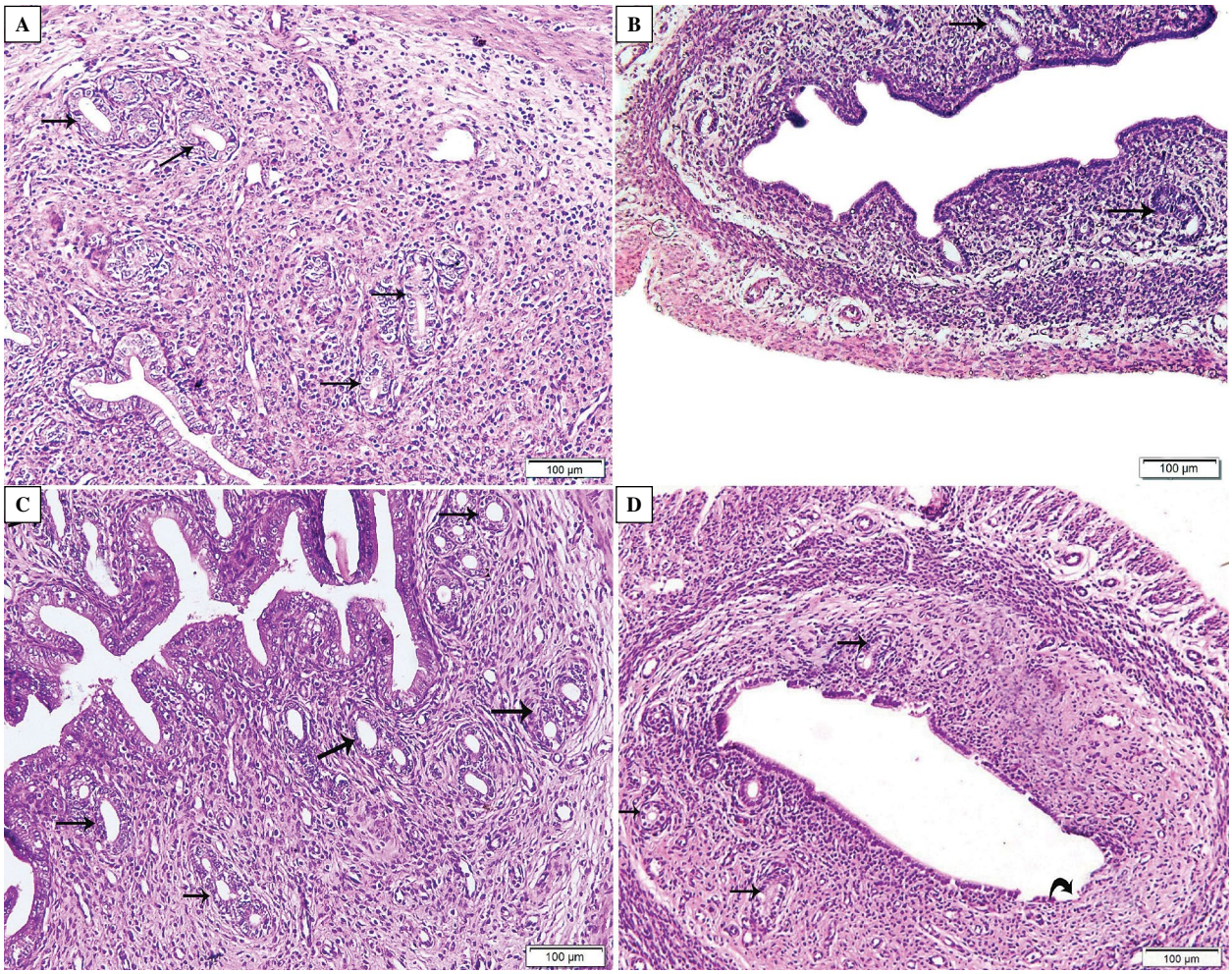

Figure 3. H&E-stained rat uterine sections. **A.** GpI (control): thick endometrium, numerous uterine glands (arrows) occupying most of the endometrial thickness and lined with simple cuboidal cells with vesicular nuclei and vacuolated cytoplasm, and intact surface epithelium. The lamina propria contains highly cellular connective tissue (CT) with stromal cells exhibiting vesicular nuclei and many leukocytic infiltrations. **B.** GpII (AS model): pronounced thinning of the endometrium with few uterine glands (arrow). **C.** GpIII (AS rats BMSCs-treated): preserved endometrial thickness, numerous uterine glands (arrows), intact surface epithelium and the stroma is highly cellular CT with many leukocytic infiltrations. **D.** GpIV (BMSCs-untreated AS rat): thin endometrium, few endometrial glands (arrow), and discontinuous surface epithelium (curved arrow). Magnification: 100×.

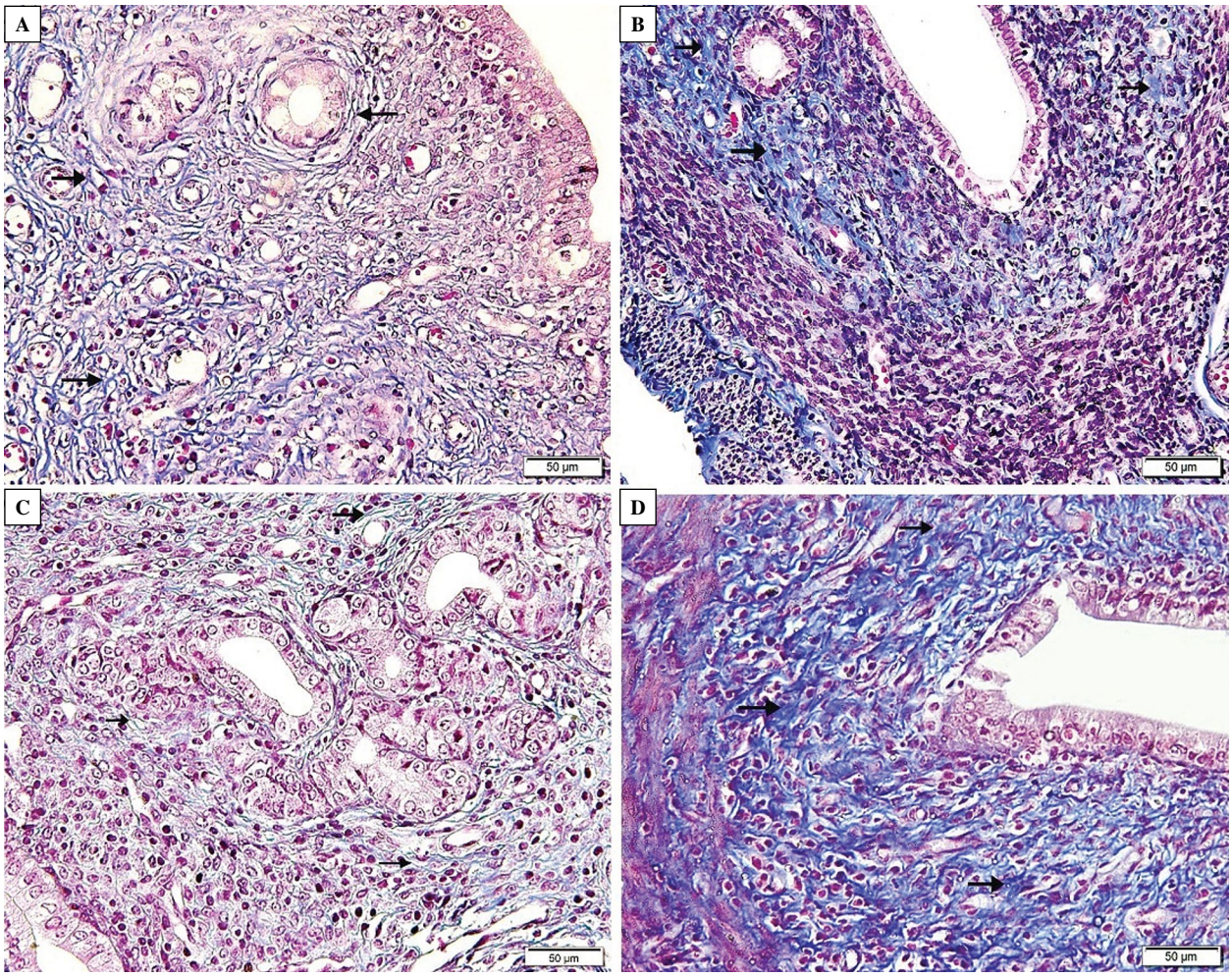

Figure 4. Uterine sections stained by Massson's trichrome method. **A.** GpI (control): fine collagen fibers (arrow). **B.** GpII (AS model): coarse collagen deposition in the lamina propria. **C.** GpIII (AS rats BMSCs-treated): fine collagen fibers between stromal cells and surrounding the glands. (D) GpIV (untreated AS): coarse collagen deposition in the endometrial stroma. Magnification: 100×.

(Fig. 4B). In **GpIV**, obvious coarse collagen deposition in the stroma of the endometrium was noted (Fig. 4D).

Effects of BM-MSCs on the features of AS endometrium

Regenerated endometrium was noted in GpIII that showed thick endometrium**,** numerous uterine glands, intact surface epithelium and highly cellular stroma with numerous leukocytic infiltrations (Fig. 3C). Besides, fine collagen fibers between the stromal cells, and surrounding the glands (Fig. 4C).

Immunohistochemical stainings

Immunohistochemical detection of PCNA in uterine sections revealed in GpI strong widespread nuclear PCNA immunoreactivity (-Ir). GpII illustrated weak PCNA-Ir in some cells of the surface epithelium, the obliterated glands, and the stromal cells. GpIII displayed widespread nuclear PCNA-Ir in the surface epithelium, the uterine glands and the stromal cells. In GpIV nuclear immunostaining was detected in the surface epithelium and some stromal cells (Figs. 5A–D, respectively).

Immunohistochemical detection of VEGF in uterine sections of GpI rats revealed widespread prominent positive immunostaining was observed. GpII showed few positive VEGF immunostaining in the stroma. In GpIII, diffuse positive immunostaining was detected in the surface epithelium, uterine glands, stromal cells, and the endothelium. GpIV showed some positive VEGF immunostaining in the surface epithelium and the stroma. (Figs. 5E–H, respectively).

Immunohistochemical detection of NF-κB revealed in GpI moderate positive immunostaining. In uterus of GpII rats, strong NF-κB-Ir was observed in the cytoplasm and cell nuclei of the surface epithelium, endometrial glands and almost all stromal cells. In GpIII, moderate NF-κB-Ir was demonstrated in the cytoplasm of the surface epithelium and in the uterine

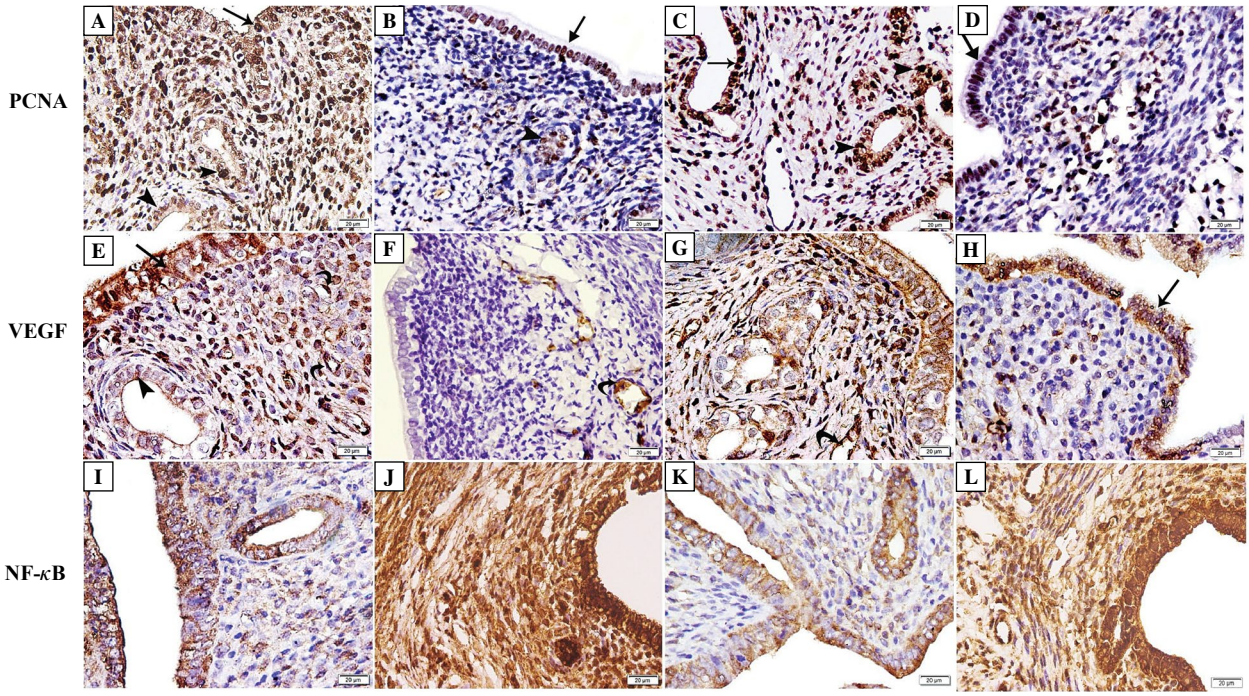

Figure 5. Immunoexpression of PCNA, VEGF, and NF-κB in the uterine section. PCNA immunohistochemical staining: **(A)** GpI: strong nuclear PCNA immunostaining in the surface epithelium (arrow), endometrial glands (arrowhead), and many stromal cells. **(B)** GpII: weak nuclear immunostaining. **(C)** GpIII: widespread nuclear immunostaining. **(D)** GpIV: weak nuclear immunostaining. VEGF immunohistochemical staining: **(E)** GpI: widespread prominent +ve immunostaining in the epithelium lining the lumen (arrow), the uterine glands (arrowheads), the stromal cells, and the blood vessels (curved arrow). **(F)** GpII: minimal +ve immunostaining detected in few stromal cells and in the endothelium (curved arrow). **(G)** GpIII: diffuse +ve immunostaining. **(H)** GpIV: some +ve immunostained cells in the surface epithelium (arrow) and in the stromal cells. NF-κB immunohistochemical staining: **(I)** GpI: mild cytoplasmic +ve immunostaining. **(J)** GpII: strong diffuse +ve cytoplasmic and nuclear immunostaining. **(K)** GpIII: mild cytoplasmic +ve immunostaining. (L) GpIV: strong diffuse +ve cytoplasmic and nuclear immunostaining. Magnification: 400×.

Table 1. The mean (± SD) of endometrial thickness, number of the uterine glands, area % of collagen deposition, number of PCNA + ve cells, area % of VEGF immunostaining, and area % of NF-κB immunostaining in the control and the experimental groups

Parameters/Groups	Gp I	Gp II	Gp III	Gp IV
Endometrial thickness [μm]	406 ± 19.3	93.7 ± 15.4*#	390.4 ± 11.3	97.5 ± 24.2*#
Number of uterine glands	8.7 ± 1.9	0.9 ± 0.7*#	8.5 ± 1.1	3.1 ± 0.7*#†
Area % of collagen deposition	20.9 ± 3.8	42.2 ± 4*#	19.8 ± 4.1	59.1 ± 3.5*#†
Number of PCNA + ve cells	54.1 ± 5.4	19.5 ± 3.4*#	45.7 ± 2.8	30.6 ± 2.4*#†
Area % of VEGF immunostaining	59.4 ± 3.6	22 ± 3.7*#	42.5 ± 3.2	33.9 ± 7.3*#†
Area % of NF-κB immunostaining	20.2 ± 7.6	50.5 ± 3.2*#	22.7 ± 7.3	52.2 ± 1.1*#

*Significant ($p < 0.05$) as compared to GpI, †Significant as compared to GpII, #Significant as compared to GpIII.

gland. GpIV displayed widespread positive cytoplasmic and nuclear NF-κB immunostaining (Fig. 5I–L).

Morphometric Study

The data of the morphometric measurements are presented in Table 1.

Regeneration of the endometrium and the uterine glands by BM-MSC

The mean thickness of the endometrium and the mean number of the endometrial glands in the BMSC-treated group showed significant ($p < 0.000$ and $p < 0.001$) increase, respectively, as compared

to GpII and GpIV groups, with a non-significant difference as compared to GpI group, thus denoting regenerative capacity of the stem cells therapy.

The antifibrotic effect of BM-MSCs

The mean area % of collagen deposition was substantially increased in the endometrium of Asherman model rats ($p < 0.000$) and recovery groups ($p < 0.002$) as compared to the control. Meanwhile, it was significantly ($p < 0.001$) decreased in GpIII with the treatment of BM-MSCs as compared to GpII indicating the antifibrotic effect of BM-MSC.

Effect of BM-MSCs on the immunoexpression of PCNA, VEGF and NF-κB

In the uterus of Asherman model and the recovery group rats, the expression of PCNA and VEGF was significantly ($p < 0.001$) decreased as compared to GpI. Also, the mean area % of NF-κB immunostaining was significantly ($p < 0.001$) increased in both groups. Stem cell therapy substantially increased the expression of PCNA and VAGF in the endometrium and significantly decreased the expression of NF-κB (Table 10).

Discussion

Asherman syndrome is referred to intrauterine synechiae due to injury of the endometrial basal layer accompanied by thin endometrium [19]. Surgery serves only to divide the adhesions within the cavity, but can do very little about the endometrial regeneration and adhesion recurrence [20]. Therefore, we tried to use bone marrow-derived mesenchymal stem cells for the regeneration of the endometrium in the experimental intrauterine synechia AS model. After the induction of AS, euthanization was performed in the estrus phase of the 3rd cycle to assess the establishment of the modeling based on the study of Cocuzza *et al*. and Kilic *et al.*, [10, 11]. Asherman syndrome is known to be one of the causes of thin endometrium. Defective uterine perfusion was assumed to be the reason for the atrophied endometrium due to limited exposure to the circulating hormones [21]. The endometrial thickness is mandatory for the successful implantation and pregnancy compared to low receptivity and pregnancy rate in case of thin endometrium [22].

The stroma of rats in GpII (AS group) showed little cellularity, few blood vessels and obvious fibrosis with substantial increase in the mean area % of the collagen deposition as compared to GpI (control) and Gp III (AS rats BMSCs-treated). Generally, fibrosis is assumed to occur as a result of interaction between the inflammatory and the fibrotic cytokines. IL-6 acts as a pro-inflammatory cytokine that is secreted mainly by inflammatory cells as macrophages and stimulates the immune response. It contributes to the development of fibrosis by modulating TGFβ signaling and stimulating the proliferation of fibroblasts, as well as the collagen production [23].

Intravenous injection of BM-MSCs revealed regenerated (increased) endometrial thickness and numerous uterine glands with intact surface and glandular epithelium, as compared to the control group, indicating regaining the normal estrous cyclic changes. Intravenous injection of stem cells has been documented to be effective in experimental studies [24, 25]. As compared to local tissue injection of stem cells, systemic administration is more easy applicable method that empowers the clinical use of this therapy [24]. Moreover, homing of the injected stem cells to the injured tissue has been documented in previous studies [6, 14] and confirmed in our present work by localization of the PKH26-labeled stem cells in the uterine tissue. Jing *et al*. [12] referred this regenerative uterine capacity to the therapeutic effect of BM-MSCs by exerting protective actions against cell damage. Exogenous BM-MSCs could home to damaged tissues where they are releasing trophic factors rather than forming engraftment. They can produce high amounts of anti-inflammatory cytokines and growth factors, and possess immunomodulatory properties [26]. A relevant phenomenon is that BM-MSCs up-regulate the anti-inflammatory cytokines, such as fibroblast growth factor-β and IL-6, and down-regulate the pro-inflammatory cytokines, such as TNF-α and IL-1β [12].

The lamina propria of the uterine sections in GpIII (BM-MSC-treated AS rats) contained highly cellular CT with numerous blood vessels and fine collagen fibers with the mean area % of collagen deposition comparable to the control rats. These results are going parallel with Sabry *et al*. [6] who documented in an induced-endometrial fibrosis rat model the antifibrotic effect of stem cells by significant decrease in IL-1 gene expression. IL-1gene expression was accused in the development of fibrosis. Similarly, systemic infusion of BM-MSCs in cutaneous radiation induced fibrosis rat model reduced skin contracture, thickening, collagen deposition and decreased expression of IL-1 in their radiated skin [27]. Ebrahim *et al*. [28], in an intrauterine adhesion female rat model, showed that MSCs secreted exosomes or vesicles, which are enriched in the extracellular environment. These vesicles have been considered as vital mediators of cellular communication and may regulate various physiological and pathological processes by transferring membrane proteins, mRNAs, and miRNAs to recipient cell [29]. Recent studies have demonstrated that vesicles can act during different stages of the inflammatory re-

sponse by transporting bioactive factors and suppress the inflammation in different animal models to restore the physiological status [30, 31].

The endometrial regeneration in AS rats induced by BM-MSC administration seems to be specifically caused by this procedure since uterine sections of rats from GpIV (untreated AS) showed thin endometrium with discontinuous surface epithelium. Few endometrial glands were seen scattered in the fibrosed endometrium suggesting poor proliferation by the tissue stem cells.

It is well known that PCNA has a crucial role in accurate DNA duplication [32]. Rats in GpII and GpIV groups demonstrated weak PCNA immunostaining in the endometrium. Meanwhile, AS BMSCs-treated rats displayed significant increase in PCNA immunostainig in the endometrial tissue indicating preservation of the proliferative capacity of the endometrial cells [33]. The bone marrow progenitor cells were documented to improve the proliferation of different injured tissues [34, 35]. Stem cell effects could be through direct homing to the injured tissue and repairing the endometrium through self-renewal, proliferation, and differentiation. In addition, mesenchymal stem cell has a paracrine effect on the surrounding cell to increase the efficacy of tissue repair [36].

Asherman syndrome is frequently associated with defective blood supply to the endometrium with subsequent impaired hormonal delivery to the endometrium resulting in thin endometrium [37]. In the present work, rats in GpII and GpIV groups displayed significant decrease in VEGF expression in the uterine tissue. In the fibrotic stroma of the endometrium of AS, thin-walled telangiectatic blood vessels are thought to cause impaired blood perfusion and tissue atrophy [38]. However, BMSC-treated AS-rats demonstrated significant diffuse VEGF immunostaining in the epithelium, stromal cells and endothelial cells indicating improved angiogenesis of the regenerated endometrium. Ebrahim *et al*. [28] postulated that the ability of MSC to repair uterine scars was associated with up-regulation of VEGF and down-regulation of collagen type I expression, in addition to promoting the regeneration of the endometrium, myometrium, and blood vessels in the uterine scars.

The NF-κB signaling pathway is considered a spark for the inflammatory process through its triggering role in the up-regulation of various pro-inflammatory genes encoding chemokines, cytokines, and adhesion molecules [39, 40]. NF-κB activation was documented in the pathogenesis of various inflammatory diseases [35]. In AS, the intrauterine adhesions are associated with increased level of the inflammatory cytokines as TGF-β, TNF-α, IL-1, and IL-18 that crosstalk with the NF-kB pathway [41]. In the present work, a significant increase in NF-κB immunostaining was detected in rats with the induced AS and the recovery group. In agreement with previous study [2], the importance of NF-κB was confirmed in the pathogenesis of human AS and animal models and suggested its role as a potential diagnostic marker and therapeutic target in the treatment of intrauterine adhesions. The immunomodulatory role and anti-inflammatory effect of stem cells were documented [2]. In a recent study, MSC-conditioned media reduced the inflammation in endotoxin-induced acute lung injury through inhibition of the activity of NF-κB and increasing the interleukin-6 and macrophage inflammatory protein level [42].

Although stem cell therapy was shown to be safe and well-tolerated in the clinical trials [43], the risk of tumorigenicity must always be evaluated with long term follow up, and during the culture- expansion stage before any therapeutic infusion [44].

In summary, application of BM-MSCs effectively promoted the endometrial regeneration in Asherman syndrome rat model through improving the proliferative capacity of the uterine tissue, inducing angiogenesis, and modulating the inflammatory process and the fibrosis.

Conflict of interest

All authors confirm that there is no conflict of interest.

References

1. Dreisler E, Kjer JJ. Asherman's syndrome: current perspectives on diagnosis and management. Int J Womens Health. 2019; 11: 191–198, doi: 10.2147/IJWH.S165474, indexed in Pubmed: 30936754.
2. Wang X, Ma N, Sun Q, et al. Elevated NF-κB signaling in Asherman syndrome patients and animal models. Oncotarget. 2017; 8(9): 15399–15406, doi: 10.18632/oncotarget.14853, indexed in Pubmed: 28148903.
3. March CM. Management of Asherman's syndrome. Reprod Biomed Online. 2011; 23(1): 63–76, doi: 10.1016/j.rbmo.2010.11.018, indexed in Pubmed: 21549641.
4. Wang J, Ju B, Pan C, et al. Application of Bone Marrow-Derived Mesenchymal Stem Cells in the Treatment of Intrauterine Adhesions in Rats. Cell Physiol Biochem. 2016; 39(4): 1553–1560, doi: 10.1159/000447857, indexed in Pubmed: 27614987.
5. Conforti A, Alviggi C, Mollo A, et al. The management of Asherman syndrome: a review of literature. Reprod Biol Endocrinol. 2013; 11: 118, doi: 10.1186/1477-7827-11-118, indexed in Pubmed: 24373209.
6. Sabry D, Mostafa A, Marzouk S, et al. Neupogen and mesenchymal stem cells are the novel therapeutic agents in regeneration of induced endometrial fibrosis in experimental rats. Biosci Rep. 2017; 37(5), doi: 10.1042/BSR20170794, indexed in Pubmed: 28883083.

7. Tang L, Chen Yu, Pei F, et al. Lithium Chloride Modulates Adipogenesis and Osteogenesis of Human Bone Marrow-Derived Mesenchymal Stem Cells. Cell Physiol Biochem. 2015; 37(1): 143–152, doi: 10.1159/000430340, indexed in Pubmed: 26303458.
8. Golpanian S, Wolf A, Hatzistergos KE, et al. Rebuilding the Damaged Heart: Mesenchymal Stem Cells, Cell-Based Therapy, and Engineered Heart Tissue. Physiol Rev. 2016; 96(3): 1127–1168, doi: 10.1152/physrev.00019.2015, indexed in Pubmed: 27335447.
9. Santamaria X, Cabanillas S, Cervelló I, et al. Autologous cell therapy with CD133+ bone marrow-derived stem cells for refractory Asherman's syndrome and endometrial atrophy: a pilot cohort study. Hum Reprod. 2016; 31(5): 1087–1096, doi: 10.1093/humrep/dew042, indexed in Pubmed: 27005892.
10. Cocuzza MA, Cocuzza M, Maciel GAR, et al. Development of an animal model for endometrial ablation using trichloroacetic acid. Fertil Steril. 2011; 95(7): 2418–2421, doi: 10.1016/j.fertnstert.2011.03.064, indexed in Pubmed: 21497335.
11. Kilic S, Yuksel B, Pinarli F, et al. Effect of stem cell application on Asherman syndrome, an experimental rat model. J Assist Reprod Genet. 2014; 31(8): 975–982, doi: 10.1007/s10815-014-0268-2, indexed in Pubmed: 24974357.
12. Jing Z, Qiong Z, Yonggang W, et al. Rat bone marrow mesenchymal stem cells improve regeneration of thin endometrium in rat. Fertil Steril. 2014; 101(2): 587–594, doi: 10.1016/j.fertnstert.2013.10.053, indexed in Pubmed: 24355044.
13. Alhadlaq A, Mao JJ. Mesenchymal stem cells: isolation and therapeutics. Stem Cells Dev. 2004; 13(4): 436–448, doi: 10.1089/scd.2004.13.436, indexed in Pubmed: 15345137.
14. Mohi El-Din MM, Rashed LA, Mahmoud Haridy MA, et al. Impact of bone marrow-derived mesenchymal stem cells on remodeling the lung injury induced by lipopolysaccharides in mice. Future Sci OA. 2017; 3(1): FSO162, doi: 10.4155/fsoa-2016-0036, indexed in Pubmed: 28344826.
15. MT AA, MA, W. Mesenchymal Stem Cells Therapy in Acute Renal Failure: Possible Role of Hepatocyte Growth Factor. J Stem Cell Res Ther. 2011; 01(03), doi: 10.4172/2157-7633.1000109.
16. Yener T, Turkkani Tunc A, Aslan H, et al. Determination of oestrous cycle of the rats by direct examination: how reliable? Anat Histol Embryol. 2007; 36(1): 75–77, doi: 10.1111/j.1439-0264.2006.00743.x, indexed in Pubmed: 17266672.
17. Bancroft JD, Gamble M. The hematoxylin and eosin. In: Theory and Practice of Histological Techniques, 6th ed. London: Churchill Livingstone. ; 2008: 121–134.
18. Bancroft JD, Gamble M. 2008. Connective tissue and stain. In: Theory and Practice of Histological Techniques, 6th ed. London: Churchill Livingstone. ; 2008: 147–150.
19. Smikle C, Khetarpal S. Asherman Syndrome. Stat Pearls [Internet], Treasure Island (FL), StatPearls Publishing. ; 2020.
20. Guo EJ, Chung JP, Poon LC, et al. Reproductive outcomes after surgical treatment of asherman syndrome: A systematic review. Best Pract Res Clin Obstet Gynaecol. 2019; 59: 98–114, doi: 10.1016/j.bpobgyn.2018.12.009, indexed in Pubmed: 30713131.
21. Senturk LM, Erel CT. Thin endometrium in assisted reproductive technology. Curr Opin Obstet Gynecol. 2008; 20(3): 221–228, doi: 10.1097/GCO.0b013e328302143c, indexed in Pubmed: 18460935.
22. Eftekhar M, Tabibnejad N, Tabatabaie A. The thin endometrium in assisted reproductive technology: An ongoing challenge. Middle East Fertility Society Journal. 2018; 23(1): 1–7, doi: 10.1016/j.mefs.2017.12.006.
23. Luckett-Chastain LR, Gallucci RM. Interleukin (IL)-6 modulates transforming growth factor-beta expression in skin and dermal fibroblasts from IL-6-deficient mice. Br J Dermatol. 2009; 161(2): 237–248, doi: 10.1111/j.1365-2133.2009.09215.x, indexed in Pubmed: 19438433.
24. Ramalho BD, Almeida FM, Sales CM, et al. Injection of bone marrow mesenchymal stem cells by intravenous or intraperitoneal routes is a viable alternative to spinal cord injury treatment in mice. Neural Regen Res. 2018; 13(6): 1046–1053, doi: 10.4103/1673-5374.233448, indexed in Pubmed: 29926832.
25. Zickri MB, Fadl SG, Metwally HG. Comparative Study between Intravenous and Intraperitoneal Stem Cell Therapy in Amiodarone Induced Lung Injury in Rat. Int J Stem Cells. 2014; 7(1): 1–11, doi: 10.15283/ijsc.2014.7.1.1, indexed in Pubmed: 24921022.
26. Fu Y, Karbaat L, Wu L, et al. Trophic Effects of Mesenchymal Stem Cells in Tissue Regeneration. Tissue Eng Part B Rev. 2017; 23(6): 515–528, doi: 10.1089/ten.TEB.2016.0365, indexed in Pubmed: 28490258.
27. Horton JA, Hudak KE, Chung EJ, et al. Mesenchymal stem cells inhibit cutaneous radiation-induced fibrosis by suppressing chronic inflammation. Stem Cells. 2013; 31(10): 2231––2241, doi: 10.1002/stem.1483, indexed in Pubmed: 23897677.
28. Ebrahim N, Mostafa O, El Dosoky RE, et al. Human mesenchymal stem cell-derived extracellular vesicles/estrogen combined therapy safely ameliorates experimentally induced intrauterine adhesions in a female rat model. Stem Cell Res Ther. 2018; 9(1): 175, doi: 10.1186/s13287-018-0924-z, indexed in Pubmed: 29954457.
29. Toh WS, Lai RC, Zhang B, et al. MSC exosome works through a protein-based mechanism of action. Biochem Soc Trans. 2018; 46(4): 843–853, doi: 10.1042/BST20180079, indexed in Pubmed: 29986939.
30. Zhang S, Teo KY, Chuah SJ, et al. MSC exosomes alleviate temporomandibular joint osteoarthritis by attenuating inflammation and restoring matrix homeostasis. Biomaterials. 2019; 200: 35–47, doi: 10.1016/j.biomaterials.2019.02.006, indexed in Pubmed: 30771585.
31. Omar A, Aboulkhair A. Do microvesicles derived from adipose mesenchymal stem cells have a therapeutic potential on Escherichia coli lipopolysaccharides-induced sepsis in Zona fasciculata of adult male albino rats? A histological study. EJH. 2018; 41(2): 204–219, doi: 10.21608/ejh.2018.13843.
32. Kang MS, Ryu E, Lee SW, et al. Regulation of PCNA cycling on replicating DNA by RFC and RFC-like complexes. Nat Commun. 2019; 10(1): 2420, doi: 10.1038/s41467-019-10376-w, indexed in Pubmed: 31160570.
33. Li B, Zhang Q, Sun J, et al. Human amniotic epithelial cells improve fertility in an intrauterine adhesion mouse model. Stem Cell Res Ther. 2019; 10(1): 257, doi: 10.1186/s13287-019-1368-9, indexed in Pubmed: 31412924.
34. Shawky LM, El Bana EA, Morsi AA. Stem cells and metformin synergistically promote healing in experimentally induced cutaneous wound injury in diabetic rats. Folia Histochem Cytobiol. 2019; 57(3): 127–138, doi: 10.5603/FHC.a2019.0014, indexed in Pubmed: 31489604.
35. Mohsen RO, Halawa AM, Hassan R. Role of bone marrow-derived stem cells versus insulin on filiform and fungiform papillae of diabetic albino rats (light, fluorescent and scanning electron microscopic study). Acta Histochem. 2019; 121(7): 812–822, doi: 10.1016/j.acthis.2019.07.007, indexed in Pubmed: 31358295.
36. Fu X, Liu Ge, Halim A, et al. Mesenchymal Stem Cell Migration and Tissue Repair. Cells. 2019; 8(8), doi: 10.3390/cells8080784, indexed in Pubmed: 31357692.

37. Miwa I, Tamura H, Takasaki A, et al. Pathophysiologic features of „thin“ endometrium. Fertil Steril. 2009; 91(4): 998–1004, doi: 10.1016/j.fertnstert.2008.01.029, indexed in Pubmed: 18328483.
38. Santamaria X, Isaacson K, Simón C. Asherman's Syndrome: it may not be all our fault. Hum Reprod. 2018; 33(8): 1374–1380, doi: 10.1093/humrep/dey232, indexed in Pubmed: 31986212.
39. Lawrence T. The nuclear factor NF-kappaB pathway in inflammation. Cold Spring Harb Perspect Biol. 2009; 1(6): a001651, doi: 10.1101/cshperspect.a001651, indexed in Pubmed: 20457564.
40. Liu T, Zhang L, Joo D, et al. NF-κB signaling in inflammation. Signal Transduct Target Ther. 2017; 2, doi: 10.1038/sigtrans.2017.23, indexed in Pubmed: 29158945.
41. Xue X, Chen Q, Zhao G, et al. The Overexpression of TGF-β and CCN2 in Intrauterine Adhesions Involves the NF-κB Signaling Pathway. PLoS One. 2015; 10(12): e0146159, doi: 10.1371/journal.pone.0146159, indexed in Pubmed: 26719893.
42. Su VYF, Lin CS, Hung SC, et al. Mesenchymal Stem Cell-Conditioned Medium Induces Neutrophil Apoptosis Associated with Inhibition of the NF-κB Pathway in Endotoxin-Induced Acute Lung Injury. Int J Mol Sci. 2019; 20(9), doi: 10.3390/ijms20092208, indexed in Pubmed: 31060326.
43. Kharaziha P, Hellström PM, Noorinayer B, et al. Improvement of liver function in liver cirrhosis patients after autologous mesenchymal stem cell injection: a phase I-II clinical trial. Eur J Gastroenterol Hepatol. 2009; 21(10): 1199–1205, doi: 10.1097/MEG.0b013e32832a1f6c, indexed in Pubmed: 19455046.
44. Caplan H, Olson SD, Kumar A, et al. Mesenchymal Stromal Cell Therapeutic Delivery: Translational Challenges to Clinical Application. Front Immunol. 2019; 10: 1645, doi: 10.3389/fimmu.2019.01645, indexed in Pubmed: 31417542.

Submitted: 10 May, 2020
Accepted after reviews: 21 September, 2020
Available as AoP: 30 September, 2020

FOLIA HISTOCHEMICA ET CYTOBIOLOGICA
Vol. 58, No. 3, 2020
pp. 219–226

ORIGINAL PAPER

VIA MEDICA

Upregulated miR-96-5p inhibits cell proliferation by targeting HBEGF in T-cell acute lymphoblastic leukemia cell line

Kaihong Xu[1], Xiao Yan[1], Guifang Ouyang[1], Jinyi Feng[2], Lilin Ye[2], Xuezhen Hu[3], Dingsheng Liu[2]*

[1]Department of Hematology, Ningbo First Hospital, Ningbo City, Zhejiang Province, 315000, China

[2]Department of Oncology and Hematology, Shanghai University of Medicine & Health Sciences Affiliated Zhoupu Hospital, Shanghai City, 201318, China

[3]Department of Emergency Medicine, The Second Affiliated Hospital and Yuying Children's Hospital of Wenzhou Medical University, Wenzhou City, Zhejiang Province, 325000, China

Abstract

Introduction. microRNAs (miRNAs) are critical for tumorigenesis and progression of T-cell acute lymphoblastic leukemia (T-ALL). MiR-96-5p has been shown to play important roles in the development of many cancers, but its roles in T-ALL have yet not been studied.

Materials and methods. miR-96-5p expression was detected in T-leukemic cells from peripheral blood of 30 patients with T-ALL using real-time quantitative PCR (RT-qPCR). TargetScan database was utilized to identify the target genes for miR-96-5p, and their target relationship was verified by western blot, dual luciferase reporter assay and RT-qPCR. The effects of miR-96-5p on the viability and proliferation of T-leukemic cells (Jurkat cells) were respectively determined using MTT and BrdU incorporation assays.

Results. miR-96-5p presented low expression levels by qPCR in peripheral blood of T-ALL patients compared to healthy volunteers. Upregulated miR-96-5p by miR-96-5p mimic transfection markedly inhibited the viability and proliferation of Jurkat cells. Furthermore, miR-96-5p negatively regulated the expression of its target gene, *HBEGF*. The decreased viability and proliferation of Jurkat cells caused by miR-96-5p over-expression was suppressed after the introduction of HBEGF plasmid.

Conclusions. The presented study showed that upregulation of miR-96-5p inhibited the viability and proliferation of Jurkat T-leukemic cells through suppressing HBEGF expression. Our study provides a novel sight for understanding the pathological mechanism of T-ALL and suggests that miR-96-5p may be a potential biomarker for the therapy and diagnosis of T-ALL. *(Folia Histochemica et Cytobiologica 2020, Vol. 58, No. 3, 219–226)*

Key words: miR-96-5p; T-cell acute lymphoblastic leukemia; Jurkat T cells; HBEGF

Introduction

Acute lymphoblastic leukemia (ALL) is a hematologic malignancy in which the bone marrow produces large numbers of lymphoid progenitor cells. It represents the most common cancer in children, with approximately 60% of ALL cases in people younger than 20 years [1]. The risk factors for ALL include environmental factors (*e.g.* X-rays, radiation, alcohol use), genetic factors (*e.g.* Down syndrome, Bloom syndrome), and infection [2]. ALL cases arise from B-cell or T-cell

Correspondence address: Dingsheng Liu
Department of Oncology and Hematology,
Shanghai University of Medicine &
Health Sciences Affiliated Zhoupu Hospital,
No. 1500 Zhouyuan Road, Pudong New District,
Shanghai City, China
phone: +86 02168135590
e-mail: QWEok67K@163.com

precursors, and are defined as B-cell ALL (B-ALL) and T-cell ALL (T-ALL) [3], respectively. T-ALL accounts for 25% of ALL cases in adults, and 10–15% of ALL cases in children [4]. Despite small numbers, T-ALL has achieved lots of attention due to its highly aggressive behavior [5]. Recently, advancements of therapeutic protocols have improved the 5-year overall survival (OS) rate to more than 80% in children with T-ALL, however, the OS rate in adult T-ALL patients is still low (approximately 50%) [6]. Furthermore, recurrence is still a huge challenge for all age groups, leading to poor prognosis [6, 7]. Hence, further improvements of therapy for T-ALL patients are required.

MicroRNAs (miRNAs) are a class of small (about 22 nucleotides), single-stranded noncoding RNAs [8, 9]. MiRNAs directly bind to the 3'-untranslated regions (3'-UTRs) of target mRNAs through base-pairing with complementary sequences, thereby regulating gene expression [10]. MiRNAs are relevant to a wide range of cellular functions such as cell differentiation, proliferation, migration, and invasion [11]. Dysfunction of miRNAs has been widely identified in many cancers, including B-ALL and T-ALL [12, 13]. For instance, miR-101 targets CXCR7 to suppress T-ALL cell invasion and proliferation *in vitro* and reduce tumor metastasis and growth *in vivo* [14]. MiR-708 can target CD47 on macrophages to promote phagocytosis, thereby eradicating T-ALL cells [15]. MiR-96-5p can target the caspase-9 gene to inhibit cell apoptosis in hepatocellular carcinoma [16]. Besides, miR-96-5p functions as an oncogenic factor to promote the proliferation of ovarian cancer cells through regulating caveolae1 [17]. MiR-96-5p also serves as a tumor suppressor to repress the breast cancer cell growth and metastasis through modulating the Wnt/β-catenin pathway [18]. Nevertheless, the role of miR-96-5p in T-ALL have yet not been described.

The aim of this study was to detect the role and molecular mechanisms of miR-96-5p in T-ALL cells. Here, we firstly determined the expression level of miR-96-5p in T-ALL patients and measured its effects on the proliferation of T-ALL cells. Then, a target gene of miR-96-5p, *HBEGF* (Heparin-binding epidermal growth factor (EGF)-like growth factor) was identified by the TargetScan database. Next, the interaction of HBEGF gene with miR-96-5p in T-ALL cells was further explored. These experiments may contribute to a better understanding on the pathological mechanism of T-ALL.

Materials and methods

T-ALL patient blood samples. This experiment was approved by the Ethical Committee of Ningbo First Hospital. Peripheral blood samples from 20 healthy volunteers and 30 patients with T-ALL were collected at Ningbo First Hospital after obtaining all patients' informed consents.

Table 1. The clinicopathologic features of acute lymphoblastic leukemia

Characteristics	Number of patients
Number	30
Gender (Male/Female)	9/21
Age (years)	22.5 (16–58)
Karyotype (Normal/Aberrant/No data available)	12/16/2
White blood cell count [$\times 10^9$/L]	12.8 (0.4–97)
Platelet count [$\times 10^9$/L]	215.6 (12–587)
Hemoglobin levels [g/L]	9.25 (3.8–18.5)

Data present median values and ranges.

The diagnosis of T-ALL was based on molecular genetics, cytochemistry, immunology, cytomorphology, and multiparameter flow cytometry. The clinical characteristics of the patients with T-ALL are presented in Table 1.

Isolation of T-leukemic cells. Peripheral blood was collected in tubes with EDTA and separated using the Ficoll density gradient centrifugation method (Ficoll-Histopaque®-1077, Sigma-Aldrich, St. Louis, MO, USA). After removing the upper layer, PBMCs (peripheral blood mononuclear cells) were collected and used for the purification of T-leukemic cells. Briefly, PBMCs were resuspended in isolation buffer, heat-inactivated fetal calf serum (FCS, Sigma-Aldrich) was added and incubated with biotinylated anti-human CD235a, CD123, CD56, CD16, CD123, CD19, and CD14 antibodies for 20 min at 4°C. Besides, Dynabeads (Dynabeads™ Untouched™ Human T Cells Kit, Thermo Fisher Scientific, Waltham, MA, USA) were washed before use according to the manufacturer's protocol. Next, the cells were centrifuged at 300 *g* at 4°C for 8 min, resuspended in isolation buffer, pre-washed Depletion Dynabeads (Thermo Fisher Scientific) were added and the cells were incubated at 25°C for 15 min, followed by placing in the magnet to obtain the supernatant containing human T cells.

Cell culture and transfection. The isolated T cells were cultured in RPMI 1640 medium with 15% FCS, 100 μg/ml streptomycin, 100 Units/ml penicillin, 10 ng/ml PMA (phorbol 12-myristate 13-acetate), 20 mM HEPES, 2 mM glutamine, 2-ME (mercaptoethanol) (all from Sigma-Aldrich) and 10 ng/ml interleukin-2 (Peprotech, Rocky Hill, NI, USA) at 37°C and in the atmosphere of 5% CO_2.

Jurkat T-leukemia cells were obtained from Cell Bank of the Chinese Academy of Sciences (Shanghai, China). These cells were incubated in RPMI 1640 medium (Gibco) supplemented with 10% FCS, 100 μg/ml streptomycin, 100 Units/ml penicillin, and glutamine (4 mM) at 37°C, 5% CO_2.

Table 2. Primer sequences

Primer	Sequences (5'–3')
miR-96-5p forward	ACGATGCACCTGTACGATCA
miR-96-5p reverse	TCTTTCAACACGCAGGACAG
HBEGF forward	CTGTCTTCGGTCTGCCTCCT
HBEGF reverse	AGACCGAAGACAGCACCA
U6 forward	GCTTCGGCAGCACATATACTAAAAT
U6 reverse	CGCTTCACGAATTTGCGTGTCAT
β-actin forward	TCACCCACACTGTGCCCATCTACGA
β-actin reverse	CAGCGGAACCGCTCATTGCCAATGG

MiRNA negative control (miR-NC), miR-96-5p mimic, inhibitor control (NC-inh) and miR-96-5p inhibitor were purchased from Thermo Fisher Scientific. HBEGF plasmid and scramble plasmid were obtained from HANBIO (Shanghai, China). For transfection, Jurkat cells were suspended in Resuspension Buffer R (Neon® Kits, Thermo Fisher Scientific) and mixed with 1 μg plasmid, 150 nM miRNA mimics or inhibitor. The mix was taken up into the Neon Pipette tip, plugged into the pipette holder and electroporated by the Neon Transfection System (Thermo Fisher Scientific) based on the protocol from the manufacturer. Then, the cells were added to 24-well plates with medium and cultured for 24 h in a humidified 5% CO_2 incubator at 37°C for further analysis.

Real-time quantitative PCR (RT-qPCR). TRIzol reagent (Invitrogen, Carlsbad, CA, USA) was used to extract total RNA. The isolated RNAs were reverse transcribed into cDNAs as PCR templates with a QuantiTect Reverse Transcription Kit (Qiagen, Hilden, Germany). Each PCR reaction including PCR templates, 1×SYBR Master Mix (Applied Biosystems, Foster City, CA, USA) and primers was carried out using an ABI Prism 7500 fast real-time PCR system (Applied Biosystems). The sequence of the primers was listed in Table 2. β-actin and U6 was used as internal controls. The relative expression of the original target transcript was presented as $2^{-\Delta\Delta Ct}$. $^{\Delta\Delta}Ct = (C_{t,\ target\ gene,\ case\ group}\text{-}C_{t,\ reference\ gene,\ case\ group})\text{-}(C_{t,\ target\ gene,\ control\ group}\text{-}C_{t,\ reference\ gene,\ control\ group})$

MTT (3-(4,5-Dimethylthiazol-2-yl)-2,5-diphenyltetrazolium bromide) assay. After transfection, the viability of Jurkat cells was evaluated using MTT assay. Jurkat cells (1×10^6/ml) were inoculated in 96-well plates, followed by incubated for 24 h. Next, MTT (3-(4,5-dimethylthiazol-2-yl)-2,5-diphenyltetrazolium bromide) (5 mg/ml, 10 μL) was added to the plates followed by incubation with the cells for another 4 h. After centrifugation for 10 min at 300 *g*, the supernatant was removed carefully, and DMSO (100 μL) was added to each well. The sample's absorbance was assessed at 570 nm using a microplate spectrophotometer (Thermo Fisher Scientific). % viable cells = $(ABS_{sample} - ABS_{blank})/(ABS_{control} - ABS_{blank}) \times 100\%$; ABS: Absorbance.

Cell proliferation assay. Jurkat cells after transfection were inoculated in 96-well plates at a density of 1×10^5 cells per ml and cultured in RPMI 1640 medium with 10% FCS for 72 h. Subsequently, the proliferation of Jurkat cells was evaluated by the colorimetric method using a BrdU Cell Proliferation ELISA kit (Roche, Merck Millipore, Burlington, MA, USA) based on the instruction. The sample's absorbance was examined at 450 nm in a microplate reader.

Dual luciferase reporter assay. The TargetScan website (http://www.targetscan.org/vert_72/) was utilized to identify the potential binding sits between *HBEGF* and miR-96-5p. The fragment of HBEGF gene containing wild-type miR-96-5p binding sites or the corresponding mutant fragment of HBEGF was cloned into pMIR-REPOR™ Luciferase vectors (Promega Madison, WI, USA), named as the HBEGF-WT reporter vector or the HBEGF-MUT reporter vector. These vectors with miRNA negative control (miR-NC) or miR-96-5p mimic were co-transfected into Jurkat cells by electroporation. In the stage of the pre-experiment, the mRNA expression of *HBEGF* detected by qPCR was used to present the efficiency of transfection, and the efficiency was high. Next, Jurkat cells were incubated at 37°C for 48 h, and subsequently the firefly luciferase activity and Renilla luciferase activity were determined with a Dual-Luciferase® 1000 Assay kit (Promega). The relative luciferase intensity = firefly luciferase activity/Renilla luciferase activity.

Western blot. After transfection, Jurkat cells were lysed with RIPA lysis buffer (Beyotime, Shanghai, China) on ice and centrifuged at 13000×*g* to obtain total protein. A BCA Protein Assay Kit (Thermo Fisher Scientific) was applied to assess the protein concentration. Proteins (20 μg) were separated on 10% SDS-PAGE gels through electrophoresis and then electro-transferred onto PVDF membranes. 5% non-fat milk was utilized to block the membranes at 25°C for 1 h. Subsequently, the membranes were incubated with primary antibodies against HBEGF (ab92620, 1/1000 dilution, ABCAM) and β-actin (ab179467, 1/5000 dilution, ABCAM) at 4°C, washed using TBS buffer with 0.05% Tween-20, and next cultured with HRP-conjugated secondary antibodies (Goat Anti-Rabbit IgG, #7074, 1:1000, Cell Signaling Technology Danvers, MA, USA) for 1 h at room temperature. Protein bands were visualized with a chemiluminescence detection kit (Aidlab Biotechnology, Beijing, China). The semi-quantification of proteins was applied using the ImageJ software, and the relative expression = the protein expression of HBEGF/the protein expression of β-actin was determined.

Statistical analysis. Each experiment involving Jurkat cells was repeated three times. Experimental data were expressed as mean ± SD. The statistics were evaluated by the GraphPad Prism 7 software (San Diego, CA, USA). Student's t test was utilized to identify differences between two groups.

One-way ANOVA with Bonferroni *post hoc* comparison test was used for analysis with multiple groups. The significant difference was defined as $p < 0.05$.

Results

Upregulated miR-96-5p inhibits the viability and proliferation of T-leukemic cells

Firstly, miR-96-5p expression in T-ALL was examined using RT-qPCR. Figure 1 showed that the levels of miR-96-5p in T-leukemic cells from peripheral blood of T-ALL patients were significantly lower compared with that from normal volunteers (**p < 0.01).

Secondly, we detected the effects of miR-96-5p on Jurkat cells. RT-qPCR showed the transfection of miR-96-5p mimic in Jurkat cells considerably up-regulated miR-96-5p expression level as compared to miRNA negative control (miR-NC) (Fig. 2A, ***p < 0.001). MTT assay suggested that miR-96-5p mimic obviously decreased the viability of Jurkat cells in comparison to miR-NC (Fig. 2B, **p < 0.01).

Furthermore, the proliferation of Jurkat cells was measured by BrdU incorporation assay. The results suggested that transfection of miR-96-5p mimic in Jurkat cells caused an obvious reduction in proliferation as compared to miR-NC transfection (Fig. 2C, *p < 0.05). Thus, miR-96-5p mimics inhibited the viability and proliferation of Jurkat cells.

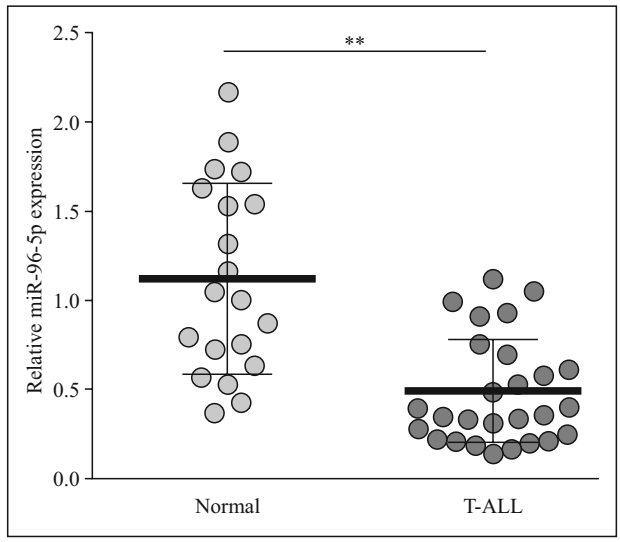

Figure 1. The down-regulated expression of miR-96-5p in T-cell acute lymphoblastic leukemia (T-ALL). RT-qPCR was used to detect the expression of miR-96-5p in T-leukemic cells from peripheral blood of T-ALL patients and healthy volunteers (normal control). **$p < 0.01$.

HBEGF is a target gene of miR-96-5p

To explore the molecular mechanism of miR-96-5p effects on Jurkat cells, we applied the TargetScan database to predict the potential target genes for miR-96-5p. HBEGF (heparin binding EGF like growth factor) was chosen as a candidate gene based on the high ranking in prediction results from the TargetScan database and its critical roles in various cancers [19, 20]. The putative binding sites were listed in Figure 3A. The interaction of HBEGF with miR-96-5p was validated via dual luciferase reporter assay. The luciferase activity in the HBEGF-WT group was down-regulated by miR-96-5p mimic in comparison to miR-NC (**p < 0.01), whereas the activity in the HBEGF-MUT group showed no significant difference (Fig. 3B). Thus, miR-96-5p was proved to directly target HBEGF. After Jurkat cells were transfected with in-

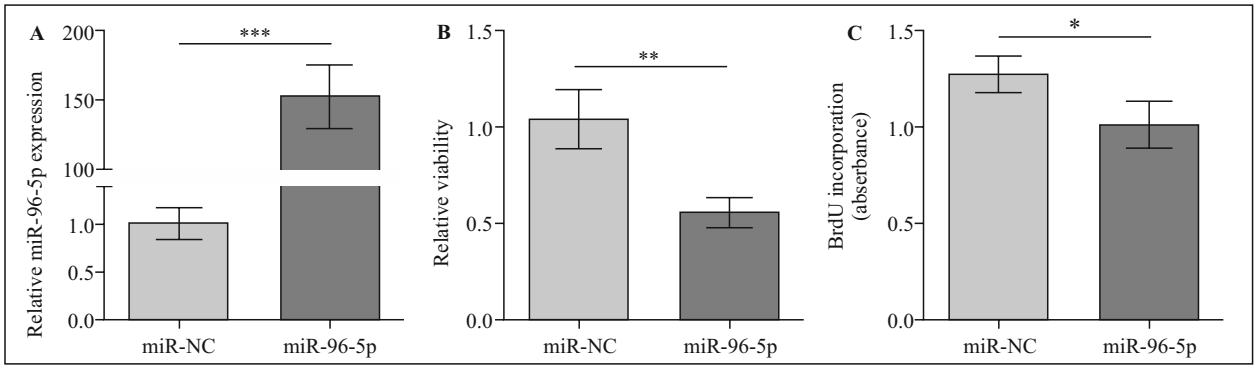

Figure 2. The effect of miR-96-5p on the viability and proliferation of Jurkat cells. **A.** RT-qPCR showed the expression of miR-96-5p was enhanced by transfection of miR-96-5p mimic as compared to miRNA negative control (miR-NC). **B.** MTT assay showed that miR-96-5p mimic suppressed the viability of Jurkat cells compared with miR-NC. **C.** BrdU incorporation assay suggested that the proliferation of Jurkat cells was inhibited by the transfection of miR-96-5p mimic as compared to miR-NC. *$p < 0.05$, **$p < 0.01$, ***$p < 0.001$.

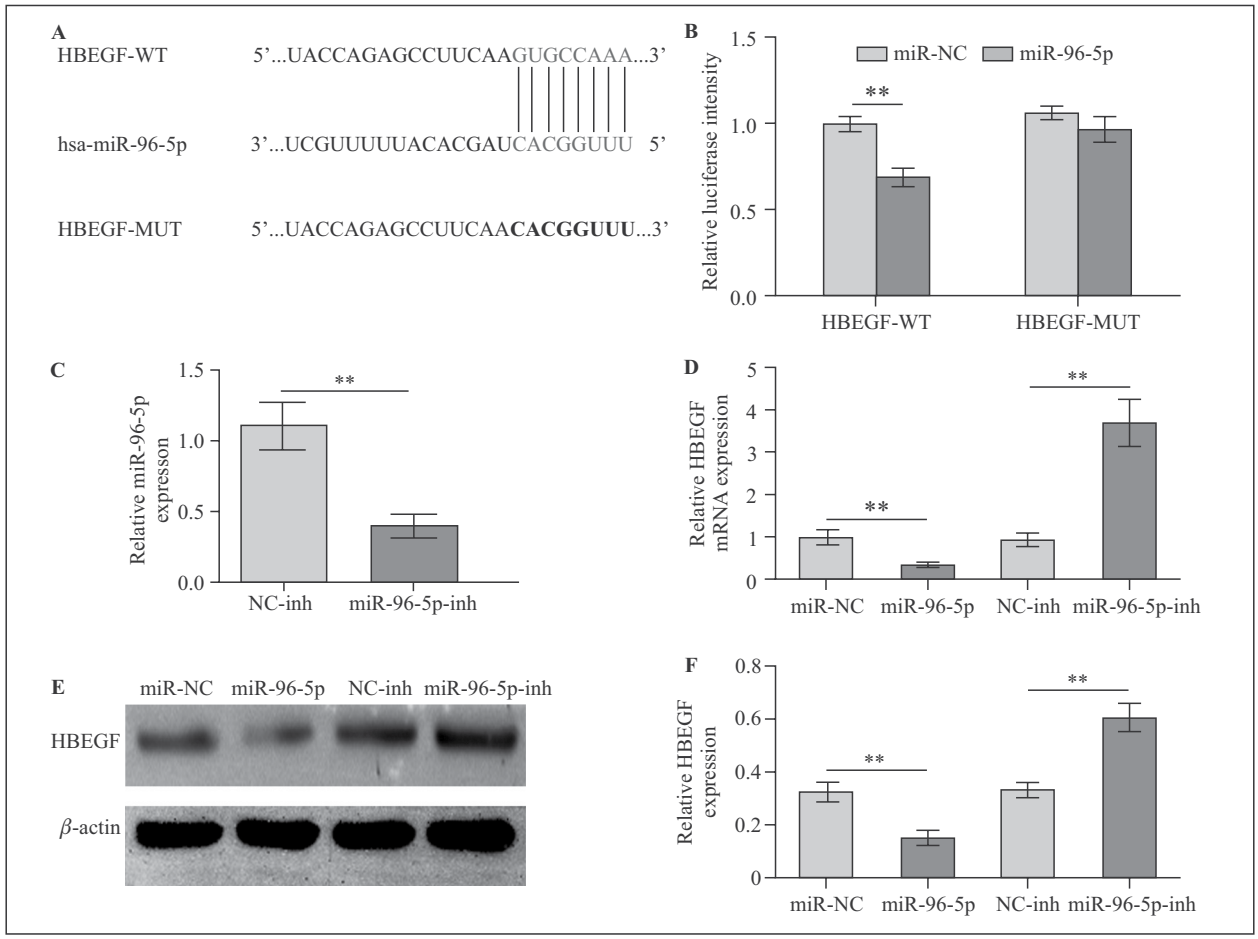

Figure 3. The relationship between miR-96-5p and HBEGF in Jurkat cells. **A.** The image of the putative binding sites between miR-96-5p and HBEGF. **B.** Dual luciferase reporter assay was used to verify the target relationship between miR-96-5p and HBEGF. Compared with miR-NC, the interaction between HBEGF-WT vector and miR-96-5p mimic decreased the luciferase activity, whereas the activity had no significant change in the HBEGF-MUT group. **C.** RT-qPCR suggested the decrease of miR-96-5p expression caused by miR-96-5p inhibitor (miR-96-5p-inh) compared with inhibitor control (NC-inh). After Jurkat cells were transfected with miR-96-5p mimic, miRNA control (miR-NC), miR-96-5p-inh or NC-inh. **D.** RT-qPCR showed HBEGF expression decreased by miR-96-5p mimic compared with miRNA control (miR-NC), but increased by miR-96-5p-inh as compared to NC-inh. **E, F.** The changing trends of HBEGF expression were further validated by western blot. $^{**}p < 0.01$.

hibitor control (NC-inh) or miR-96-5p inhibitor, miR-96-5p inhibitor greatly decreased miR-96-5p expression in comparison to NC-inh (Fig. 3C, $^{**}p < 0.01$). As shown in Figure 3D, compared with miR-NC, miR-96-5p mimic markedly down-regulated the mRNA expression levels of HBEGF ($^{**}p < 0.01$), and yet miR-96-5p inhibitor up-regulated HBEGF mRNA expression in comparison to NC-inhibitor ($^{**}p < 0.01$). Additionally, the protein expression of HBEGF was decreased by miR-96-5p mimic as compared to miR-NC ($^{**}p < 0.01$), while the protein level of HBEGF was increased by miR-96-5p inhibitor compared with NC-inhibitor ($^{**}p < 0.01$, Figs. 3E and 3F). Collectively, miR-96-5p could directly target HBEGF and negatively regulate HBEGF expression.

Upregulated miR-96-5p inhibits the viability and proliferation of T lymphocytes through regulating HBEGF

To detect the effects of miR-96-5p/HBEGF on T lymphocytes, Jurkat cells were transfected with miR-96-5p mimic combined with or without HBEGF plasmid. As shown in Figure 4A, compared with miR-NC+vector, miR-96-5p mimic obviously down-regulated the mRNA expression of HBEGF ($^{**}p < 0.01$) and HBEGF plasmid up-regulated HBEGF expression ($^{**}p < 0.01$). Besides, the co-transfection of miR-96-5p mimic with HBEGF plasmid significantly decreased the expression of HBEGF compared with the transfection of HBEGF plasmid alone ($^{**}p < 0.01$). Furthermore, western blot further confirmed that the

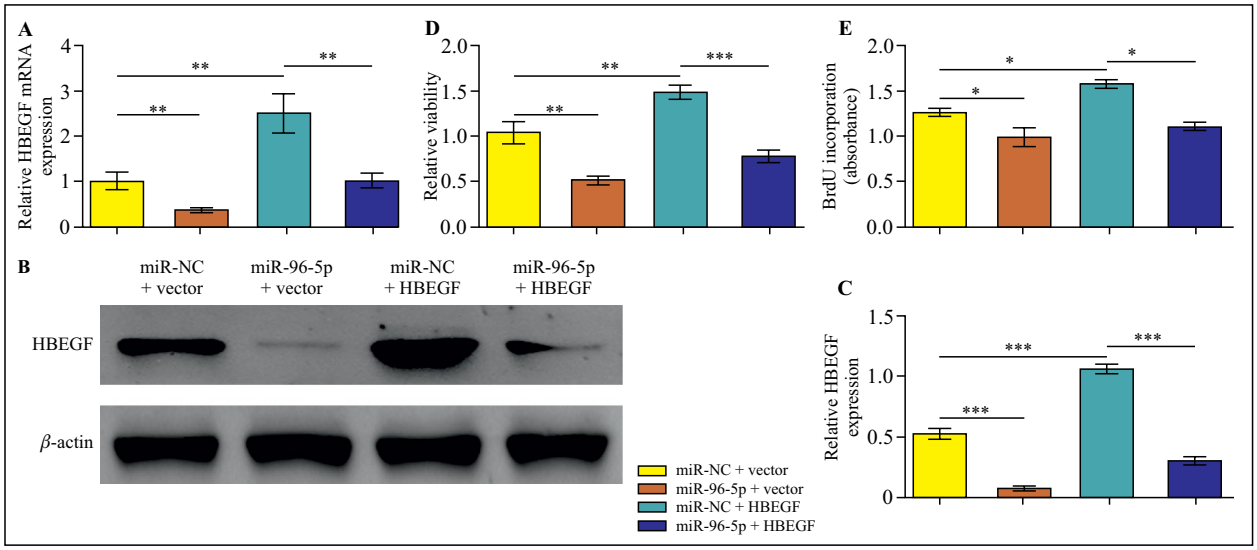

Figure 4. miR-96-5p targets HBEGF to regulate the viability and proliferation of Jurkat cells. Jurkat cells were transfected with miR-96-5p mimic + HBEGF plasmid, miR-96-5p mimic + scramble plasmid (vector), miRNA control (miR-NC) + HBEGF plasmid, or miR-NC + vector. **A.** RT-qPCR revealed HBEGF expression was increased by HBEGF plasmid and decreased by miR-96-5p mimic compared with miR-NC + vector, and the increase of HBEGF expression induced by HBEGF plasmid was changed by the co-transfection of miR-96-5p mimic with HBEGF plasmid. **B, C.** The changing trends of HBEGF expression were further validated by western blot. **D.** MTT assay showed the viability of Jurkat cells was inhibited by miR-96-5p mimic and enhanced by HBEGF plasmid compared with miR-NC + vector, and the enhancement in the cell viability caused by HBEGF plasmid was weakened by the co-transfection of miR-96-5p mimic with HBEGF plasmid. **E.** BrdU incorporation assay indicated that the cell proliferation had the same change tendency with **(D)** after Jurkat cells were transfected with those vectors. $^{*}p < 0.05$, $^{**}p < 0.01$, $^{***}p < 0.001$.

increase of HBEGF protein expression induced by HBEGF plasmid was weakened by the introduction of miR-96-5p mimic (***p < 0.001, Figs. 4B and 4C). Moreover, the viability of Jurkat cells was markedly enhanced by HBEGF plasmid compared with miR-NC+vector (**p < 0.01), which was weakened by the introduction of miR-96-5p mimic (Fig. 4D). Furthermore, HBEGF plasmid promoted the proliferation of Jurkat cells as compared to miR-NC+vector (*p<0.05), and yet this promotive effect was suppressed by the co-transfection of miR-96-5p mimic with HBEGF plasmid (*p<0.05) (Fig. 4E). Therefore, upregulated miR-96-5p inhibited the viability and proliferation of T lymphocytes through suppressing HBEGF expression.

Discussion

Despite the remarkable improvements in the treatment of T-ALL, approximately 20% children with T-ALL and 50% adult T-ALL patients still fail first-line therapy [6]. Especially, the recurrence result in a very poor prognosis in T-ALL patients [7]. It is reported that T-ALL is relevant to large numbers of genetic abnormalities, which facilitate the development of malignant lymphoid progenitors [21]. Thus, exploring the detailed molecular mechanism of T-ALL is important for improving therapeutic methods. MiRNAs have been applied to many clinical and preclinical studies in various diseases, among which some miRNAs have been proved to be closely associated with the pathogenesis of T-ALL [22]. For instance, miR-96-5p functions as a potential oncogenic factor or tumor suppressor in several cancers [16–18]. Gao *et al.* have shown that miR-96-5p can target CTNND1 to affect the activation of Wnt/β-catenin signaling resulting in the inhibition of the proliferation and invasion of breast cancer cells [18]. Zhang *et al.* have indicated that miR-96-5p negatively regulates SFRP4 to inhibit cervical cancer cell apoptosis and facilitate the cell viability and metastasis [23]. miR-96-5p has important functions in the proliferation and survival of B-cell malignancies [24, 25]. Nevertheless, there is no data regarding the roles of miR-96-5p in T-ALL. Thus, our study determined miR-96-5p expression levels in T-leukemic cells from peripheral blood of T-ALL patients and found the patients with aberrantly low expression of miR-96-5p as compared to that from healthy volunteers. Moreover, we used miR-96-5p mimic to upregulate the expression of

miR-96-5p, which markedly repressed the viability and proliferation of T-leukemic cells. Thus, miR-96-5p, as a new and potent biomarker, might be used for the therapy and diagnosis of T-ALL.

To further explore the molecular mechanisms of miR-96-5p in T-leukemic cells, TargetScan database was used to identify the potential target genes of miR-96-5p, among which HBEGF was chosen as a candidate. Despite the fact that HBEGF had a high ranking in prediction results of the TargetScan database, HBEGF, as a heparin-binding member of the EGF family [26], has been found to be a potent growth factor associated with tumorigenesis [19]. For instance, HBEGF stimulates EGFR expression and induces angiogenesis of bone marrow endothelial cells in multiple myeloma mouse model [27]. HBEGF over-expression promotes the invasion of gastric cancer cells [28]. Moreover, HBEGF has been observed to be over-expressed in T-ALL cells and associate with the cell survival [20]. In the present study, the direct target relationship between HBEGF and miR-96-5p was confirmed by dual luciferase reporter assay. In addition, miR-96-5p was observed to negatively regulate HBEGF expression.

MiRNAs are proved to mediate posttranscriptional regulation of genes to participate in a wide range of biological processes [29]. MiR-96-5p can target CTNND1 to regulate Wnt/β-catenin signaling and thus inhibit the invasion and proliferation of breast cancer [18]. MiR-212 represses the metastasis and growth of epithelial ovarian cancer through controlling HBEGF [26]. Regulation of HBEGF by miR-1192 affects the C2C12 cell osteogenic differentiation [30]. Our study also revealed that the promotive effects on the viability and proliferation of T-leukemic cells induced by HBEGF plasmid transfection were suppressed by the introduction of miR-96-5p mimic. Therefore, miR-96-5p could target HBEGF expression to regulate the viability and proliferation of T-leukemic cells.

In conclusion, our study found the aberrantly low expression of miR-96-5p in peripheral blood mononuclear cells of T-ALL patients. Additionally, upregulated miR-96-5p repressed the viability and proliferation of T-leukemic Jurkat cells through controlling HBEGF expression. Thus, miR-96-5p may be a potential biomarker. These findings contribute to a better understanding of the molecular mechanism of the functional role of miR-96-5p in T-ALL.

Funding

This work was supported by Natural Science Foundation of Ningbo Municipality (Grant No. 2017A610210 (Grant No.2017A610177) and Discipline Construction Program of Pudong New District Health Bureau of Shanghai (Grant No. PWZzk2017-31).

Competing interests

The authors state that there are no conflicts of interest.

Contribution of authors

KX and DL designed the study, supervised the data collection, analyzed the data, XY interpreted the data and prepare the manuscript for publication, and JF, LY and XH supervised the data collection, analyzed the data and reviewed the draft of the manuscript. All authors have read and approved the manuscript.

Availability of data and materials

All data generated or analyzed during this study are included in this published article.

References

1. Malard F, Mohty M. Acute lymphoblastic leukaemia. The Lancet. 2020; 395(10230): 1146–1162, doi: 10.1016/s0140-6736(19)33018-1, indexed in Pubmed: 32247396 .
2. Jacobson S, Tedder M, Eggert J. Adult acute lymphoblastic leukemia: a genetic overview and application to clinical practice. Clin J Oncol Nurs. 2016; 20(6): E147–E154, doi: 10.1188/16.CJON.E147-E154, indexed in Pubmed: 27857258.
3. Follini E, Marchesini M, Roti G. Strategies to overcome resistance mechanisms in T-cell acute lymphoblastic leukemia. Int J Mol Sci. 2019; 20(12), doi: 10.3390/ijms20123021, indexed in Pubmed: 31226848.
4. Bongiovanni D, Saccomani V, Piovan E. Aberrant signaling pathways in T-cell acute lymphoblastic leukemia. Int J Mol Sci. 2017; 18(9), doi: 10.3390/ijms18091904, indexed in Pubmed: 28872614.
5. Drobna M, Szarzyńska-Zawadzka B, Dawidowska M. T-cell acute lymphoblastic leukemia from miRNA perspective: Basic concepts, experimental approaches, and potential biomarkers. Blood Rev. 2018; 32(6): 457–472, doi: 10.1016/j.blre.2018.04.003, indexed in Pubmed: 29703513.
6. Evangelisti C, Chiarini F, McCubrey JA, et al. Therapeutic targeting of mTOR in T-cell acute lymphoblastic leukemia: An Update. Int J Mol Sci. 2018; 19(7), doi: 10.3390/ijms19071878, indexed in Pubmed: 29949919.
7. Maude SL, Teachey DT, Porter DL, et al. CD19-targeted chimeric antigen receptor T-cell therapy for acute lymphoblastic leukemia. Blood. 2015; 125(26): 4017–4023, doi: 10.1182/blood-2014-12-580068, indexed in Pubmed: 25999455.
8. Zhang L, Tang Y, Zhu X, et al. Overexpression of MiR-335-5p promotes bone formation and regeneration in mice. J Bone Miner Res. 2017; 32(12): 2466–2475, doi: 10.1002/jbmr.3230, indexed in Pubmed: 28846804.
9. Ji Y, Wang D, Zhang B, et al. MiR-361-3p inhibits ñamyloid accumulation and attenuates cognitive deficits through targeting BACE1 in Alzheimer's disease. J Integr Neurosci. 2019; 18(3): 285–291, doi: 10.31083/j.jin.2019.03.1136, indexed in Pubmed: 31601077.

10. Bartel DP. MicroRNAs: genomics, biogenesis, mechanism, and function. Cell. 2004; 116(2): 281–297, doi: 10.1016/s0092-8674(04)00045-5, indexed in Pubmed: 14744438.
11. Sandoval-Bórquez A, Polakovicova I, Carrasco-Véliz N, et al. MicroRNA-335-5p is a potential suppressor of metastasis and invasion in gastric cancer. Clin Epigenetics. 2017; 9: 114, doi: 10.1186/s13148-017-0413-8, indexed in Pubmed: 29075357.
12. Tutar Y. miRNA and cancer; computational and experimental approaches. Curr Pharm Biotechnol. 2014; 15(5): 429, doi: 10.2174/1389201015051408281613335, indexed in Pubmed: 25189575.
13. Nucera S, Giustacchini A, Boccalatte F, et al. miRNA-126 orchestrates an oncogenic program in b cell precursor acute lymphoblastic leukemia. Cancer Cell. 2016; 29(6): 905––921, doi: 10.1016/j.ccell.2016.05.007, indexed in Pubmed: 27300437.
14. Yang XY, Sheng Ye. miR-101 Represses T-cell acute lymphoblastic leukemia by targeting CXCR7/STAT3 axis. Oncol Res. 2019; 27(9): 997–1006, doi: 10.3727/096504018X15439207752093, indexed in Pubmed: 30837035.
15. Huang W, Wang WT, Fang Ke, et al. MIR-708 promotes phagocytosis to eradicate T-ALL cells by targeting CD47. Mol Cancer. 2018; 17(1): 12, doi: 10.1186/s12943-018-0768-2, indexed in Pubmed: 29368647.
16. Iwai N, Yasui K, Tomie A, et al. Oncogenic miR-96-5p inhibits apoptosis by targeting the caspase-9 gene in hepatocellular carcinoma. Int J Oncol. 2018; 53(1): 237–245, doi: 10.3892/ijo.2018.4369, indexed in Pubmed: 29658604.
17. Hao H, Liu Q, Wu D, et al. Tetrahydropalmatine reduces cell death and improves functional recovery after traumatic spinal cord injury in rats. Trop J Pharm Res. 2019; 18(5): 703–711, doi: doi: http://dx.doi.org/10.4314/tjpr.v18i4.4.
18. Gao XH, Zhang YL, Zhang ZY, et al. MicroRNA-96-5p represses breast cancer proliferation and invasion through Wnt/ñcatenin signaling via targeting CTNND1. Sci Rep. 2020; 10(1): 44, doi: 10.1038/s41598-019-56571-z, indexed in Pubmed: 31913290.
19. Yang CC, Chang KW. Eicosanoids and HB-EGF/EGFR in cancer. Cancer Metastasis Rev. 2018; 37(2-3): 385–395, doi: 10.1007/s10555-018-9746-9, indexed in Pubmed: 29936588.
20. Kunami N, Yotsumoto F, Ishitsuka K, et al. Antitumor effects of CRM197, a specific inhibitor of HB-EGF, in T-cell acute lymphoblastic leukemia. Anticancer Res. 2011; 31(7): 2483–2488, indexed in Pubmed: 21873163.
21. Bond J, Marchand T, Touzart A, et al. An early thymic precursor phenotype predicts outcome exclusively in HOXA-overexpressing adult T-cell acute lymphoblastic leukemia: a Group for Research in Adult Acute Lymphoblastic Leukemia study. Haematologica. 2016; 101(6): 732–740, doi: 10.3324/haematol.2015.141218, indexed in Pubmed: 26944475.
22. Rashed WM, Hamza MM, Matboli M, et al. MicroRNA as a prognostic biomarker for survival in childhood acute lymphoblastic leukemia: a systematic review. Cancer Metastasis Rev. 2019; 38(4): 771–782, doi: 10.1007/s10555-019-09826-0, indexed in Pubmed: 31807971.
23. Zhang H, Chen R, Shao J. MicroRNA-96-5p facilitates the viability, migration, and invasion and suppresses the apoptosis of cervical cancer cells by negatively modulating SFRP4. Technol Cancer Res Treat. 2020; 19: 1533033820934132, doi: 10.1177/1533033820934132, indexed in Pubmed: 32527205.
24. Alinari L, Mahasenan KV, Yan F, et al. Selective inhibition of protein arginine methyltransferase 5 blocks initiation and maintenance of B-cell transformation. Blood. 2015; 125(16): 2530–2543, doi: 10.1182/blood-2014-12-619783, indexed in Pubmed: 25742700.
25. Mensah AA, Cascione L, Gaudio E, et al. Bromodomain and extra-terminal domain inhibition modulates the expression of pathologically relevant microRNAs in diffuse large B-cell lymphoma. Haematologica. 2018; 103(12): 2049–2058, doi: 10.3324/haematol.2018.191684, indexed in Pubmed: 30076183.
26. Wei LQ, Liang HT, Qin DC, et al. MiR-212 exerts suppressive effect on SKOV3 ovarian cancer cells through targeting HBEGF. Tumour Biol. 2014; 35(12): 12427–12434, doi: 10.1007/s13277-014-2560-2, indexed in Pubmed: 25201063.
27. Rao L, Giannico D, Leone P, et al. HB-EGF-EGFR signaling in bone marrow endothelial cells mediates angiogenesis associated with multiple myeloma. Cancers (Basel). 2020; 12(1), doi: 10.3390/cancers12010173, indexed in Pubmed: 31936715.
28. Shimura T, Yoshida M, Fukuda S, et al. Nuclear translocation of the cytoplasmic domain of HB-EGF induces gastric cancer invasion. BMC Cancer. 2012; 12: 205, doi: 10.1186/1471-2407-12-205, indexed in Pubmed: 22646534.
29. Tian XP, Huang WJ, Huang HQ, et al. Prognostic and predictive value of a microRNA signature in adults with T-cell lymphoblastic lymphoma. Leukemia. 2019; 33(10): 2454––2465, doi: 10.1038/s41375-019-0466-0, indexed in Pubmed: 30953029.
30. Yu S, Geng Q, Ma J, et al. Heparin-binding EGF-like growth factor and miR-1192 exert opposite effect on Runx2-induced osteogenic differentiation. Cell Death Dis. 2013; 4: e868, doi: 10.1038/cddis.2013.363, indexed in Pubmed: 24136232.

Submitted: 13 May, 2020
Accepted after reviews: 19 August, 2020
Available as AoP: 7 September, 2020

FOLIA HISTOCHEMICA ET CYTOBIOLOGICA
Vol. 58, No. 3, 2020
pp. 227–234

ORIGINAL PAPER

VIA MEDICA

RhTSG-6 inhibits IL-1β-induced extracellular matrix degradation and apoptosis by suppressing the p38, and JNK pathways in nucleus pulposus cells

Shishen Pei[1, 2, 3], Jinwei Ying[2], Yan Zhang[2], Linhao Su[2], Shi Cheng[2], Dike Ruan[1, 2]

[1]The Second School of Clinical Medicine, Southern Medical University, Guangzhou, China
[2]Department of Orthopedic, Navy General Hospital, Beijing, People's Republic of China
[3]Department of Orthopedic Surgery, The 4th People's Hospital of Hengshui City, Hebei, People's Republic of China

Abstract

Introduction. Intervertebral disc degeneration (IDD) is one of the major causes of low back pain (LBP) which seriously affects health and normal physical activity. Recombinant human tumor necrosis factor-α (TNF-α) induced protein 6 (rhTSG-6) has been reported to have therapeutic effects on a variety of inflammatory diseases, but the effect and mechanism of rhTSG-6 action in IDD are not fully understood. The present study was aimed to explore the functional role of rhTSG-6 in interleukin (IL)-1β-induced nucleus pulposus (NP) cell model.

Materials and methods. Experimental human NP cells were isolated from the patients with idiopathic scoliosis and treated with culture medium containing IL-1β (10 ng/mL) for 24 hours to induce extracellular matrix degradation and apoptosis, simulating an IDD model *in vitro.* The viability of NP cells was analyzed by the CCK-8 assay. The relevant mRNA and protein levels were measured by RT-qPCR and western blot. The apoptosis of NP cells was determined by flow cytometry analysis and western blot.

Results. Compared with the NP cells without IL-1β treatment, IL-1β caused approximately 70% reduction in the viability of NP cells, while RhTSG-6 partly increased the decrease of IL-1β on cell viabilities. Moreover, treatment with rhTSG-6 considerably attenuated the upregulation of extracellular matrix (ECM)-catabolic factors (MMP-3, MMP-13, ADAMTS-4, and ADAMTS-5), and increased the downregulation of ECM-anabolic factor (collagen II) in NP cells induced by IL-1β, indicating that ECM degradation was suppressed. Furthermore, rhTSG-6 also protected NP cells from IL-1β-induced apoptosis. Mechanically, rhTSG-6 inhibited the activation of members of mitogen-activated protein kinase (MAPK) pathway by blocking the phosphorylation of p38, c-Jun N-terminal kinase (JNK) and ERK in IL-1β-induced NP cells.

Conclusions. RhTSG-6 can attenuate ECM degradation and apoptosis in IL-1β-induced NP cells by inhibiting the p38, JNK and ERK pathways, which may contribute to its potential application in the therapy of IDD. (*Folia Histochemica et Cytobiologica 2020, Vol. 58, No. 3, 227–234)*

Key words: intervertebral disc degeneration; rhTSG-6; extracellular matrix degradation; apoptosis; IL-1β; nucleus pulposus cells

Introduction

Low back pain (LBP) is a common and multifactorial debilitating disease worldwide, leading to severe disability and a significant socio-economic burden [1]. Intervertebral disk degeneration (IDD) is believed to be one of the leading causes of LBP, which confuses 80% of the world's population [2]. Intervertebral disks (IVDs) are very important components of the human spine structure, maintaining the stability of the spine. IVDs are composed of the inner glycosaminoglycans (GAGs)-rich nucleus pulposus (NP) surrounded by the outer collagen-rich annulus fibrosus (AF) and cartilaginous endplate (CEPs) [3]. As

Correspondence address: Dike Ruan,
Department of Orthopedic, Navy General Hospital,
NO. 6 Fucheng Road,
Beijing 100048, China
e-mail: peishishenspine@163.com

the IDD progressed, the levels of pro-inflammatory cytokines (including TNF-α, IL-1β, IL-6 and etc.) and cell apoptosis increased. Moreover, during IDD the production of extracellular matrix (ECM)-catabolic proteinases [including disintegrin and metalloproteinase with thrombospondin motifs (ADAMTS, which is a superfamily of 26 secreted molecules composed of ADAMTS proteases and ADAMTS-like proteins, and has the function of degrading ECM [4] and matrix metalloproteinases (MMPs)] were elevated, while the synthesis of type II collagen and aggrecan was decreased in NP tissue [5, 6]. Admittedly, up-regulated ADAMTS (including ADAMTS-4 and ADAMTS-5) and matrix MMPs (including MMP-1, MMP-3, MMP-7, MMP-9, and MMP-13) are responsible for the degradation of ECM components [4, 7, 8]. Therefore, inhibiting NP cell apoptosis and ECM degradation by NP cells may be therapeutic targets for delaying IDD.

IL-1β and other pro-inflammatory cytokines are expressed at high levels in degenerative IDD tissues and cells and have been demonstrated to play essential roles in development of IDD [9–11]. IL-1β has also been reported to regulate pathological processes of NP cells in the disk, including inflammatory response, cell apoptosis, and MMP production and ECM homeostasis, further leading to destruction of the physiological structure and function of IVD and the instability of the spine, which ultimately causing LBP [12, 13]. Induction of NP cells with IL-1β has been widely reported as an *in vitro* model for simulating the process of IVD [14–16]. Mechanically, reversing the effect of IL-1β on the cell apoptosis and ECM degradation of NP cells may delay the progression of IDD.

Tumor necrosis factor-α (TNF-α)-induced protein 6 (TSG-6) is a 35 kDa protective inflammatory response protein that mediates inflammatory cell migration, adhesion, involvement in immune regulation and extracellular matrix remodeling by binding to hyaluronic acid, chondroitin sulfate or proteoglycans, and thus plays an inflammatory regulatory role [17–21]. Numerous evidences have demonstrated that administration of recombinant human TSG-6 (rhTSG-6) has been used in a variety of disease models and has demonstrated a broad and strong anti-inflammatory effect. Tuo *et al.* demonstrated that rhTSG-6 could stabilize retinopathy in Ccl2 -/- /Cx3cr1 -/- mice [22]. Li *et al.* found that rhTSG-6 could regulate microglia polarization in rats with subarachnoid hemorrhage and reduce inflammatory brain injury [23]. The protective effects of rhTSG-6 have also been well studied in osteoarthritis. TSG-6 is reported to be up-regulated in rheumatoid arthritis and osteoarthritis and as a biomarker for the progression of knee osteoarthritis [24, 25]. Mindrescu *et al.* indicated that rhTSG-6 improved collagen-induced arthritis in DBA/1J mice [26]. Tellier *et al.* suggested that TSG-6 could attenuate cartilage damage in a rat model of osteoarthritis [27]. A recent study showed that TSG-6 secreted by bone marrow mesenchymal stem cells (BMSCs) attenuated IL-1β-induced NP cell degeneration by inhibiting the activation of the TLR2/ /NF-κB signaling pathway [28]. However, the effects of rhTSG-6 on apoptosis and ECM degradation in IL-1β-induced NP cells still remain unclear.

In this study, we aimed to investigate the influence of rhTSG-6 on ECM degradation and apoptosis in IL-1β-induced NP cells and to explore its potential molecular mechanism.

Materials and methods

Isolation and culture of NP cells. NP cells were isolated from 10 patients with idiopathic scoliosis (average age 22.8 years, range 18–45) as described in previous studies [15, 28]. Thereafter, NP cells were cultured in DMEM/F12 (Gibco, Rockville, MD, USA) containing 10% fetal bovine serum (FBS) and 1% penicillin-streptomycin mix at 37°C in a humidified atmosphere with 5% CO_2.

Cell viability analysis. Cell viability was evaluated by Cell Counting Kit-8 (CCK-8; Dojindo Co, Kumamoto, Japan). The NP cells were seeded in a 96-well plate at a density of 5×10^5 cells/well until reaching 80–90% confluence. The cells were treated with different concentrations of rhTSG-6 (0, 0.5, 1, 1.5, 2 μg/mL) to determine its effects on viability of NP cells. The cells were pre-treated with different concentrations of rhTSG-6 (0, 0.5, 1, 1.5, 2 μg/mL) for 2 h in NP cells then treated with or without 10 ng/mL IL-1β for 24 h at 37°C. Subsequently, 10 μL of CCK-8 solution was added into each well and the cells were incubated at 37°C for 2 h. The optical density at 450 nm was measured using a microplate reader (BioTek Instruments, Inc., Winooski, VT, USA).

RNA extraction and reverse transcription-quantitative polymerase chain reaction (RT-qPCR). Total RNAs were extracted from cells and using TRIzol reagent (Invitrogen, Carlsbad, CA, USA) according to the manufacturer's protocol. First-strand cDNA was reverse transcribed from RNAs using reverse transcriptase kit (Takara, Dalian, China). qRT-PCR was performed using SYBR Green PCR Master Mix (Applied Biosystems, Carlsbad, CA, USA). Relative expression levels were calculated with the $2^{-\Delta\Delta Ct}$ method and normalized to GAPDH. The sequence of primers used for RT-qPCR analysis were as follows: MMP-3, forward: 5'-AAAATCAAGCAG-CGGCGAAG-3', and reverse: 5'-CTCGCGCATAAAAG-CGTCTG-3'; MMP-13, forward: 5'-GATGCCTACTGGGT

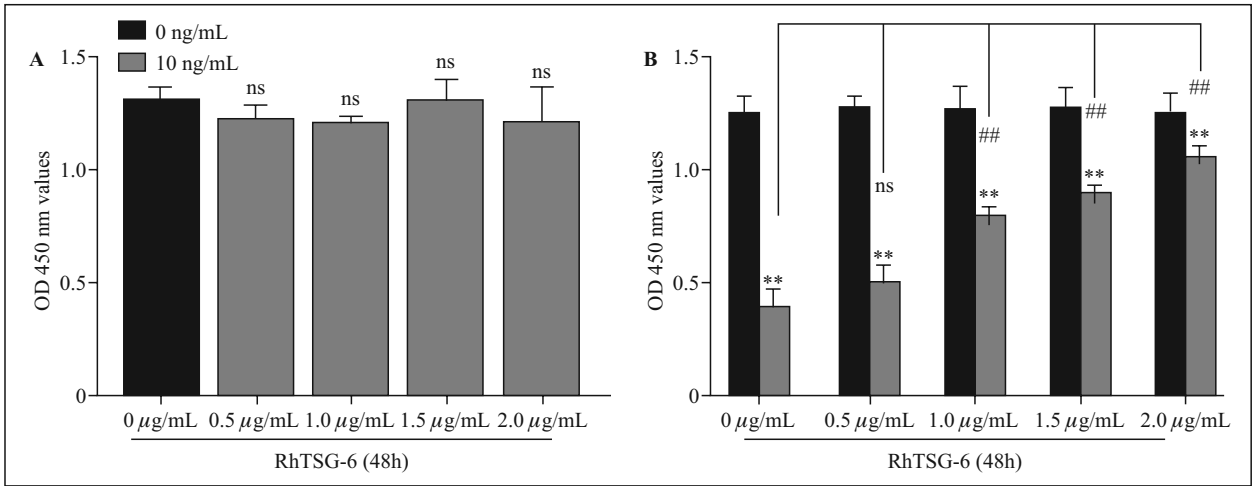

Figure 1. Cell viability of human NP cells following treatment with rhTSG-6 and IL-1β. **A.** Nucleus pulpous (NP) cells were incubated in DMEM/F12 medium containing 10% fetal bovine serum (FBS) and 1% penicillin-streptomycin mix for 24 h and then indicated concentrations of rhTSG-6 were added for 48 h. Thereafter, viability of NP cells was measured by a CCK-8 assay as described in Methods. **B.** Effect of rhTSG-6 on the viability of NP cells stimulated by IL-1β as detected by a CCK-8 assay. Data are expressed as mean ± SD, $^{**}P < 0.01$, *vs.* 0 ng/mL IL-1β group; $^{\#\#}P < 0.01$, *v*s. 10 ng /mL IL-1β+ 0 μg/mL rhTSG-6 group.

GGAG-3' and reverse: 5'-AAAGACGGAAATGGGAGA-3'; ADAMTS-4, forward: 5'-ACCCAAGCATCCGCAATC-3' and reverse: 5'-TGCCCACATCAGCCATAC-3'; ADAMTS-5, forward: 5'-GACAGTTCAAAGCCAAAGACC-3' and reverse: 5'-TTTCCTTCGTGGCAGAGT-3'; Collagen II, forward: 5'-CTCCATGTTGCAGAAG ACTTTCA-3' and reverse: 5'-TTCATGCATCCGCTAGTCCCTTCT-3'; GAPDH, forward: 5′-CGAGATCCCTCCAAAATCAA-3′ and reverse: 5′-TTCACACCCATG ACGAACAT-3′.

Western blot. Total proteins were extracted by using RIPA lysis buffer (Beyotime Biotechnology Co., Ltd., Shanghai, China) and separated with 10% SDS-PAGE and transferred onto a PVDF membrane. After blocking with 5% non-fat milk in TBST for 1 h, the membranes were incubated overnight at 4°C with the following primary antibodies: anti-MMP3 (ab52915, 1:1000, Abcam), anti-MMP13 (ab39012, 1:3000, Abcam), anti-ADAMTS4 (ab185722, 1:500, Abcam), anti-ADAMTS5 (ab41037, 1:250, Abcam), anti-Collagen II (ab34712, 1:1000, Abcam), anti-Bcl-2 (ab196495, 1:1000, Abcam), anti-cleaved caspase-3 (ab49822, 1:500, Abcam), anti-p38 (ab170099, 1:1000, Abcam), phosphor-p38 (1:1000, ab195049, Abcam), anti-JNK (1:1000, #9258, Cell Signaling), anti-phospho-JNK (1:1000, #4668, Cell Signaling), anti-ERK (1:500, ab17942, Abcam), anti-phospho-ERK (1:500, ab214362, Abcam), followed by incubation with the HRP-labeled secondary antibody at room temperature for 1h. The bands were then visualized by electrogenerated chemiluminescence reagent (Pierce, Rockford, IL, USA), and analyzed by using Image J software. GAPDH was used as an internal control.

Flow cytometry analysis. Cell apoptosis was determined using the Annexin V-FITC Apoptosis Detection kit (Beyotime Biotechnology Co., Ltd., Shanghai, China) according to the manufacturer's instructions. Briefly, cells were collected, washed, and stained with 10 μL of Annexin V-FITC buffer and 10 μL of propidium iodide (PI) in dark for 30 minutes at room temperature. Then the stained cells were analyzed using a FACS flow cytometer (BD Biosciences, San Jose, CA, USA).

Statistical analysis. All data were expressed as mean ± SD of three independent experiments. Statistical analysis was performed by using SPSS20.0 (SPSS, Inc., Chicago, IL, USA). Significant differences were evaluated using student's t test or one-way ANOVA. $P < 0.05$ was considered as statistically significant.

Results

Cell viability of human NP cells following treatment with rhTSG-6

Firstly, NP cells were treated with different concentrations (0, 0.5, 1, 1.5, 2 μg/mL) of rhTSG-6, and cell viabilities were determined by using CCK-8 assay. As revealed in Figure 1A, the results suggested that rhTSG-6 was not cytotoxic and had no effect on the proliferation of NP cells. Subsequently, NP cells were stimulated by 10 ng/mL IL-1β for 24 h to evaluate whether rhTSG-6 can alleviate the cytotoxic effects of IL-1β on NP cells. Our findings showed that IL-1β caused approximately 70% reduction in the viability of NP cells, while rhTSG-6 co-treatment could grad-

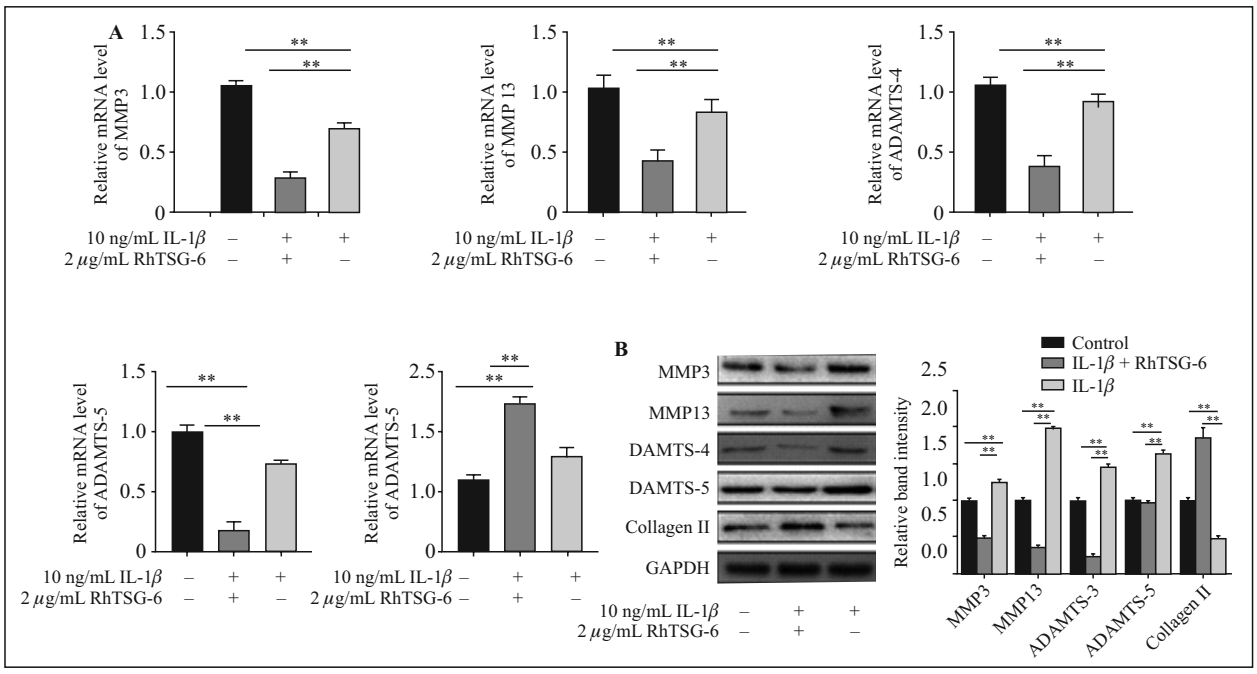

Figure 2. Inhibitory effects of rhTSG-6 on IL-1β-induced expression of ECM components in human NP cells. **(A)** RT-qPCR and **(B)** Western blot analyses were used to evaluate the mRNA and protein expression of MMP3, MMP13, ADAMTS-4, ADAMTS-5 and collagen II. GAPDH served as an internal control. Data are expressed as mean ± SD, $^{**}P < 0.01$.

ually reverse the inhibitory effect of IL-1β on cellular viability in a dose-dependent manner, especially at the concentration of 2 μg/mL (Fig. 1B). Therefore, the concentration of rhTSG-6 used in our subsequent experiments was 2 μg/mL.

Inhibitory effects of rhTSG-6 on IL-1β-induced ECM degradation in human NP cells

To investigate whether rhTSG-6 affects IL-1β-induced ECM degradation in human NP cells, the expression levels of the mRNA and protein associated with ECM progression of NP cells were detected by western blot and RT-qPCR (Fig. 2A and B). The results showed that IL-1β significantly increased the mRNA and protein expression levels of MMP3, MMP13, ADAMTS-4 and ADAMTS-5, but decreased the mRNA and protein expression level of collagen II, whereas co-treatment with rhTSG-6 partly reversed the effects induced by IL-1β.

RhTSG-6 protects NP cells against IL-1β-induced apoptosis

Since cell apoptosis is closely related to the development of IDD, our study further explored the effect of rhTSG-6 on apoptosis of IL-1β-induced NP cells. Flow cytometry analysis demonstrated that IL-1β increased the apoptosis rate of NP cells, whereas rhTSG-6 prevented the apoptosis of NP cells induced by IL-1β. Consistently, the protein level of Bcl-2 (anti-apoptotic protein) was decreased, and the expression level of cleaved caspase-3 (pro-apoptotic protein) was increased in the IL-1β-stimulated NP cells, whereas the effects induced by IL-1β stimulation were alleviated by rhTSG-6 treatment (Fig. 3C).

Effects of rhTSG-6 on the IL-1β-induced activation of p38, JNK and ERK signaling pathways in NP cells

To elucidate the potential mechanisms responsible for rhTFG-6 protective effect on IL-1β-induced NP cells, we evaluated the role of rhTFG-6 in regulating p38 and JNK pathways. As displayed in Figure 4A, the levels of phosphorylated p38, phosphorylated JNK and phosphorylated ERK were significantly increased by IL-1β treatment, indicating activation of the p38, JNK and ERK pathways in the IL-1β-treated human NP cells. However, co-treatment with rhTFG-6 markedly inhibited IL-1β-induced activation of the p38, JNK and ERK pathways.

Discussion

IDD is a major cause of LBP which seriously endangers public health and has become a serious public health problem with high disease rate, disability rate and high medical costs [29, 30]. IDD is characterized by

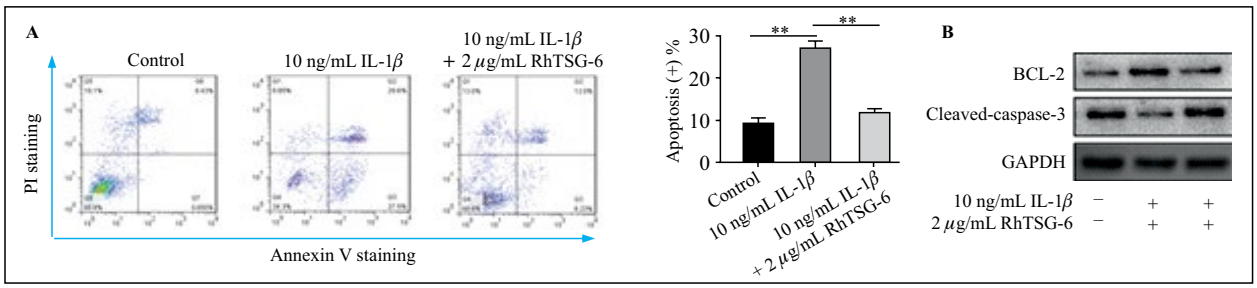

Figure 3. RhTSG-6 protects NP cells against IL-1β-induced apoptosis. **A.** Flow cytometry was used to detect the cell apoptosis of NP cells by the Annexin V-FITC Apoptosis Detection kit. **B.** Western blot analysis was used to determine the protein expression of Bcl-2 and cleaved caspase-3. GAPDH served as an internal control. Data are expressed as mean ± SD, $^{**}P < 0.01$.

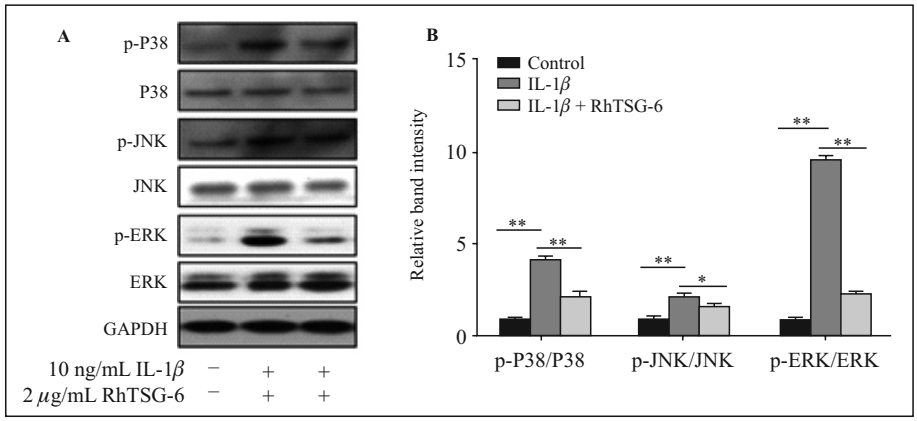

Figure 4. Effects of rhTSG-6 on the IL-1β-induced activation of p38, JNK and ERK in NP cells. **A.** The effects of rhTSG-6 on p38, p-P38, JNK, p-JNK, ERK and p-ERK were determined by western blot analysis. GAPDH served as an internal control. Data are expressed as mean ± SD, $^{*}P < 0.05$, $^{**}P < 0.01$.

increased apoptosis of NP cells and hyperactive ECM degradation [11]. Current evidence suggests that decreasing NP cell apoptosis and increasing expression of some important ECM components may provide a therapeutic strategy for IDD [31–33]. In this study, in vitro model of IDD degeneration was successfully constructed by IL-1β-induced NP cells. We provided the first evidence that in human IL-1β-treated NP cells rhTSG-6 has inhibitory effects on cell apoptosis and expression of ECM-degrading molecules, and that potential regulatory mechanism is mediated by the activation of p38, JNK and ERK pathways.

TSG-6 is a pleiotropic regulatory protein secreted by pro-inflammatory mediator-induced (including TNF-α and IL-1β) immune cells (such as neutrophils, monocytes, macrophages, medullary dendritic cells), and stromal cells (such as fibroblasts and smooth muscle cells) [34–36]. TSG-6 is quickly activated early in the inflammatory process and plays an anti-inflammatory role. The protective effects of TSG-6 secreted by bone marrow mesenchymal stem cells in IDD has been proved by a recent study, which focused on the mechanism of reducing inflammation, especially its role in inhibiting the expression of inflammatory cytokines *via* TLR2/NF-κB signaling [28]. Since the mechanism of inhibiting IDD may involve many aspects, the present study explored the effects of exogenous addition of rhTSG-6 on the changes of some important ECM components' expression and cell apoptosis in IL-1β-induced NP cells. Consistent with the results of the previous study [28], rhTSG-6 decreased the expression of MMP3 and MMP13, and increased the expression of collagen II in IL-1β-induced NP cells. In addition, ECM-catabolic proteinases (ADAMTS-4 and ADAMTS-5) were also inhibited by exogenous rhTSG-6. Furthermore, the inhibitory effect of rhTSG-6 on IL-1β-induced NP cell apoptosis was demonstrated by flow cytometry and western blot analysis. These results reveal that rhTSG-6 has the potential to regulate the progression of IDD by inhibiting ECM degradation and cell apoptosis of NP cells.

IDD-associated inflammation is capable of activating various intracellular signaling pathways that mediate the production of downstream effectors that are closely related to the progression of IDD [37]. P38, JNK and ERK, as important members of mitogen-activated protein kinase (MAPK) pathway, have been reported as key signaling pathways regulating IDD [38–42]. Hua *et al.* demonstrated that icariin, an anti-inflammatory drug isolated from Epimedium brevicornum, inhibits IL-1β-induced inflammatory response and ECM reduction through suppressing the p38/MAPK pathway in human NP cells [43]. Lin *et al.* suggested that Propionibacterium acnes induces IDD by promoting NP cell apoptosis *via* the TLR2/ /JNK/mitochondrial-mediated pathway [44]. Besides, a recent study proved that simvastatin suppresses IL-1β-induced cell apoptosis and ECM degradation by inhibiting the p38, JNK and ERK phosphorylation [16]. Therefore, the activation of p38, JNK and ERK signaling pathway may exacerbate IDD. RhTSG-6 has been reported to inhibit p38, JNK and ERK pathways in various disease models [28, 45–47]. Hence, we supposed that p38, JNK and ERK pathways might be involved in the regulatory effects of rhTSG-6 on degradation of ECM and cell apoptosis in the *in vitro* IDD model. To confirm our hypothesis, western blot was performed to detect the expression changes of p-p38, p-JNK, and p-ERK. The results revealed that rhTSG-6 could inhibit the P38, JNK and ERK pathway, thus explaining the effects of rhTSG-6 on NP cell apoptosis and possible ECM degradation described above.

In conclusion, this study suggested that rhTSG-6 could inhibit the IL-1β-induced ECM degradation and cell apoptosis through inhibiting the P38, JNK and ERK pathways and should be further investigated as a possible novel therapeutic approach treatment for IDD.

Acknowledgements

Not applicable.

Funding

This work was supported by National Natural Science Foundation of China (Grant No.81472121).

Ethics approval and consent to participate

The present study was approved by the Ethics Committee of Southern Medical University, Guangzhou, China.

Competing interests

The authors declare that they have no competing interests.

Availability of data and materials

All data generated or analyzed during this study are included in this published article.

Authors' contributions

RDK and PSS conceived and designed the experiments, YJW and ZY analyzed and interpreted the results of the experiments, SLH and CS performed the experiments.

References

1. Hoy D, March L, Brooks P, et al. Measuring the global burden of low back pain. Best Pract Res Clin Rheumatol. 2010; 24(2): 155–165, doi: 10.1016/j.berh.2009.11.002, indexed in Pubmed: 20227638.
2. Jensen C, Riis A, Petersen K, et al. Economic evaluation of an implementation strategy for the management of low back pain in general practice. PAIN. 2017; 158(5): 891–899, doi: 10.1097/j.pain.0000000000000851, indexed in Pubmed: 28114182.
3. Chen YC, Su WY, Yang SH, et al. In situ forming hydrogels composed of oxidized high molecular weight hyaluronic acid and gelatin for nucleus pulposus regeneration. Acta Biomater. 2013; 9(2): 5181–5193, doi: 10.1016/j.actbio.2012.09.039, indexed in Pubmed: 23041783.
4. Mead TJ, Apte SS. ADAMTS proteins in human disorders. Matrix Biol. 2018; 71-72: 225–239, doi: 10.1016/j.matbio.2018.06.002, indexed in Pubmed: 29885460.
5. Wu B, Meng C, Wang H, et al. Changes of proteoglycan and collagen II of the adjacent intervertebral disc in the cervical instability models. Biomed Pharmacother. 2016; 84: 754–758, doi: 10.1016/j.biopha.2016.09.077, indexed in Pubmed: 27716589.
6. Li Y, Li K, Han X, et al. The imbalance between TIMP3 and matrix-degrading enzymes plays an important role in intervertebral disc degeneration. Biochem Biophys Res Commun. 2016; 469(3): 507–514, doi: 10.1016/j.bbrc.2015.12.020, indexed in Pubmed: 26686417.
7. Tang BL. ADAMTS: a novel family of extracellular matrix proteases. Int J Biochem Cell Biol. 2001; 33(1): 33–44, doi: 10.1016/s1357-2725(00)00061-3, indexed in Pubmed: 11167130.
8. Jabłońska-Trypuć A, Matejczyk M, Rosochacki S. Matrix metalloproteinases (MMPs), the main extracellular matrix (ECM) enzymes in collagen degradation, as a target for anticancer drugs. J Enzyme Inhib Med Chem. 2016; 31(sup1): 177–183, doi: 10.3109/14756366.2016.1161620, indexed in Pubmed: 27028474.
9. Yang W, Yu XH, Wang C, et al. Interleukin-1ñin intervertebral disk degeneration. Clin Chim Acta. 2015; 450: 262–272, doi: 10.1016/j.cca.2015.08.029, indexed in Pubmed: 26341894.
10. Chen J, Xuan J, Gu YT, et al. Celastrol reduces IL-1ñinduced matrix catabolism, oxidative stress and inflammation in human nucleus pulposus cells and attenuates rat intervertebral

disc degeneration in vivo. Biomed Pharmacother. 2017; 91: 208–219, doi: 10.1016/j.biopha.2017.04.093, indexed in Pubmed: 28458159.
11. Risbud MV, Shapiro IM. Role of cytokines in intervertebral disc degeneration: pain and disc content. Nat Rev Rheumatol. 2014; 10(1): 44–56, doi: 10.1038/nrrheum.2013.160, indexed in Pubmed: 24166242.
12. Johnson ZI, Schoepflin ZR, Choi H, et al. Disc in flames: Roles of TNF-α and IL-1β in intervertebral disc degeneration. Eur Cell Mater. 2015; 30: 104–16; discussion 116, doi: 10.22203/ecm.v030a08, indexed in Pubmed: 26388614.
13. Lee J, Song J, Baek M, et al. Interleukin-1β induces angiogenesis and innervation in human intervertebral disc degeneration. Journal of Orthopaedic Research. 2010; 29(2): 265–269, doi: 10.1002/jor.21210, indexed in Pubmed: 20690185.
14. Hua W, Zhang Y, Wu X, et al. Icariin Attenuates interleukin-1β-induced inflammatory response in human nucleus pulposus cells. Curr Pharm Des. 2018; 23(39): 6071–6078, doi: 10.2174/1381612823666170615112158, indexed in Pubmed: 28619001.
15. Kang L, Yang C, Yin H, et al. MicroRNA-15b silencing inhibits IL-1ñinduced extracellular matrix degradation by targeting SMAD3 in human nucleus pulposus cells. Biotechnol Lett. 2017; 39(4): 623–632, doi: 10.1007/s10529-016-2280-3, indexed in Pubmed: 28039556.
16. Tu Ji, Li W, Zhang Y, et al. Simvastatin inhibits IL-1β-induced apoptosis and extracellular matrix degradation by suppressing the NF-kB and MAPK pathways in nucleus pulposus cells. Inflammation. 2017; 40(3): 725–734, doi: 10.1007/s10753-017-0516-6, indexed in Pubmed: 28188410.
17. Lee TH, Wisniewski HG, Vilcek J. A novel secretory tumor necrosis factor-inducible protein (TSG-6) is a member of the family of hyaluronate binding proteins, closely related to the adhesion receptor CD44. J Cell Biol. 1992; 116(2): 545–557, doi: 10.1083/jcb.116.2.545, indexed in Pubmed: 1730767.
18. Nentwich H, Mustafa Z, Rugg M, et al. A Novel allelic variant of the humanTSG-6gene encoding an amino acid difference in the CUB module. J Biol Chem. 2002; 277(18): 15354–15362, doi: 10.1074/jbc.m110765200, indexed in Pubmed: 11854277.
19. Lee RH, Pulin AA, Seo MJ, et al. Intravenous hMSCs improve myocardial infarction in mice because cells embolized in lung are activated to secrete the anti-inflammatory protein TSG-6. Cell Stem Cell. 2009; 5(1): 54–63, doi: 10.1016/j.stem.2009.05.003, indexed in Pubmed: 19570514.
20. Parkar A, Kahmann J, Howat S, et al. TSG-6 interacts with hyaluronan and aggrecan in a pH-dependent manner via a common functional element: implications for its regulation in inflamed cartilage. FEBS Letters. 1998; 428(3): 171–176, doi: 10.1016/s0014-5793(98)00523-7.
21. Blundell CD, Mahoney DJ, Almond A, et al. The link module from ovulation- and inflammation-associated protein TSG-6 changes conformation on hyaluronan binding. J Biol Chem. 2003; 278(49): 49261–49270, doi: 10.1074/jbc.M309623200, indexed in Pubmed: 12972412.
22. Tuo J, Cao X, Shen D, et al. Anti-inflammatory recombinant TSG-6 stabilizes the progression of focal retinal degeneration in a murine model. J Neuroinflammation. 2012; 9: 59, doi: 10.1186/1742-2094-9-59, indexed in Pubmed: 22452753.
23. Li R, Liu W, Yin J, et al. TSG-6 attenuates inflammation-induced brain injury via modulation of microglial polarization in SAH rats through the SOCS3/STAT3 pathway. J Neuroinflammation. 2018; 15(1): 231, doi: 10.1186/s12974-018-1279-1, indexed in Pubmed: 30126439.
24. Bayliss MT, Howat SL, Dudhia J, et al. Up-regulation and differential expression of the hyaluronan-binding protein TSG-6 in cartilage and synovium in rheumatoid arthritis and osteoarthritis. Osteoarthritis Cartilage. 2001; 9(1): 42–48, doi: 10.1053/joca.2000.0348, indexed in Pubmed: 11178946.
25. Wisniewski HG, Colón E, Liublinska V, et al. TSG-6 activity as a novel biomarker of progression in knee osteoarthritis. Osteoarthritis Cartilage. 2014; 22(2): 235–241, doi: 10.1016/j.joca.2013.12.004, indexed in Pubmed: 24333293.
26. Mindrescu C, Thorbecke GJ, Klein MJ, et al. Amelioration of collagen-induced arthritis in DBA/1J mice by recombinant TSG-6, a tumor necrosis factor/interleukin-1-inducible protein. Arthritis Rheum. 2000; 43(12): 2668–2677, doi: 10.1002/1529-0131(200012)43:12<2668::AID-ANR6>3.0.CO;2-E, indexed in Pubmed: 11145024.
27. Tellier LE, Treviño EA, Brimeyer AL, et al. Intra-articular TSG-6 delivery from heparin-based microparticles reduces cartilage damage in a rat model of osteoarthritis. Biomater Sci. 2018; 6(5): 1159–1167, doi: 10.1039/C8BM00010G, indexed in Pubmed: 29564448.
28. Yang H, Tian W, Wang S, et al. TSG-6 secreted by bone marrow mesenchymal stem cells attenuates intervertebral disc degeneration by inhibiting the TLR2/NF-κB signaling pathway. Lab Invest. 2018; 98(6): 755–772, doi: 10.1038/s41374-018-0036-5, indexed in Pubmed: 29483622.
29. Luoma K, Riihimäki H, Luukkonen R, et al. Low back pain in relation to lumbar disc degeneration. Spine (Phila Pa 1976). 2000; 25(4): 487–492, doi: 10.1097/00007632-200002150-00016, indexed in Pubmed: 10707396.
30. Fontana G, See E, Pandit A. Current trends in biologics delivery to restore intervertebral disc anabolism. Adv Drug Deliv Rev. 2015; 84: 146–158, doi: 10.1016/j.addr.2014.08.008, indexed in Pubmed: 25174310.
31. Lu L, Hu J, Wu Q, et al. Berberine prevents human nucleus pulposus cells from IL1-β-induced extracellular matrix degradation and apoptosis by inhibiting the NFκB pathway. Int J Mol Med. 2019; 43(4): 1679–1686, doi: 10.3892/ijmm.2019.4105, indexed in Pubmed: 30816449.
32. Wang Ke, Chen T, Ying X, et al. Ligustilide alleviated IL-1-β--induced apoptosis and extracellular matrix degradation of nucleus pulposus cells and attenuates intervertebral disc degeneration in vivo. Int Immunopharmacol. 2019; 69: 398–407, doi: 10.1016/j.intimp.2019.01.004, indexed in Pubmed: 30785069.
33. Chai X, Si H, Song J, et al. miR-486-5p inhibits inflammatory response, matrix degradation and apoptosis of nucleus pulposus cells through directly targeting FOXO1 in intervertebral disc degeneration. Cell Physiol Biochem. 2019; 52(1): 109––118, doi: 10.33594/000000008, indexed in Pubmed: 30790508.
34. Milner CM, Day AJ. TSG-6: a multifunctional protein associated with inflammation. J Cell Sci. 2003; 116(Pt 10): 1863––1873, doi: 10.1242/jcs.00407, indexed in Pubmed: 12692188.
35. Wisniewski HG, Vilček J. Cytokine-induced gene expression at the crossroads of innate immunity, inflammation and fertility: TSG-6 and PTX3/TSG-14. Cytokine Growth Factor Rev. 2004; 15(2-3): 129–146, doi: 10.1016/j.cytogfr.2004.01.005, indexed in Pubmed: 15110797.
36. Day AJ, Milner CM. TSG-6: A multifunctional protein with anti-inflammatory and tissue-protective properties. Matrix Biol. 2019; 78-79: 60–83, doi: 10.1016/j.matbio.2018.01.011, indexed in Pubmed: 29362135.
37. Wuertz K, Vo N, Kletsas D. Boos NJECM. Inflammatory and catabolic signalling in intervertebral discs: the roles of NF-KB and MAP kinases. 2012; 23: 103–19, doi: 10.22203/ecm.v023a08, indexed in Pubmed: 22354461.
38. Studer RK, Aboka AM, Gilbertson LG, et al. p38 MAPK inhibition in nucleus pulposus cells: a potential target for treating intervertebral disc degeneration. Spine (Phila Pa 1976). 2007;

32(25): 2827–2833, doi: 10.1097/BRS.0b013e31815b757a, indexed in Pubmed: 18246004.
39. Studer RK, Gilbertson LG, Georgescu H, et al. Kang JDJJoOR. p38 MAPK inhibition modulates rabbit nucleus pulposus cell response to IL-1. 2008; 26(7): 991–8, doi: 10.1002/jor.20604, indexed in Pubmed: 18302237.
40. Klawitter M, Quero L, Klasen J, et al. Curcuma DMSO extracts and curcumin exhibit an anti-inflammatory and anti-catabolic effect on human intervertebral disc cells, possibly by influencing TLR2 expression and JNK activity. J Inflamm (Lond). 2012; 9(1): 29, doi: 10.1186/1476-9255-9-29, indexed in Pubmed: 22909087.
41. Tsai TT, Guttapalli A, Agrawal A, et al. MEK/ERK signaling controls osmoregulation of nucleus pulposus cells of the intervertebral disc by transactivation of TonEBP/OREBP. J Bone Miner Res. 2007; 22(7): 965–974, doi: 10.1359/jbmr.070322, indexed in Pubmed: 17371162.
42. Marazza A, Tekari A, Roth E, et al. Investigation into ERK, JNK and p38 downstream signaling pathways: an anti-inflammatory approach against the Intervertebral Disc Degeneration; 2015.
43. Hua W, Zhang Y, Wu X, et al. Icariin Attenuates interleukin-1β-induced inflammatory response in human nucleus pulposus cells. Curr Pharm Des. 2018; 23(39): 6071–6078, doi: 10.2174/1381612823666170615112158.
44. Lin Y, Jiao Y, Yuan Ye, et al. Propionibacterium acnes induces intervertebral disc degeneration by promoting nucleus pulposus cell apoptosis via the TLR2/JNK/mitochondrial-mediated pathway. Emerg Microbes Infect. 2018; 7(1): 1, doi: 10.1038/s41426-017-0002-0, indexed in Pubmed: 29323102.
45. Zhang C, Zhang B, Wang H, et al. Tumor necrosis factor alpha-stimulated gene-6 (TSG-6) inhibits the inflammatory response by inhibiting the activation of P38 and JNK signaling pathway and decreases the restenosis of vein grafts in rats. Heart Vessels. 2017; 32(12): 1536–1545, doi: 10.1007/s00380-017-1059-3, indexed in Pubmed: 28975447.
46. Um S, Kim HY, Lee JH, et al. TSG-6 secreted by mesenchymal stem cells suppresses immune reactions influenced by BMP-2 through p38 and MEK mitogen-activated protein kinase pathway. Cell Tissue Res. 2017; 368(3): 551–561, doi: 10.1007/s00441-017-2581-4, indexed in Pubmed: 28247086.
47. Liu Yi, Yin Z, Zhang R, et al. MSCs inhibit bone marrow-derived DC maturation and function through the release of TSG-6. Biochem Biophys Res Commun. 2014; 450(4): 1409–1415, doi: 10.1016/j.bbrc.2014.07.001, indexed in Pubmed: 25014173.

Submitted: 3 June, 2020
Accepted after reviews: 1 September, 2020
Available as AoP: 16 September, 2020

INSTRUCTIONS FOR AUTHORS

MANUSCRPIT SUBMISSION

Folia Histochemica et Cytobiologica accepts manuscripts (original articles, short communications, review articles) from the field of histochemistry, as well as cell and tissue biology. Each manuscript is reviewed by independent referees. Book reviews and information concerning congresses, symposia, meetings etc., are also published.

All articles should be submitted to FHC electronically online at www.fhc.viamedica.pl where detailed instruction regarding submission process will be provided.

AUTHOR'S STATEMENT

The manuscript must be accompanied by the author's statement that it has not been published (or submitted to publication) elsewhere.

GHOSTWRITTING

Ghostwriting and guest-authorship are forbidden. In case of detecting ghost written manuscripts, their actions will be taking involving both the submitting authors and the participants involved.

The corresponding author must have obtained permission from all authors for the submission of each version of the paper and for any change in authorship. Submission of a paper that has not been approved by all authors may result in immediate rejection.

COST OF PUBLICATION

The cost of publication of accepted manuscript is 800 Euro.

OFFPRINTS

PDF file of each printed paper is supplied for the author free of charge. Orders for additional offprints should be sent to the Editorial Office together with galley proofs.

ORGANIZATION OF MANUSCRIPT

The first page must include: the title, name(s) of author(s), affiliation(s), short running head (no more than 60 characters incl. spaces) and detailed address for correspondence including e-mail. Organization of the manuscript: 1. Abstract (not exceeding one typed page — should consist of the following sections: Introduction, Material and methods, Results, Conclusions); 2. Key words (max. 10); Introduction; Material and methods; Results; Discussion; Acknowledgements (if any); References; Tables (with legends); Figures; Legends to figures.

In a short communication, Results and Discussion should be written jointly. Organization of a review article is free.

TECHNICAL REQUIREMENTS

Illustrations (line drawings and halftones) — either single or mounted in the form of plates, can be 85 mm, 125 mm, or 175 mm wide and cannot exceed the size of 175 × 250 mm. The authors are requested to plan their illustrations in such a way that the printed area is eco-nomically used. Numbers, inscriptions and abbreviations on the figures must be about 3 mm high. In case of micrographs, magnification (*e.g.* × 65 000) should be given in the legend. Calibration bars can also be used. For the best quality of illustrations please provide images in one of commonly used formats e.g. *.tiff, *.png, *pdf (preferred resolution 300 dpi). Color illustrations can be published only at author's cost and the cost estimate will be sent to the author after submission of the manuscript. Tables should be numbered consecutively in Arabic numerals and each table must be typed on a separate page. The authors are requested to mark the places in the text, where a given table or figure should appear in print. Legends must begin on a new page and should be as concise as necessary for a self-sufficient explanation of the illustrations. PDF file of each paper is supplied free of charge.

CITATIONS

In References section of article please use following American Medical Association 9th Ed. citation style. Note, that items are listed numerically in the order they are cited in the text, not alphabetically. If you are using a typewriter and cannot use italics, then use underlining.

Authors: use initials of first and second names with no spaces. Include up to six authors. If there are more than six, include the first three, followed by et al. If no author is given, start with the title. **Books:** include the edition statement (ex: 3rd ed. or Rev ed.) between the title and place if it is not the first edition. **Place:** use abbreviations of states, not postal codes. **Journals:** abbreviate titles as shown in *Index Medicus*. If the journal does not paginate continuously through the volume, include the month (and day). **Websites:** include the name of the webpage, the name of the entire website, the full date of the page (if available), and the date you looked at it. The rules concerning a title within a title are *not* displayed here for purposes of clarity. See the printed version of the manual for details. For documents and situations not listed here, see the printed version of the manual.

EXAMPLES

Book:

1. Okuda M, Okuda D. *Star Trek Chronology: The History of the Future.* New York: Pocket Books; 1993.

Journal or Magazine Article (with volume numbers):

2. Redon J, Cifkova R, Laurent S et al. Mechanisms of hypertension in the cardiometabolic syndrome. *J Hypertens.* 2009; 27(3):441–451. doi: 10.1097/HJH.0b013e32831e13e5.

Book Article or Chapter:

3. James NE. Two sides of paradise: the Eden myth according to Kirk and Spock. In: Palumbo D, ed. *Spectrum of the Fantastic*. Westport, Conn: Greenwood; 1988:219–223.

When the manufacturers of the reagents etc. are mentioned for the first time, town, (state in the US) and country must be provided wheras for next referral only the name of the firm should be given.

Website:

4. Lynch T. DSN trials and tribble-ations review. Psi Phi: Bradley's Science Fiction Club Web site. 1996. Available at: http://www.bradley.edu/campusorg/psiphi/DS9/ep/503r.htm. Accessed October 8, 1997.

Journal Article on the Internet:

5. McCoy LH. Respiratory changes in Vulcans during pon farr. *J Extr Med* [serial online]. 1999;47:237–247. Available at: http:// //infotrac.galegroup.com/itweb/nysl_li_liu. Accessed April 7, 1999.